Printing the Personal Aircraft of Tomorrow - Final Report

Design Synthesis Exercise
Spring 2014 - Group 12

Faculty of Aerospace Engineering

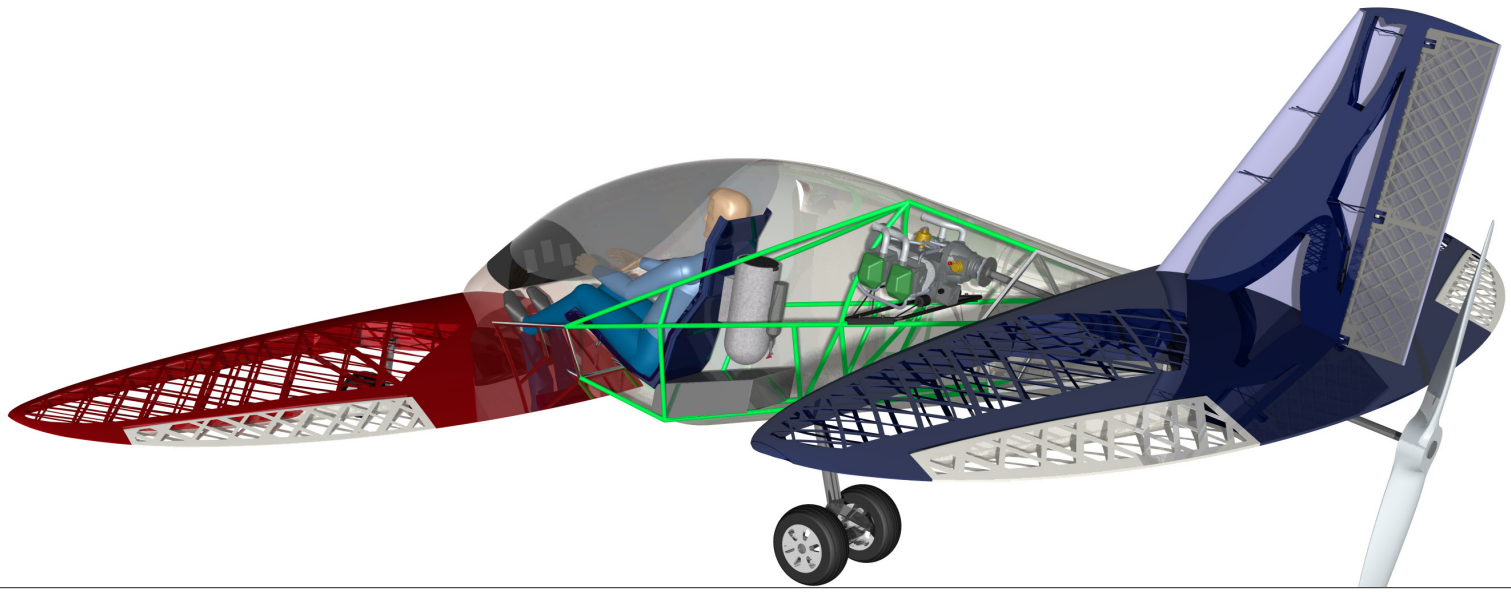

TU Delft Delft University of Technology

Challenge the future

This report may find you in black and white print. Due to the vast amount of figures requiring color, not everything might be legible. The complete PDF of the report is therefore made available on the following link:

Printing the Personal Aircraft of Tomorrow

Final Report

Design Synthesis Exercise Spring 2014

Barten, K.P.A.M.
De Bie, M.
Cheylus, T.P.A.
van de Grift, I.
Jux, C.
van der Linden, S.
Opgenoord, M.M.J.
Peelman, S.H.M.
Stoter, K.F.S.
van Zanten, F.J.

DATE:	July 1, 2014
TUTOR:	C.D. Rans
COACHES:	F. Tian
	H.J. Tol

Faculty of Aerospace Engineering
Delft University of Technology

Preface

This Final Report holds all details regarding the development and design of a personal aircraft using only Additive Manufacturing (AM) techniques for at least all the load carrying structures. This work has been carried out by the ten Aerospace Engineering Bachelor students from DSE project group 12. This Final Report concludes all design activities from this eleven week project.

The Final Report focuses on the detailed design phase, but also gives a general overview of the project. Readers particularly interested in the conceptual design phase are advised to consult Chapter 2, while those who are especially interested in all detailed technical aspects are urged to have to look at Chapters 3 through 5. The subsequent evaluation of the design is elaborated on Chapter 7.

We would like to express our deep gratitude to our tutor, Dr. Calvin Rans for his enthusiasm and very helpful guidance throughout the project. His willingness to give his time so generously has been very much appreciated. We would also like to give our special thanks to coaches Fengnian Tian and Henry Tol for their provided feedback during the meetings and reviews. Furthermore, we would like to express our gratitude to Dr. Ir. Matthijs Langelaar, Ir. Jan Hol, Ir. Michiel Schuurman and Ir. Hessel Benedictus from TU Delft for their expert knowledge shared with the team. The team is also particularly grateful for the provided license for Abaqus ATOM by *Dassault Systèmes* and for the availability of the CFD cluster from Formula Student Team Delft (DUT Racing). Our special thanks are extended to the staff of *Materialise* and *LayerWise* for the valuable information about Additive Manufacturing given during a company visit and to the staff of ILT for their valuable help regarding the airworthiness.

Delft, July 1, 2014

Table of Contents

Summary

In connection with the technical progress of the growing Additive Manufacturing industry, the possible introduction of this technology in full scale aircraft structures has been researched. The research has been focused on the application of this unique, layerwise manufacturing technique in the Light Sport Aircraft category. Consequently, the design freedom provided by this technology is incorporated in an aircraft design featuring an airframe structure manufactured by Additive Manufacturing technologies only.

To draw the full advantage of the new design freedom, but also to cope with the limitations introduced by Additive Manufacturing, a unique "bottom-up top-down" concept development strategy is proposed: effects of manufacturing method and material choice on aircraft components are investigated, then these observations are combined to come up with optimized aircraft configurations, of which the best concept is subsequently broken down into concepts for its constituents. The concept emerging this design process is a tandem wing aircraft comprising aerodynamically efficient, elliptical wings.

The two lifting surfaces omit the need for a horizontal stabilizer, further increasing aerodynamic efficiency. The danger of blanketing effects is eliminated by adequate positioning of the wings. However, the overall configuration still needs to be investigated further to guarantee stability and control in all flight conditions and to meet the stall speed requirements specified in the Light Sport Aircraft regulations.

In the detailed structural design phase Topology Optimization software lends itself well for additively manufactured products and has been used for the structural sizing of the vertical stabilizer and the wing root sections. The software output can be closely resembled with Additive Manufacturing. The drawback is the complexity of this software and the large effort required to implement the software output into a final design. The potential of Topology Optimization software in combination with Additive Manufacturing could be demonstrated in a case study, and it is recommended to invest more resources in this area. For all other airframe components, a conventional, beam, column and sheet based sizing approach is chosen. The results of these are then adjusted to draw benefits from Additive Manufacturing. For the latter, ideas are often inspired by nature and a bionic design is realized.

Besides the alternative sizing approach, alternative materials are considered for structural components. Consequently, polymer structures contribute significantly to the constitution of the airframe.

The challenges of Additive Manufacturing encountered in the detailed design stage are two fold: on the technical side, the current build envelope as well as the uncertainty about the part's fatigue properties and directional dependent behavior represent the most constraining factors. Especially for large components it is questionable whether Additive Manufacturing is the favorable technology at this point in time; In general, also for small scale products, more research needs to be performed to reduce fatigue and anisotropy related safety factors. From a design perspective, the observed freedom

in shape allows various solutions, which effectively slows down the design process. It is recommended that systems engineering methods are developed specifically for the design of additively manufactured components.

A design evaluation has shown that it is possible to build an additively manufactured aircraft, but that at the time it is advisable to use Additive Manufacturing for specific components only. Furthermore, a cost & market analysis has proven that manufacturing costs are incommensurably high compared to existing Light Sport Aircraft. Regarding the technologies' impact on sustainability more research needs to be done. An extensive list, suggesting research items to increase the feasibility of Additive Manufacturing in aerospace industries concludes the report.

Chapter 1

Introduction

Additive Manufacturing, commonly known as 3D-printing, is a technology which carries the potential of being a game changer in the manufacturing industry. Its unique approach of building objects in a layerwise fashion eliminates a great deal of geometric limitations present in classical manufacturing processes. Thereby, it allows for steps of improvements in structural and aerodynamic performance of aerospace structures. However, until today, additively manufactured products represent small scale objects when comparing to typical aerospace structures. It is the objective of DSE group 12 to push this promising technology to the next level, and to design a manned experimental aircraft that has its entire airframe constructed using additive manufacturing technologies.

The purpose of this report is to present the final design of this aircraft, to reflect on the design process and to outline limitations that currently prevent the completion of this major step in building a fully additively manufactured aircraft. The designed aircraft is a technology demonstrator and will for this reason be certified under a special experimental airworthiness certificate in the Light Sport Aircraft category. The mission driving the demonstrator design comprises a two hour loiter phase at 4000 ft altitude with a loiter speed of 85 kts. The demonstrator shall be operated from Lelystad airport in The Netherlands.

To familiarize the reader with the contents of this report and the final design, the concept development and selection phase is briefly summarized in the following. Furthermore, the final aircraft layout is presented including 3-view drawings.

1.1 Concept Development & Selection

The design challenge faced in this project is exceptional in the sense that it features the application of Additive Manufacturing to full scale aircraft components. But even more unique is the sequence of first selecting a manufacturing technology and then tailoring the design towards this process. This design environment requires a review and adjustment of classical design approaches.

The concept development process is one item which exemplifies this change in design strategy. Instead of a classical top-down development process it is decided to start the concept generation process at a component level and to follow a "bottom-up top-down" strategy. At the first level, it is investigated how the material selection influences specific component designs. For this analysis two focus groups are formed, one for polymer and one for metal construction. In the consecutive step, this knowledge is combined to generate aircraft configurations tailored to the needs and limitations of Additive Manufacturing. With the aircraft configuration selected, concepts for individual components of this specific aircraft layout are created and traded-off. The latter are then further developed in the detailed design phase. This process is evaluated in Chapter 2.

The following detailed design phase required a reconsideration of the design philosophy which

was to be used. In this stage of the project, the design freedom of the AM technologies emerged. Additive Manufacturing lends itself very well for the application of Topology Optimization software. Such software, based on Finite Element Method analysis, iteratively optimizes a structure under a given load case by removing excessive material. The application of Additive Manufacturing allows to resemble the output of such optimization software without large simplifications. This tool provides the basis for the first of the two design strategies followed by the team. The second philosophy chosen by the team is based on conventional sizing methods, including beam, column and sheet models. The results of this design approach are then fine-tuned and optimized to draw additional advantages from the AM technologies. Inspiration for such adjustments are drawn from nature, following a biomimetic design approach. The design philosophies together with the structural design is presented in Chapter 4.

1.2 Final Design

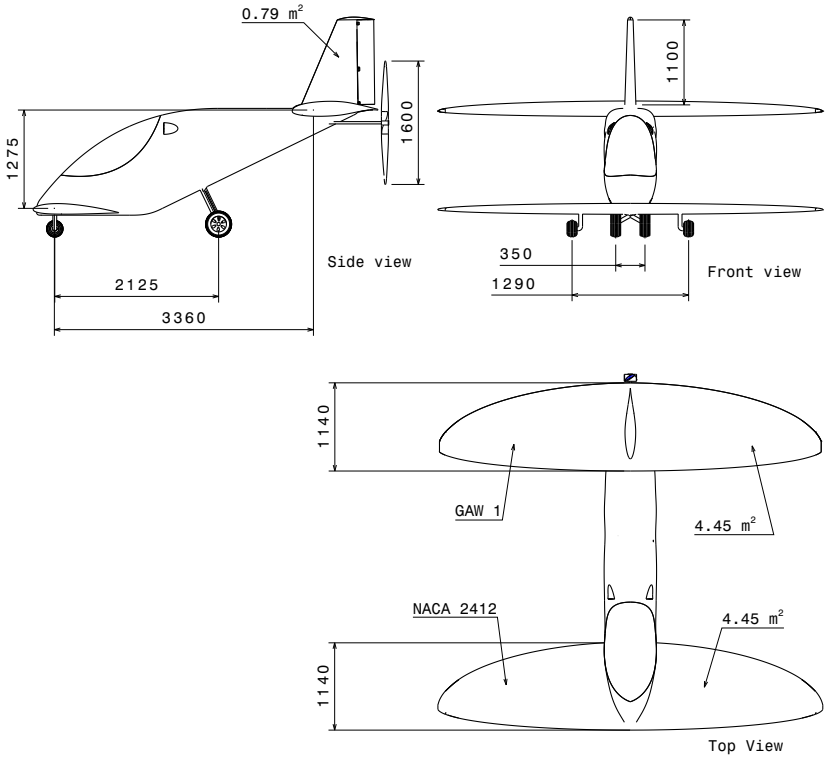

Figure 1.1: 3-View drawing of the tandem aircraft, length dimensions in $[mm]$

The final concept that emerged from the developed selection process is a tandem wing aircraft. A separation of the lifting surfaces is desired to reduce the required wingspan and thereby the induced bending loads. These two wings have elliptical planforms to enhance the aerodynamic performance, which is further increased by moving the back wing higher up to move it out of the wake of the front wing. A 3-view drawing of the design is shown in Figure 1.1. The design of the outer shape of the aircraft is discussed in Chapter 3, while the structural design of the aircraft is discussed extensively in Chapter 4.

The internal aircraft layout has an major impact on the center of gravity location which in turn drives the design for stability and controllability, a critical aspect of the tandem wing aircraft. The final internal layout is briefly summarized and illustrated in Figure 1.2. Detailed information on the design decisions related to the internal layout is provided in Chapter 5.

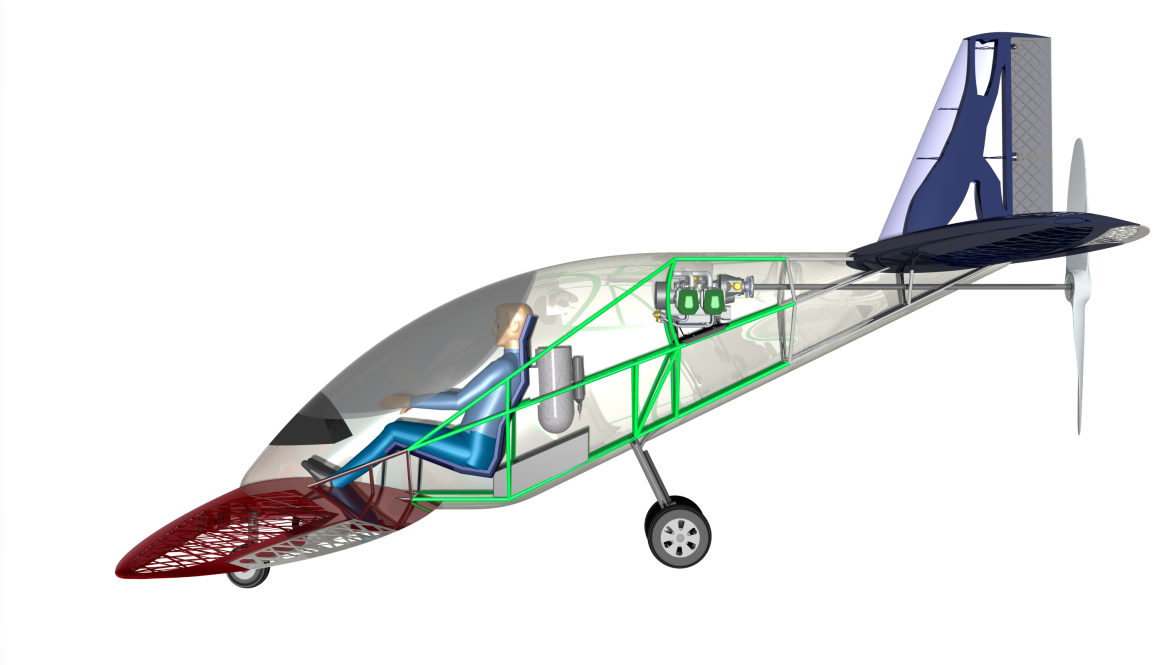

Figure 1.2: Render of the final internal layout

Lastly, the technologies' impact on the aircraft's sustainability aspects, its operational and logistics requirements, including a production plan are evaluated and a market analysis is presented. Manufacturing related aspects are discussed in Chapter 6. The evaluation of the final design can be found in Chapter 7, with Chapter 8 presenting recommendations for future work.

Chapter 2

Top-level Concept Selection

This chapter discusses the trade-off process that is implemented for the selection of the final aircraft design. The trade-off methodology is explained together with its results. In addition, some previous concepts are briefly described and the details behind the final concept are presented.

2.1 Concept Development & Trade-off Process

The concept development and selection stage has been split up in three general phases as is depicted in Figure 2.1. Phase 0 comprised of an extensive literature study. One sub-team performed specific research into the application of metal AM products, while the second sub-team investigated structural components made of plastics. After having obtained specific AM knowledge the team was redivided into three groups. This second division preluded phase I of the concept development and selection. The mission Functional Flow Diagram (FFD) as seen in Appendix B shows the functions that will be performed to achieve a successful mission. After considering this FFD, three sub-teams went into phase I of the design. One team focused on conventional configuration concept development, the second on aerodynamically beneficial concepts and the third team on structurally efficient concepts. These teams generated up to five concepts each. The concepts were assessed on a Class I weight estimation and general layout characteristics after which a first trade-off was conducted. It should be noted that this was an intra-team trade-off. Many of the first stage concepts could be disregarded quite easily through basic reasoning and feasibility calculations would be a waste of resources. In phase II the teams worked out the chosen concept of each of the three groups in more detail. In the development stage of these concepts were developed in more detail and a Class II weight estimation was conducted, after which the concepts were traded-off. The second selection phase was an inter-team trade-off. After one of the three concepts had been selected it continued to the detailed design phase. The total process of the concept development and selection is shown in Figure 2.1, where the three different phases are shown horizontally. It should be noted that the possibility of adaption of superior solutions of other concepts into the final design was also included in phase II. An example of this hybrid design is implementation of superior wings of one concept into another to ultimately come up with a better final design.

For the trade-off itself the Analytical Hierarchy Process (AHP) was used. Graphical comparison was used to verify the AHP outcome. AHP is a mathematics and psychology based process that is used for multi-criteria decision making. It proves particularly valuable in group decision making [1].

Concerning the phase II trade-off it was decided to structure the trade-off criteria in correspondence with the classes of requirements which were determined in the Baseline Report [2]. The main criteria are related to *Performance, Manufacturing, Structural Layout, Scheduling, Regulations, Sustainability*

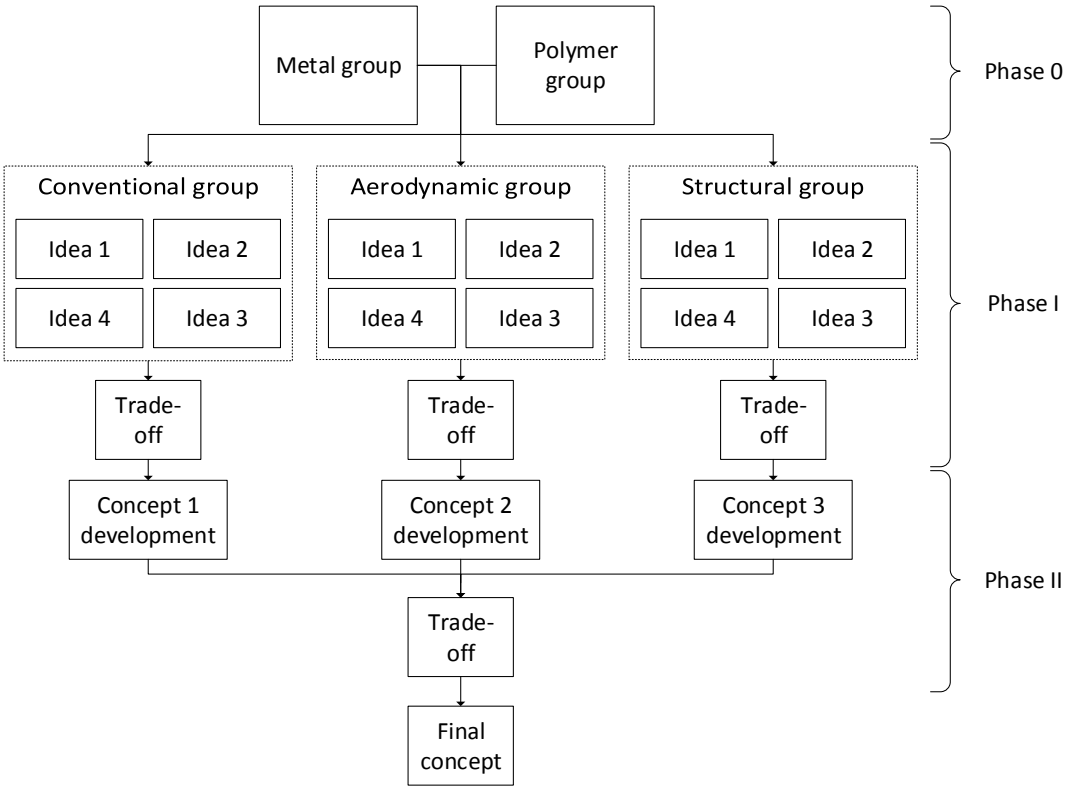

Figure 2.1: Concept development and selection process overview

and Others. Compliance with the operational requirements is a "killer-requirement" and determines whether a design can progress into the final selection or if it is excluded from the process. The criteria are evaluated on the following aspects:

- **Performance:** The main performance parameter is chosen to be L/D. As a second criterion the stability behavior is assessed due to the risk associated with this criterion in unconventional aircraft configurations.
- **Manufacturing:** Two parameters are defined to assess the performance of the design options in terms of manufacturing. The first is the extent to which a concept benefits from the AM technologies. The second is to what extent the projects focus can stay on AM when developing a final design.
- **Structural layout:** Two parameters were selected to judge this criterion. These are the Operational Empty Weight and Part Integrity. Assessment of the first one is trivial, however judgement of the second is not. Part Integrity is based on the scalability of parts and thus on the amount of joints required and the ability to join separate structures.
- **Scheduling:** Any project is limited to some extent by the available time. The ability to complete the design in this time frame is what is assessed in this criterion.
- **Regulations:** "Ease of Certification" is used as the trade-off criterion for this category.
- **Sustainability:** For assessment of this criterion the selected criteria are energy consumption, material waste and cost. Together they are a good basis for sustainability evaluation.
- **Others:** The three parameters added in this category comprise of the "level of innovation" in the design solutions, the academic value and aesthetics.

Table 2.1 shows the relative weight of each of the criteria. For the process of getting to these weights, one is referred to the Midterm Report [3].

Table 2.1: Individual weight factors for the overall trade-off

Criteria	Weight [%]
Manufacturing	30.34
Performance	18.22
Structural	18.22
Regulations	9.45
Scheduling	9.45
Sustainability	9.45
Others	4.86

2.2 Final Concept

Prior to the final concept selection, three concepts are worked out in more detail. These concepts are the tandem wing aircraft, the blended wing body and the conventional, glider inspired aircraft, which were subsequently worked out in more detail in phase II of the concept development phase. However, this document focuses on the evaluation of the selected concept, as such the detailed findings of the concept development phase are not shown in this report. The interested reader is referred to the Midterm Report [3] for detailed information on the individual concepts. The distinguishing features of the three concepts are briefly summarized in the following.

The tandem wing aircraft is specifically tailored to the needs of Additive Manufacturing. It limits the loads on joints by distributing the lift over two lifting surfaces. Thereby it allows for greater use of non-metallic parts which in turn is more sustainable, considering energy consumption during production. Furthermore, it fits well in the scope of the project.

The blended wing body draws its advantages from AM technologies by its complexity in shape which can now easily be printed. Therefore, it excels in aerodynamic performance when compared to its competitors. Furthermore, following a class II weight estimation it is expected to be the lightest concept which is a result of the lift distribution which is largely concentrated in the central wing section. However, the complexity in design of a blended wing body will drive the focus of the project away from Additive Manufacturing and further introduce a scheduling risk.

The most conventional design is the elliptical, glider inspired concept. The maturity of this design allows for comparably easy certification procedures while keeping the focus on AM technologies. However, due to its very large wingspan it suffers a weight disadvantage over the other concepts which results from the limited build volume in Additive Manufacturing, requiring multiple highly loaded joints.

Conducting the trade-off of the three concepts, using the methodology described in Section 2.1, the tandem aircraft appears to be the most feasible contender for the purpose of this project. The complete trade-off matrix is shown in Table 2.2.

The chosen tandem wing concept features two elliptical wings to enhance aerodynamic performance, as seen in Figure 2.2. Opposed to the low mounted front wing, the aft wing is in a high wing configuration to escape the wake of the front wing, thereby increasing the aerodynamic efficiency and stability of the aircraft. The vertical stabilizer is connected to the aft wing while the engine and the propeller are positioned in a pusher configuration. The latter configuration is chosen to increase pilot visibility and reduce the frontal area of the fuselage structure. The fixed landing gear is a tricycle installation

Table 2.2: Trade-off table for the phase II concept selection

	Weight [%]	Elliptical wing (Conventional)	Blended wing (Aerodynamic)	Tandem wing (Structural)
Manufacturing	30.34			
AM benefits	21.23	○	+	○
AM focus	9.10	+	−	+
Performance	18.22			
L/D	14.58	○	+	○
Stability	3.64	+	−	○
Structures	18.22			
OEW	12.75	−	+	○
Assembly	5.47	−	−	+
Regulations	9.45	+	○	○
Sustainability	9.45	−	○	+
Scheduling	9.45	+	−	○
Others	4.85			
Innovation	1.94	−	+	+
Academic value	1.94	○	+	+
Aesthetics	0.97	○	+	+
Final grade		0.0203	0.2575	**0.2887**

with the aft gear carrying the main loads and featuring a small wheel separation. The front gear is integrated in the wing structure while being separated by a larger distance to increase ground stability.

As a first performance analysis and sizing tool, Class I & II weight estimations are iterated. In the class I estimation a wing-loading versus power-loading ($W/S - W/P$) diagram is generated as can be seen in Figure 2.3. In this diagram a design point is decided upon the constraints that make up the red non-design space. These results are subsequently used for the Class II estimations. The results of this analysis provide the starting point for the detailed design phase. Again, detailed background on assumptions and methodology can be found in the Midterm Report [3]. From this diagram it can be concluded that the critical performance requirements are maneuvering and stall. The take-off, landing and climb-rate requirements are therefore not critical in the design. The results from the Class I estimation were fed into a Class II estimation to set the major design parameters and to set a mass budget for each major component. These major design parameters and the mass budget can be found in Tables 2.4(a) and 2.4(b), respectively.

The power budget for the final concept is less elaborate due to the small number of electric systems.

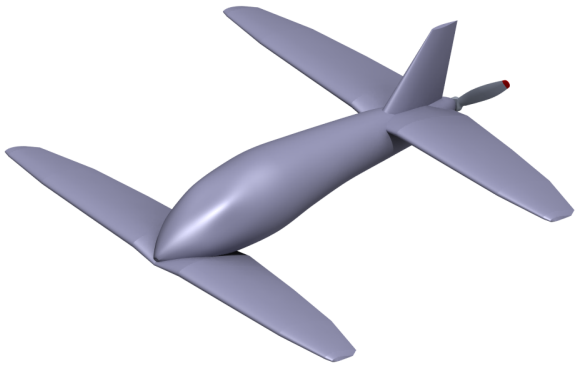

Figure 2.2: Chosen concept resulting from the overall trade-off

The power for loitering was estimated using an L/D ratio of 11, with a propeller efficiency of 65% [4]. The required take-off power is not assumed to be critical due to the long runway that can be used to perform the mission. Furthermore, the estimated power usage of avionics equipment is 50 W, while for communication another 20 W is reserved [5]. The final power budget is listed in Table 2.3.

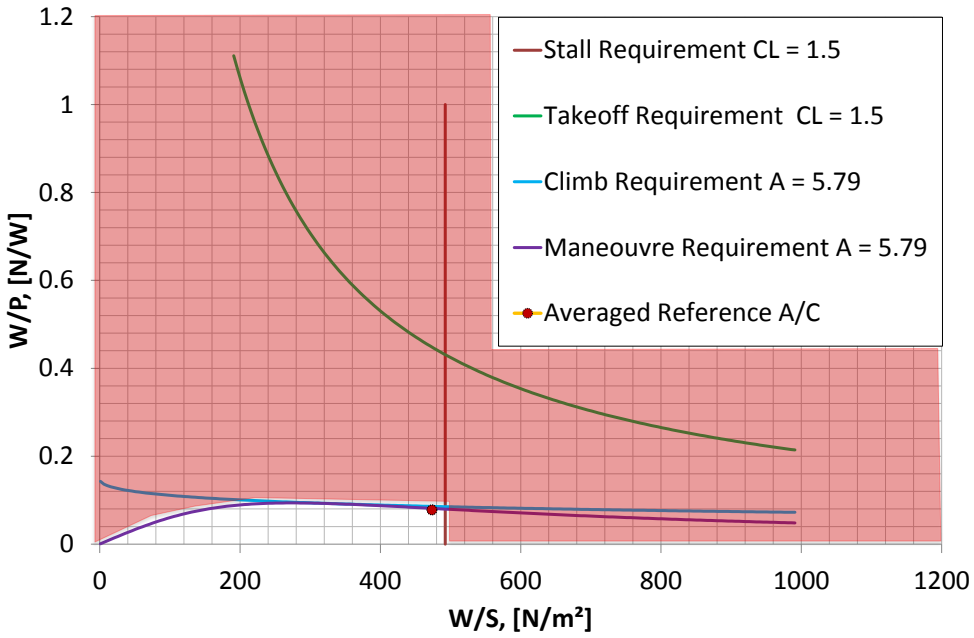

Figure 2.3: Example wing-loading vs. power-loading diagram

Table 2.3: Power budget during loiter

Subsystem	Power $[kW]$
Propulsive power	26.7
Avionics	0.050
Communication	0.020

Table 2.4: Weights and sizes resulting from the Class I & II estimations of the conceptual design phase.

(a) Major design parameters at the end of the first Class II weight estimation for the tandem concept

Parameter	Value	Unit
Maximum take-off weight	445.9	kg
Lifting surface area	8.9	m^2
Aspect ratio	5.5	$-$
Lift to Drag ratio	11	$-$
Wingspan	4.95	m
Fuselage length	4.5	m
Maximum fuselage width	0.8	m
Maximum fuselage height	1.2	m
Maximum fuselage perimeter	2.8	m
Aspect ratio (vertical tailplane)	2	$-$
Surface area (vertical tailplane)	1.64	m^2
Take-off power	54.85	kW
Shock strut length for main gear	0.4	m
Mission fuel weight	44.7	kg

(b) Class II weight estimation of the tandem wing concept

Parameter	Value	Unit
Wing	83.5	kg
Vertical tail	6.1	kg
Fuselage	66.2	kg
Nacelle	9.2	kg
Landing gear	28.6	kg
Fuel system	3.0	kg
Flight control system	7.2	kg
Electronics	17.9	kg
Furnishing	5.4	kg
Engine	64.0	kg
Propeller	10.0	kg
Operative empty	301.2	kg
Fuel	44.7	kg
Payload	100.0	kg
Maximum take-off	445.9	kg

Chapter 3

Design for Aerodynamics, Stability & Control

Designing a tandem aircraft does not come without a thorough stability and controllability analysis. Contrary to traditional aircraft layouts, with a main wing and an empennage, the tandem aircraft has two lifting surfaces on both extremities of the fuselage. In addition both lifting surfaces generate approximately the same amount of lift and the exact distribution needs to be determined for aircraft controllability. To achieve static stability, the neutral point needs to be located behind the CG and different parameters affecting its location are investigated. The requirements for stability and controllability, as well as the overall performance requirements, dictate the airfoil selection and overall aerodynamic design. Finally the propeller selection is also described in this section since it provides one of the main aerodynamic forces.

3.1 Design for Stability

The stability analysis of the aircraft is aimed at positioning the neutral point of the aircraft. The neutral point of the aircraft is the point where the resultant change in aerodynamic forces due to a change in angle of attack is zero. In order to have static stability this point should always be located behind the CG.

The method used to determine the stability of the aircraft is based on the DATCOM method. However, this method allows the user to find the horizontal tail to main wing surface ratio required for a certain neutral point location. Since the tandem aircraft has two equal wing surfaces, plotting the S_h/S ratio as a function of the neutral point location would not yield usable results. Hence a new equation was derived expressing the distance between the front and the back wing aerodynamic centers as a function of the neutral point location. It was then possible to create the first half of the scissor plot shown in Figure 3.1. Equation (3.1) was used to calculate the location of the neutral point.

$$x_{np} = x_{ac_1} + \frac{(1 - \frac{\mathrm{d}\epsilon}{\mathrm{d}\alpha})(\frac{V_2}{V_1})^2}{\frac{C_{L_{\alpha_1}}}{C_{L_{\alpha_2}}} + (1 - \frac{\mathrm{d}\epsilon}{\mathrm{d}\alpha})(\frac{V_2}{V_1})^2} x_w \tag{3.1}$$

The preliminary design set the distance between both aerodynamic centers to be 3.5 m. Knowing this distance, the C_{L_α}'s that allowed the neutral to be behind the CG could be determined. The values found were 4.29 and 5.48 for the front and the back wing respectively and the neutral point is located at 2.04 m from the aircraft's nose. Based on the Class II weight estimation, the CG was located at 1.95 m of the nose. Hence the aircraft is statically stable.

The main difficulty of the stability analysis was to find a suitable variable to put in relation with the location of the neutral point. The S_h/S ratio used it in the DATCOM method was not well suited to the tandem aircraft. Thus, rethinking the equation in a way to could yield appropriate results was the main challenge. Fortunately, using the distance between both aerodynamic centers enable an effective determination of the neutral point with respect to an important parameter of the aircraft. The remaining task was then to derive the correct relation between the distance between both aerodynamic centers and the position of the neutral point with respect to the nose.

3.2 Design for Controllability

The procedure to determine the controllability of the aircraft is also the DATCOM method. It consists creating the second half of the scissor plot in order to obtain a CG range in which the aircraft is both stable and controllable. The main parameters that influence the controllability of the aircraft are the C_L and the entire aircraft's C_{m_α}.

Equation (3.2) was derived to compute the distance between the wing's aerodynamic centers as a function of the location of the neutral point. Using this equation it was possible to create the second half of the scissor plot shown in Figure 3.1. Following the creation of the scissor plot, it was possible to determine the lift distribution between the two wings. The front wing needs to generate 55% of the lift, while the aft wing should account for 45% of the overall lift. For the aircraft to have such a lift distribution, the front wing should have an incidence angle of 4.08°, while the aft one should have an incidence angle of −1.53°.

$$x_{wing} = \left(\frac{C_{L_{1_{cruise}}}}{C_{L_{2_{cruise}}} (\frac{V_2}{V_1})^2} + 1 \right) (x_{np} - x_{ac_1}) + \frac{C_{m_{ac_1}} + C_{m_{ac_2}} (\frac{V_2}{V_1})^2}{C_{L_{2_{cruise}}} (\frac{V_2}{V_1})^2} \tag{3.2}$$

The same DATCOM method is used for the controllability as to determine the stability range of the aircraft. Therefore, the same limitations in the method are present.

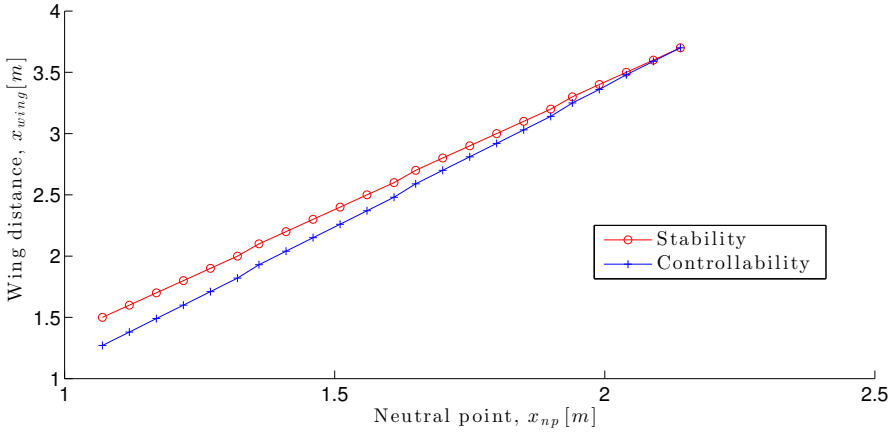

Figure 3.1: Scissor plot of the tandem airplane

3.2.1 Control Surfaces

The elevator is probably the most important control surface since it enables the pilot to pitch up the aircraft, allowing it to rotate for take-off and to keep it trimmed during the flight. It was decided to place the elevators are located on the back wing. The aft placement of the elevators is a consequence of the position of the wings with respect to the CG. The lift acting on the back wing creates a nose down pitching moment about the CG. Hence, locating the elevator on the back wing deceases its lift

and increases its drag: these two factors facilitate the upwards pitching maneuver at take-off. In the design of the elevator a method developed by Sadraey [6] was employed. The final dimension of the elevator are given in Table 3.1.

Table 3.1: Control surface parameters

Control surface	Wing span ratio [−]	Chord length ratio [−]	Minimum and Maximum deflection [°]
Elevator	$0.48b$	$0.23c$	± 25
Aileron	$0.48b$	$0.23c$	± 5

In Table 3.1 the values b and c refer to the span length and chord length of one wing.

The purpose of the ailerons is to provide roll control to the aircraft. The ailerons are located on the front wing of the aircraft since the elevators are located on the aft wing. Due to the unconventional design of the aircraft, the ailerons are located in a more forward location with respect to the aircraft's CG than for conventional aircraft. This results in an adverse yawing motion: as the aircraft rolls, the lower wing is subject to a higher relative angle of attack resulting in a higher lift and drag. Subsequently, the lower wing will create an overall yawing moment. Hence, roll control of this tandem aircraft can only be achieved by correcting the yawing moment with the rudder. Furthermore, the distance of the ailerons from the CG will also create a pitching moment that will need to be compensated with the elevators. The ailerons were also designed using the method proposed by Sadraey [6]. Finally the aileron parameters are listed in Table 3.1. As it can be seen in Table 3.1, the elevators and the ailerons have the same design parameters. This is a big advantage with respect to manufacturing. On the other hand, the deflection of the ailerons needs to be limited to 5 degrees to limit the roll velocity of the aircraft. The way it is designed now, the time the aircraft takes to achieve a 30° bank angle is 1.6 s. The actuation system takes this small aileron deflection into account and a more detailed explanation is given in Section 3.2.2.

Finally the vertical stabilizer and rudder are sized. These are sized at the same time as their contribution to the aircraft stability and controllability is of the same nature; the rudder's purpose is to increase the effect of the vertical tail. The first step in designing a vertical stabilizer is to determine the required surface area. Subsequently the basic area dimensions such as the aspect ratio, taper ratio and the sweep angle.

The primary task of the vertical tail is to keep the aircraft from sideslipping by creating a counter yawing moment. A sideslip angle can be induced by discrepancies in the tangential force of the wings by for instance gusts. Also when in sideslipping flight, one wing will produce a different tangential force than the other by for instance wing-fuselage interaction. These forces cause the moments that have to be countered by the vertical tail. Equation (3.3) shows the relation that can be derived for the vertical tail area. The coefficient c_{VT} in this equation can be determined from reference aircraft. For homebuild aircraft a value of 0.04 is found [7]. This leads to a vertical stabilizer surface area of $0.79\,m^2$.

$$S_{VT} = c_{VT} \frac{b_{wing} S_{wing}}{L_{VT}} \tag{3.3}$$

After having determined the surface area, the entire vertical tail layout can be fixed by determining the aspect ratio, taper ratio and sweep angle. These values are not critical for the general performance and stability of the aircraft. An extensive analysis would be required to make a sound decision. For this stage in the designing it is advised to choose values in between 0.3 and 0.6 for the taper ratio

and in between 1.3 and 2.0 for the aspect ratio [7], therefore averaged values of 1.6 for the aspect ratio and 0.5 for the taper ratio are chosen. This leads to a b_{VT} of $1.1\,m$. Finally the sweep angle is chosen such that the trailing edge is unswept. This will allow for placing the whole vertical tail as far backward as possible without interfering with the propeller.

Now that the basic layout of the vertical tail is determined, the rudder can be sized. From reference aircraft it is found that the rudder surface area is usually around 30% of the vertical tail area [6]. To keep the control system as simple and lightweight as possible, an unswept hinge-line is desirable. This results in the final layout shown in Figure 3.2. This type of tail does appear more often in LSA which provides confidence in the design [8].

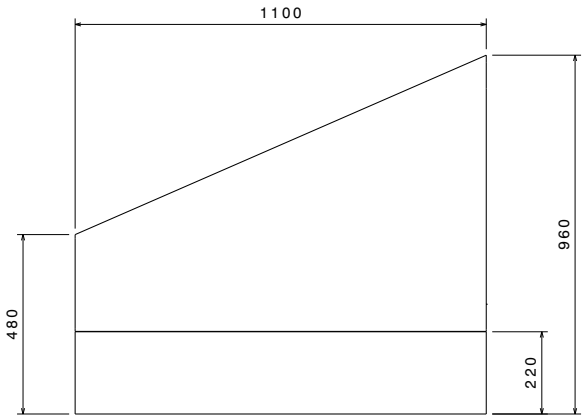

Figure 3.2: Basic dimensions and layout of the vertical stabilizer in $[mm]$

3.2.2 Control Actuation System

The control actuation system of the tandem aircraft will consist of a stick that commands both pitch and roll (elevators and ailerons respectively) and pedals that control yaw (the rudder). The actuation system consists of wire rope cables connected to the stick or the pedals on one extremity and to the control surfaces on the other side. They are directed to the control surface by means of pulleys. Since the control surface need to be moved in two directions (upward and downward) two cables per control surface are required. Hence a total of ten cables (two for each elevator and aileron and two for the rudder) are necessary to control the aircraft at all time. The layout of the cables is a result of the motion the control surface need to have. These different motions are the following:

- The elevators, located on the back wing, need to be moved in the same direction (upwards or downwards) when they are used. Hence, pulling the control stick towards the pilot should result in a upward deflection of both elevators, pitching the aircraft upwards. Pushing the stick away from the pilot should deflect the elevators downwards and pitch the aircraft downwards.
- The ailerons, located on the front wing need to be deflected in opposite directions when a rolling maneuver is initiated. Moving the stick to the right should roll the aircraft to the right: the left aileron is deflected downwards and the right aileron is deflected downwards. Moving the stick to left will yield a left roll and the ailerons will be deflected the opposite way. It should be noted here that activating the ailerons will create an adverse yaw motion due to the increase in drag on the wing deflected downwards. Hence the pilot should also use the rudder if he wishes to do a pure rolling motion.
- The rudder is controlled with two pedals. When pushing the left pedal a left yaw motion should be initialed and vice versa.

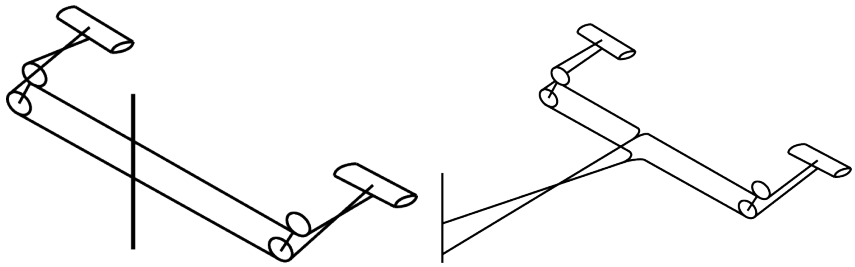

(a) Aileron layout

(b) Elevator layout

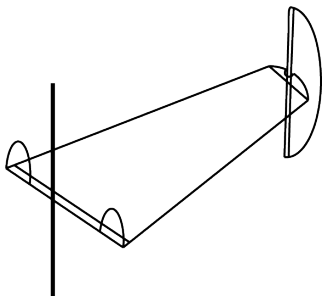

(c) Rudder layout

Figure 3.3: Control actuation system layout

A graphical layout of the control surfaces can be seen in Figure 3.3. The mass budget allocated to the flight controls from the Class II weight estimation is 7.2 kg, as listed in Table 2.4. One requirement AMA-Tech.-Manu.-3 states that the maximum weight of the actuation system should never be higher than 10% of the MTOW. Given the MTOW of the tandem aircraft, this requirement is fulfilled and has a large safety margin if the weight of the cables is higher than expected.

Finally, the control stick should not be to sensitive to a pilot's input. This is especially true for the aileron actuation: the maximum aileron deflection is 5°. Hence, a damping system should be embedded in the aircraft's control stick, at least for right and left deflections.

3.3 Airfoil Selection

From the final concept, as outlined in Section 2.2, the overall aerodynamic shape has been determined and in Section 3.2 the vertical tail has been sized. The airfoils for these aerodynamic surfaces still have to be selected. For both wings distinct airfoils have been selected for stability reasons while the vertical tail also requires an individual airfoil. The selection and trade-off procedure for these airfoils is discussed in this section. It should be noted that all aerodynamic computations are based on the Reynolds Number at loitering conditions, which is found to be $Re = 2,952,912$.

3.3.1 Wings

From literature on the design process in the LSA category, it is found that the airfoil selection for such aircraft is less critical [7, 9], therefore the airfoil selection process for such aircraft is not very detailed. This is mostly due to the fact that existing airfoils which are widely used in the category (such as the NACA 2412), are quite good and for most homebuilt aircraft one therefore does not look further. However, during an investigation into the stability of tandem aircraft it is found that the $C_{L\alpha}$ of the wings is important for the stability, justifying a more extensive airfoil selection process. The result of that investigation shows that the $C_{L\alpha}$ for the front wing should be as low as possible, while the $C_{L\alpha}$ for the back wing should be as large as possible (see Section 3.2). Thus, two different trade-offs are

to be performed for the front and back wing, but the same pool of airfoils is used in that trade-off.

The airfoils are selected on the basis of, amongst others, their performance at the design conditions and at maximum C_l condition. In the course *AE2101 Aerospace Design and Systems Engineering Elements II* [10], it is recommended to set the airfoil design lift coefficient 10% higher than the aircraft C_L at the design point - in this case halfway through the loitering phase. From the investigation into the controllability (see Section 3.2), it was pointed out that the front wing should account for 55 % and the back wing 45 % of the total lift. However, the airfoil selection is still based on 50 % lift for both wings, since it allows for a faster selection process and the 5 % difference is insignificant. Thus, the airfoils are selected for a C_l of 0.4962. Still, the performance is checked for the 55 % and 45 % lift contribution throughout the whole loitering phase, that is, at minimum and maximum weight.

In Reference [10] also a correction factor between $C_{L_{max}}$ and $C_{l_{max}}$ is given. For unswept wings at a Mach number lower than 0.2, this boils down to $C_{L_{max}} = 0.9\,C_{l_{max}}$. Therefore, the $C_{l_{max}}$ of the airfoil should be higher than 1.66 to meet Req. AMA-Con.-FAA-1-2 which requires, for this aircraft, a $C_{L_{max}}$ of 1.5.

From literature [9, 11, 12], a large pool of 35 airfoils is selected. These include, amongst others, NACA-24 series, NACA-44 series (as suggested by [9]), NACA-65 series, the Clark Y (commonly used in small homebuilts), Selig airfoils and the NACA-22 series (used on the Supermarine Spitfire [12]). All these airfoils are analysed extensively using `XFOIL` [13] after which a preliminary selection was made. Airfoils which have a $C_{l_{max}}$ lower than 1.66 are directly omitted. For several NACA series, only the best airfoil of that series is selected (for example, for the 24 series, the 2412 was selected). Then, airfoils with clearly too high drag values and no clear benefit on other criteria are removed from the pool. Eventually, five airfoils progressed to the final trade-off. These airfoils are shown in Figure 3.4: the NASA/Langley/Whitcomb LS1-0417 (hereafter referred to as simply GAW-1), the NACA 65415, NACA 37015, NACA 2412 and NACA 2211. The NACA 37015 and NACA 2412 are recommended by Husa in [9]. The NACA 2211 is interesting because it is used on the Supermarine Spitfire, which is relevant to the current aircraft because it also features an elliptical planform.

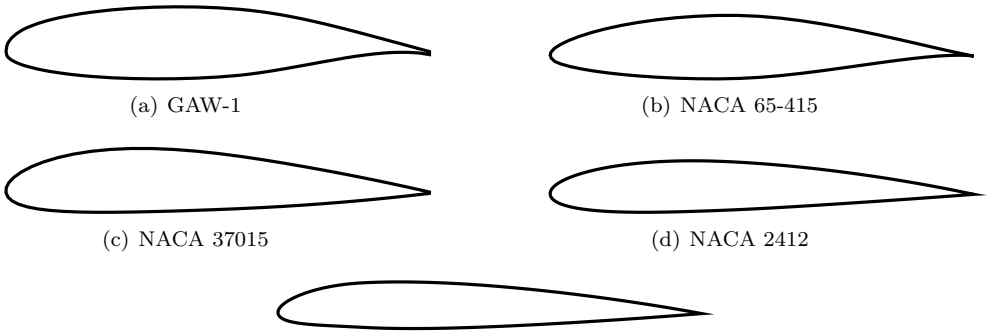

(a) GAW-1 (b) NACA 65-415

(c) NACA 37015 (d) NACA 2412

(e) NACA 2211

Figure 3.4: Airfoils used in trade-off

For the front wing six different criteria are used for the trade-off, while for the back wing one additional criterion is used. These are explained below in order of importance. The first four are based on measurable, quantitative parameters while the last three are determined qualitatively.

Lift rate coefficient, C_{l_α}

Considering stability can be problematic for tandem aircraft, and the C_{L_α} of the wings is important, this criterion is given the highest weight. For the front wing the airfoil with the lowest C_{l_α} is given the highest weight, while for the back wing the airfoil with the highest C_{l_α} is given

the highest weight. In general, a score of -1 is awarded for the weakest performance and a score of $+1$ indicates the strongest performance. Scores in between the two extrema are interpolated.

Moment coefficient around 0.25c at the design conditions, $C_{m_{0.25c}}$

For controllability, it is important to have the aerodynamic moment coefficient as close to zero as possible. Considering all selected airfoils feature a negative $C_{m_{0.25c}}$, the airfoil with the least negative $C_{m_{0.25c}}$ scores best as this is most beneficial to unite stability and controllability. This criterion is given a high weight, since for the chosen tandem concept, design for stability and control is especially important. Note that it is assumed that the aerodynamic center is located at the quarter chord point on the airfoil.

Drag coefficient at design conditions, C_d

The drag coefficient of the airfoil is very important for the overall L/D of the aircraft, justifying its high weight in the trade-off process.

Maximum lift coefficient, $C_{l_{max}}$

The maximum lift coefficient is important, but considering that in the preliminary selection already all airfoils are omitted which have a too low $C_{l_{max}}$, this criterion is somewhat less important. For the back wing however, it becomes more important, as the back wing should, for stability reasons, stall at a higher angle of attack than the front wing.

Stall characteristics

The aircraft should also have good stall characteristics. That is, the aircraft should not suddenly lose all its lift when the aircraft goes slightly over its maximum angle of attack. Sharp stall behavior is given a score of -1, while smooth stall is given a score of 1. The score for this criterion is determined qualitatively by looking at the $C_l - \alpha$ curve as shown in Figure 3.5(a).

Minimum Drag Zone (MDZ)

It is beneficial if an airfoil has an extended zone in which it has minimum drag - the laminar bucket. This also aids in the climb performance of the aircraft [9]. Again, this score is determined qualitatively from the $C_l - C_d$ curve as depicted in Figure 3.5(b).

Elevator effectiveness

For the back wing airfoil, the camber at the end of the airfoil is important for the effectiveness of the elevator. The elevator section may have to produce downforce, thus having a highly cambered airfoil reduces the amount of downforce the elevator section can generate. This is not a showstopper, but it should be included in the trade-off. The score for this criterion is determine qualitatively from the airfoil cross-sections illustrated in Figure 3.4. Of course, this criterion is only used for the back wing.

In order to determine proper weights for the different criteria, again the AHP process is used. This method is further explained in Section 2.1. The resulting weights can be found in Tables 3.2(a) and 3.2(b).

The final trade-off for both wings can be found in Tables 3.2(a) and 3.2(b) for the front and back wing, respectively. Thus, the NACA 2412 is chosen for the front wing, while the back wing features the GAW-1 airfoil.

Concluding, five airfoils were selected from a larger pool of 35 airfoils. These five airfoils continued to a separate trade-off for the front and the back wing, respectively. The most distinct difference between the two is that for the front wing a low C_{l_α} is better, while for the back wing airfoils with a high C_{l_α} have a clear advantage. Eventually, the NACA 2412 is selected for the front wing, while the

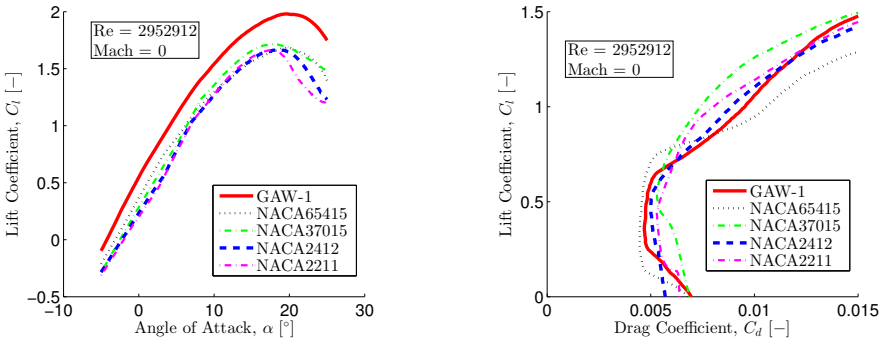

(a) C_l - α (b) C_l - C_d (Focused on design area)

Figure 3.5: Polars for airfoils used in trade-off

	C_d @ des.	$C_{m_{0.25c}}$ @ des.	C_{l_α}	$C_{l_{max}}$	Stall Charac.	MDZ	Score
Weight	0.203	0.203	0.340	0.117	0.069	0.069	
GAW-1	0.44	-1.00	-1.00	1.00	-1.00	1.00	-0.34
NACA 65415	1.00	-0.30	-0.09	-0.87	-1.00	1.00	0.01
NACA 37015	-0.79	0.58	0.23	-0.66	1.00	1.00	0.09
NACA 2412	-0.05	0.63	0.95	-0.97	0.00	0.00	**0.33**
NACA 2211	-1.00	1.00	1.00	-1.00	0.00	0.00	0.22

(a) Front wing

	C_d @ des.	$C_{m_{0.25c}}$ @ des.	C_{l_α}	$C_{l_{max}}$	Stall Charac.	MDZ	Elevator	Score
Weight	0.176	0.176	0.294	0.176	0.066	0.066	0.047	
GAW-1	0.44	-1.00	1.00	1.00	-1.00	1.00	-1.00	**0.33**
NACA 65415	1.00	-0.30	0.09	-0.87	-1.00	1.00	-1.00	-0.05
NACA 37015	-0.79	0.58	-0.23	-0.66	1.00	1.00	0.00	-0.09
NACA 2412	-0.05	0.63	-0.95	-0.97	0.00	0.00	1.00	-0.30
NACA 2211	-1.00	1.00	-1.00	-1.00	0.00	0.00	1.00	-0.42

(b) Back wing

Table 3.2: Trade-off tables for the airfoil selection

GAW-1 proves to be most suitable for the back wing. The NACA 2412 is one of the most widely used airfoils in the LSA category due to its good overall performance. The GAW-1 airfoil's main advantages include low drag at the design condition, but a high $C_{l_{max}}$ allowing the rear wing to stall later than the front wing, with the only large disadvantage its highly negative moment coefficient (almost three times larger than the value for the NACA 2412).

3.3.2 Vertical Tail

According to Raymer [7], the airfoil for the vertical tail is not critical for small aircraft, most of them simply use the NACA 0009 and the NACA 0012. The NACA 64A015 airfoil is also commonly used [6]. Thus, the airfoil selection was limited to the NACA 00 series (9% to 12%) and the NACA 64A015. The final airfoil was selected on the basis of three criteria: drag at $\alpha = 0$, thickness of the airfoil and the lift rate coefficient C_{L_α}. The second criterion stems from the fact that with a thicker airfoil the moment of inertia at the root is higher, thereby reducing the overall weight. C_{L_α} is important for the weathervane stability (C_{n_β}), which mostly determines the effectiveness of the vertical tail.

These airfoils were analysed using `XFOIL` to quantify the first and third criterion, the results of which are shown in Figure 3.6. As seen, the lift rate coefficients of the five airfoils are too close to make a selection on the basis of that criterion alone. Larger differences occur in the drag values, which for NACA 64A015 are quite low and also extended over multiple angle of attack due to a Minimum

Drag Zone. Moreover, it is a 15% thick airfoil which therefore gives significant structural benefits. Therefore, the NACA 64A015 airfoil is used for the vertical tail.

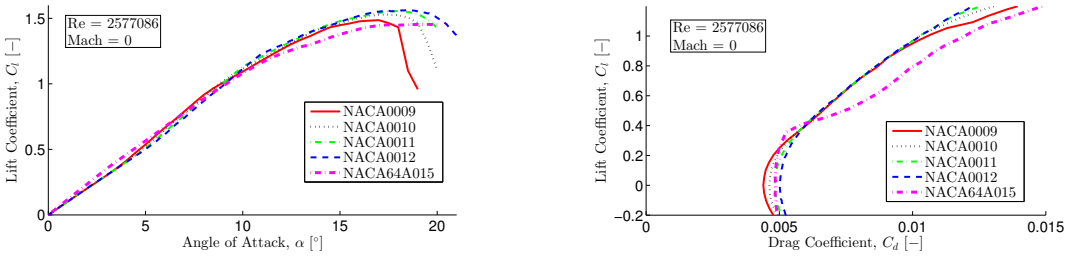

(a) C_l - α (b) C_l - C_d

Figure 3.6: Lift and drag polars for vertical tail airfoil selection

3.4 Overall Aerodynamic Design

The overall aerodynamic layout of the tandem aircraft was already mostly fixed in the conceptual design phase, as explained in Section 2.2. The two elliptical wings have the same wing area (4.45 m^2) with a span of 5 m. The front wing is positioned in a low-wing configuration, while the back wing is located at the very end of the fuselage in a high-wing configuration. This overall layout is chosen to reduce the downwash of the front wing on the back wing, and conversely the upwash of the back wing on the front wing. This not only increases the overall aerodynamic efficiency, but also significantly benefits the stability of the aircraft, as explained in Section 3.1. The NACA 2412 airfoil is used on the front wing and the GAW-1 airfoil is used for the back wing. The wings have different incidence angles with respect to the fuselage since during cruise, 55% of the lift should be generated by the front wing with the back wing accounting for the remaining part. This is decided to maximize the efficiency during cruise by minimizing the deployment of the elevator, as explained in Section 3.2.

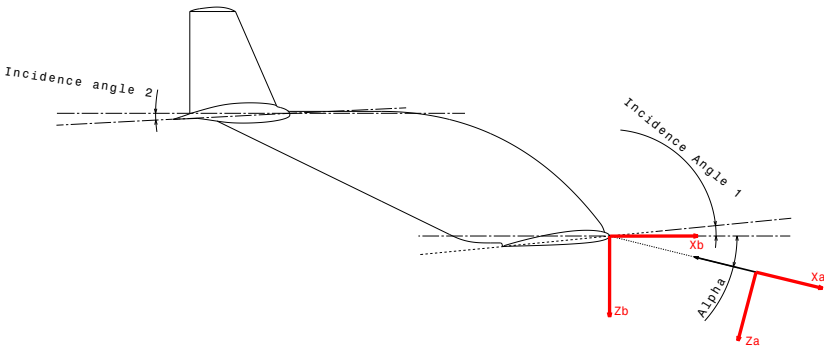

Figure 3.7: Definition of aerodynamic angles

An initial estimation for the incidence angles has been made in the controllability design (Section 3.2). The angle of attack and incidence angle definition can be found in Figure 3.7. These are defined such that at zero angle of attack of the aircraft the vertical distance between the front and back wing is maximum as seen from the aerodynamic reference frame. At this angle of attack the downwash should therefore be minimal, which is the reason the aircraft is designed to fly at zero degree angle of attack during loitering. However, a first CFD analysis showed that at zero angle of attack of the aircraft, it only produced half the lift it was supposed to during loiter. Subsequently, a simple 3D `XFLR5` [14] analysis was performed to find the incidence angles at which the aircraft should produce enough lift for $\alpha = 0°$. This analysis was performed for the front and back wing separately

as well as combined together in a tandem configuration, the results of which are shown in Figure 3.8. It is decided to omit the fuselage in this computation as the XFLR5 program is known to output bad results when the fuselage is added [15]. The fuselage is however taken into account in the final CFD computations.

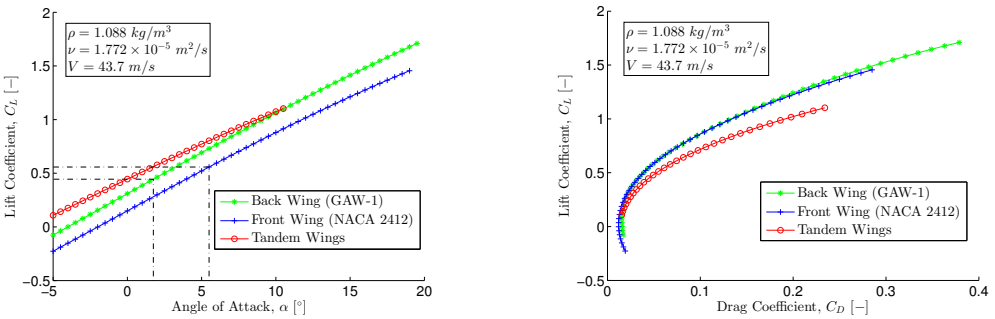

(a) C_L - α (b) C_L - C_D

Figure 3.8: Lift and drag polars for the front and back wing separately and combined

From Figure 3.8(a) the required incidence angles for the wings are determined to let the front wing account for 55% of the required lift with the back wing accounting for the rest. These angles are determined to be 5.50° for the front wing and 1.75° for the aft wing and are also indicated in Figure 3.8(a). However, examining Figure 3.8(a) in more detail shows that there might be a problem in stability. The design for stability relies significantly on the difference in C_{L_α} between the front and rear wing, while the results from XFLR5 do not show a significant difference between the two, as listed in Table 3.3. Using the C_{L_α} from the XFLR5 results, the stability analysis from Section 3.1 indicates that the aircraft is not stable anymore. The DATCOM method is a tested procedure used extensively in industry, therefore confidence in these results is not misplaced. However, the XFLR5 results cannot be ignored and therefore, a more in-depth investigation using CFD and preferably wind tunnel tests have to be conducted.

Table 3.3: Comparison between DATCOM results and XFLR5 results

	Units	DATCOM Results	XFLR5 Results
Front wing incidence angle, i_{w_1}	[°]	4.08	5.50
Front wing lift Rate coefficient, $C_{L_{\alpha_1}}$	[1/°]	4.29	3.94
Back wing incidence angle, i_{w_2}	[°]	-1.53	1.75
Back wing lift Rate coefficient, $C_{L_{\alpha_2}}$	[1/°]	5.49	4.43

In the stability analysis it has been identified that the blanketing of the rear wing is a risk for the current configuration. This phenomenon occurs when the front wing stalls and the full aft wing is covered by the wake of the front wing. Therefore, the front wing does not produce lift any more, while the lift on the back wing also reduces significantly because it has to work in highly turbulent, separated flow. Consequently, the aircraft rapidly loses altitude while it is hard to recover from it, since both wings are ineffective. This phenomenon only occurs if the aft wing is positioned in the wake of the front wing at high angles of attack. According to Sadraey [6] this is a large risk for the configuration determined in the conceptual design, which has to be mitigated in the detailed design phase. There are basically two ways to mitigate this risk: One is to change the overall configuration, and the other is to tweak the design of the front wing preventing a full stall of that wing. The first option would mean that the aft wing has to move significantly downward. This downward shift is approximately 55 cm (estimated from Sadraey [6]), which would increase the downwash $d\varepsilon/d\alpha$ by

as much as 73%. From the stability analysis it follows that the neutral point would shift forward an unacceptable 20 *cm*. The wing could also move upward, but that requires an upward shift of at least 40 *cm* which would add significant weight. Therefore, the second option has been chosen for the aircraft.

Most mitigation strategies for the blanketing effect mostly focus on warning the pilot of an imminent stall in order to correct for it. The most simple systems include stick shakers or a warning system which gives an audible warning when a certain angle of attack is reached. Other systems focus on letting the inboard part of the front wing stall first to give both a warning to the pilot and reduce the lift on the front to let the aircraft pitch nose down again. Roskam [8] recommends two ways to achieve this, either through a forward swept wing or through applying twist to have the tip at a lower angle of attack ("washout") . The first option would require significant changes to the design as forward swept wings introduce larger torsion at the root. The second option could be a better alternative as AM allows for incorporating a complex twist distribution in the wing easily. However, the same effect can be achieved with a large stall strip on the leading edge of the inboard wing. This is a triangular aerodynamic device which ensures that the inboard section stalls first. This then warns the pilot since the separated flow will hit the rear wing which will introduce large vibrations into the aircraft. Also, the overall lift on the front wing is reduced which induces a correcting pitch down moment. The stall strip on the aircraft will cover 10% of the total span, that is, 25 *cm* on each wing-half. As an extra safety measure also vortex generators will be applied to the outboard tip sections to further ensure that these sections stall at a higher angle of attack. Since also the back wing has a significantly higher $C_{L_{max}}$, one can be confident that the stability at high angles of attacks is ensured.

Thus, the correct incidence angles for a controllable aircraft have been determined, while also some mitigation strategies for the risk of blanketing have been decided on. This leads the way for fully evaluating the final aerodynamic design in Section 7.2.

3.5 Propeller Design

The propeller has a few criteria it has to fulfill. Firstly, during loiter the propeller should be as efficient as possible. Secondly, the propeller has to be able to function at the power specified in the Phase II of the conceptual design. The limiting factor at a higher RPM could be the tip speed, which cannot approach Mach 1 without severe consequences for the drag and efficiency. Weight, which in turn affects the CG, should also be taken in account. To find the best propeller several of them are traded off using the following criteria:

- The efficiency of the propeller during loiter.
- The efficiency of the propeller at maximum power.
- The estimated weight of the propeller.

To design the propeller an applet called `JavaProp` was used [16]. `JavaProp` uses inputs and constraints like the diameter, flight speed, RPM, power, angle of attack and airfoil to create a propeller that is as efficient as possible for the given constraints. After a design is chosen one has to check whether the propeller can be used at the maximum amount of power. To do so `JavaProp` provides a table that relates the power and RPM combination to the efficiency, stall and thrust. Afterwards, a trade-off is conducted for the propellers. By the requirements the propeller can only be a fixed pitch propeller, therefore any other type of propellers were not considered.

Table 3.4: The input in the JavaProp applet for the selected propellers

Propeller parameter	Unit	Propeller 1	Propeller 2	Propeller 3
Number of blades, n_b	$[-]$	3	3	2
Diameter, d	$[m]$	1.5	1.6	1.6
Revolutions per minute, RPM	$[1/m]$	1000	990	1000
Spinner diameter, d_s	$[m]$	0.20	0.20	0.20
Flight velocity, V	$[m/s]$	43.7	43.7	43.7
Power, P	$[W]$	22000	21500	22000
Airfoil	$[-]$	Clark Y	Clark Y	Clark Y
Angle of attack, α	$[^\circ]$	4.0	4.0	5.0

The variable inputs for the design of the propeller are the propeller diameter, the number of blades, the airfoil used and the angle of attack of the propeller. The constraints are the flight velocity, the diameter and the RPM which is linked to the power. The inputs are shown in Table 3.4. The power and RPM of the engine are found in the engine's data sheet [17].

An increase of the propeller diameter increases the efficiency but increases the size and weight of the propeller. The size of the propeller is however restricted by the clearance angle and thereby the position of the landing gear. Increasing the number of blades increases the efficiency but also increases the weight of the propeller. The airfoil used influences the efficiency and the stall speed of the propeller, however very few airfoils are available to test in JavaProp. Lastly, the angle of attack has a major effect on the efficiency but also decreases the maximum stall speed of the airfoil. The propeller is designed with a Reynolds number of $100,000$.

The propeller diameter was set to a maximum diameter of 1.6 m since this is the maximum diameter possible, in order to maximize efficiency. The angle of attack is maximized to the stall limit to further increase the efficiency. Therefore, in the trade-off a baseline propeller is defined to be a propeller with a 1.6 m diameter. This baseline propeller is compared with a smaller diameter propeller and a two blade propeller.

The output of the JavaProp calculation is shown in Table 3.5, the thrust in this table has to be higher than the drag during loiter which is calculated to be 398 N using an L/D of 11 and the weight of the aircraft during loitering. Based on this constraint the power and RPM are determined at which the aircraft flies during loiter. Finally, checks are done whether the propeller can function at the power requirement found in the Class I estimation and if it can provide enough thrust for the aircraft to take-off. Assuming a one kilometer take-off distance and a take-off L/D of 10 the required take-off thrust is found to be 609 N.

Table 3.5: Output of the JavaProp applet for the selected propeller

Propeller parameter	Unit	Propeller 1	Propeller 2	Propeller 3
Cruise thrust, T_{cruise}	$[N]$	400.54	398.68	403.53
Maximum thrust, T_{max}	$[N]$	1151.6	1195.7	1103.6
The twist at $\frac{3}{4} \times R$, $\varepsilon_{t_{0.75R}}$	$[^\circ]$	45.8	42.5	43.8

Table 3.6: Associated propeller data as used in the trade-off

Criteria	Unit	Propeller 1	Propeller 2	Propeller 3
Propeller efficiency during loiter, η_{loiter}	$[-]$	80.313	82.568	80.95
Propeller efficiency at maximum power, η_{max}	$[-]$	54.98	56.458	55.63
Weight estimation	$[-]$	0	-	+

In Table 3.6 the important values for each propeller as used in the trade-off are shown. The greater the efficiency the better, however, since the aircraft spends most of its time in loiter, the loiter efficiency is much more important than the efficiency at maximum power. The weight estimation was, however, purely qualitatively. Considering the efficiency Propeller 2 is the best propeller out of the three, however the weight is also considered. Adding weight influences the stability negatively through a shift in the CG and has a negative influence on the overall performance of the aircraft. The weight that is saved by only using two blades is deemed significant enough to offset the small loss in propeller efficiency. Therefore, Propeller 3 was chosen as the final design.

For the propeller most likely metal has to be used. In that case,different types of Additive Manufacturing can be used. If current production facilities should be used to create the blade, Direct Energy Deposition is the best contender to make the blade in one printing session. A blade build out of multiple sections has a high chance of having an inconsistency in the surface where the sections meet. However, if the accuracy is sufficiently high, it is possible to manufacture the blade from of multiple sections and multiple materials. On the other hand, the increase in building size for Power Bed Fusion that is expected by *Layerwise*, as discussed in Section 4.3, could result in an entire blade to be printed using PBF. The advantage of using PBF over DED is that the former allows for thinner structures, which allows for a better optimized structure to be printed. If the metal blade is over designed it is likely that propeller blades made from polymers are lighter than their metal counterparts while still meeting the requirements.

Chapter 4

Detailed Structural Design

This chapter focuses on the core topic of this report: additively manufacturing the structure of an airplane. The first part details common misconception about AM and develops the design philosophy of the team. The manufacturing techniques, as well as the materials they can print, that were chosen for the tandem aircraft are also detailed in this chapter. Following these sections, the detailed design of two main aircraft part is given, namely the fuselage and the wings. Subsequently, the detailed design of the vertical tail, the landing gear and the engine mount described. This chapter is concluded with a detailed analysis on the various joining techniques that were specifically design for the tandem aircraft.

4.1 Additive Manufacturing Constraints & Difficulties

While Additive Manufacturing technology is praised as the revolutionizing future manufacturing technique, one large misconception is spread: *Additive Manufacturing allows to manufacture anything.* - This is truly not the case. Indeed, AM technologies enable the creation of complex and revolutionary structures in single parts, but still, AM technologies have their limitations as well. To better understand the difficulties encountered during the design process of the tandem aircraft, it is important to point out the most restraining limitations.

Build Volume. Depending on the process, build volumes are limited. The largest metallic parts which can be manufactured span a maximum dimension of $2.0 \times 1.5 \times 0.75\,m$, while the largest polymer counterparts can reach a volume of $2.1 \times 0.8 \times 0.7\,m$.

Overhang. The orientation in which a part is build up is crucial since maximum overhang angles vary with manufacturing techniques. This effect can partially be overcome by printing support structures. However, this increases cost and time requirements. Typical overhang limits for commercial desktop printers are about 30°.

Materials. Available materials are process dependent. Requirements are very different, but characteristics such as reflectivity and reactivity can drive the material selection. Thus, material and process selection need to go hand in hand.

Anisotropy. Typically, additively manufactured parts show anisotropic material characteristics. The origin in this phenomenon lies in the connections between the individual layers. For this reason, it is important to consider the build direction. Furthermore, cooling rates effect residual stresses which remain in the parts and possibly cause anisotropic behavior.

Tolerances. Especially when considering thin walled structures, tolerances play a crucial role. For AM processes these may be significantly larger than known from conventional manufacturing methods. Again, this characteristic is largely process dependent.

Surface Finish. This effect compares to the previous point. Considering the application in aircraft design, predominantly aerodynamic surfaces, one needs to be aware of the mostly rough surface finish of additively manufactured parts. In this context, it may require post-processing activities.

Time. Rapid prototyping is often used as an equivalent term for Additive Manufacturing. However, this term leads to the perception that parts are build in a very short time. This is certainly not the case when considering larger build volumes. Time requirements scale with the number of layers required and therefore also with build direction. It can take multiple days for a part to be printed.

Besides the limitations that are encountered in Additive Manufacturing it still provides a great design freedom compared to conventional manufacturing technologies. Precisely this design freedom proved to be a harmful factor in the aircraft design and development process: The variety of design options that can be considered is extremely large, and thus, trading off all design possibilities becomes a time consuming process. Furthermore, design methodologies, analysis methods and sizing tools taught in academia are tailored to conventional designs. These are mainly based on the use of sheets, beams and columns. It proves difficult to escape this way of designing and sizing of structural components. Thus, inspiration for design solutions of some components is obtained from nature, also known as biomimicry.

In conclusion, Additive Manufacturing provides technologies which allow for unconventional design approaches but at the same time, it also requires experience in design and new approaches in sizing and analyzing solutions. As this project is the first exposure of the team to this technology, time needed to be invested to get acquainted with this new design environment.

4.2 Overall Design Philosophy

The design-freedom of Additive Manufacturing translates into different design philosophies which can be used. The major philosophy considered by the team is the use of Topology Optimization software. This software determines the optimal material distribution, given a certain design space, the material properties and the several applied load cases. The exact working principle is explained in Appendix C. In brief, the initial design space is meshed and a FEM analysis is executed. Then, the density of low strained respectively stressed elements is lowered by the program and the process is repeated until an optimal structure is obtained. This design approach is promising as it can provide unconventional and lightweight designs. However, the big drawback of this design philosophy is its time requirement: Initializing and running a topological optimisation takes multiple days. In addition the obtained result still needs to be smoothened and redrawn to generate a manufacturable design. For this reason this design strategy is only used for a few parts while others are designed in a more conventional manner. Independent of the chosen strategy the team tries to take the biggest advantage of the AM technologies.

It is decided to use Topology Optimization for two major parts: The vertical tail and the wing root. The reason to optimize these two parts differs. The vertical tail is chosen as it presents a part of limited size with a rather simple load case. Thus, it is ideal to gain experience with TO-software as it can be expected to be less time consuming. The design cycle of the vertical tail from the definition of its design space up to the final structural design and its FEM validation is illustrated in Figure 4.1. A

more general case study, validating Topology Optimization results, is a major item of the verification & validation activities presented in Section 7.5.

Next, the wing root sections are chosen as they represent some of the most highly loaded parts in the aircraft. This design philosophy is illustrated in Figure 4.1. Additionally, the wing roots integrate the remainder of the wings, the fuselage as well as the landing gear in the front and the vertical tail in the rear. Thus, complex load paths and transfers are present and therefore, it is expected that an optimization cycle of the wing roots provides considerable weight savings. However, defining all load cases in the Topology Optimization software is a time-consuming process.

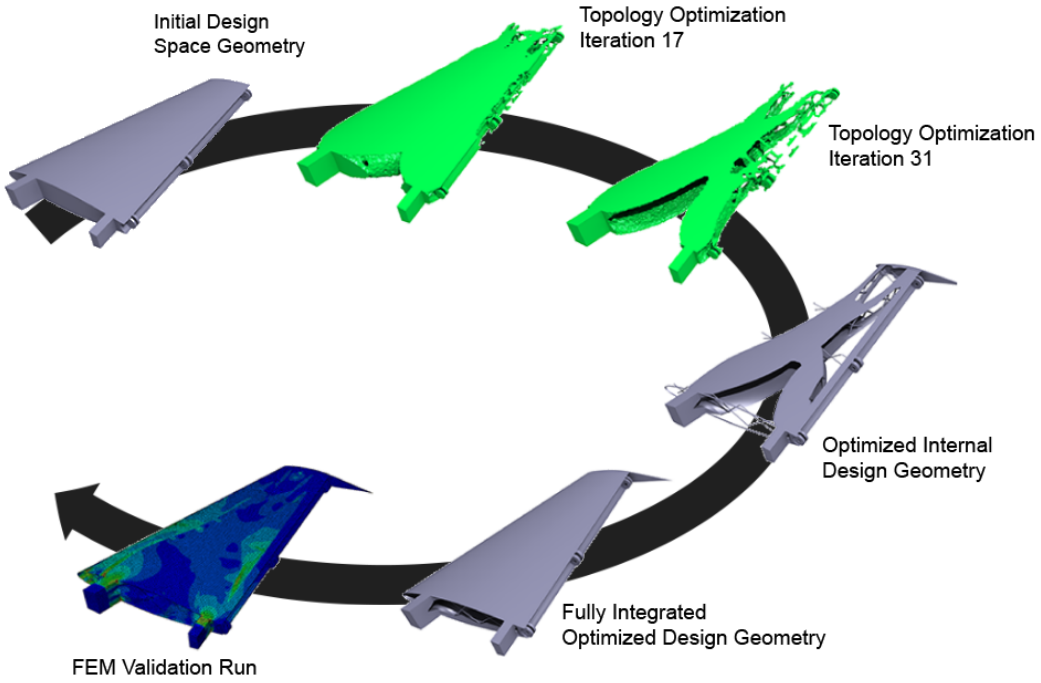

Figure 4.1: Illustration of the design process of the vertical tail

For all other aircraft components a conventional design strategy is chosen, mainly due to time-constraints. The detailed individual design approaches and sizing models are further explained in Sections 4.4 to 4.8. Once a conventional design is determined it is investigated how this can be fine-tuned such that advantages are drawn from using AM technologies. For some parts, subelements which are loaded in a single load-case are optimized in Topology Optimization software on a small scale. This is done for the fuselage-shear panels, for instance. It should be noted that some components, including the fuselage structure, still have a rather classical look. It is recommended that further investigation into these structures is done in a consecutive analysis.

Following the strategy chosen by the team, the final design is developed as shown in Figure 4.2. Besides the optimized vertical tail and wing roots, the fuselage-, landing gear- and engine mount design are discussed in more detail in the consecutive sections. Finally, joining concepts for these major components are discussed in Section 4.9.

4.3 Additive Manufacturing Processes & Materials

Generally, the AM processes can be grouped in two categories: those that manufacture using metal and those that use polymers. The relevant processing methods are summarized in this section.

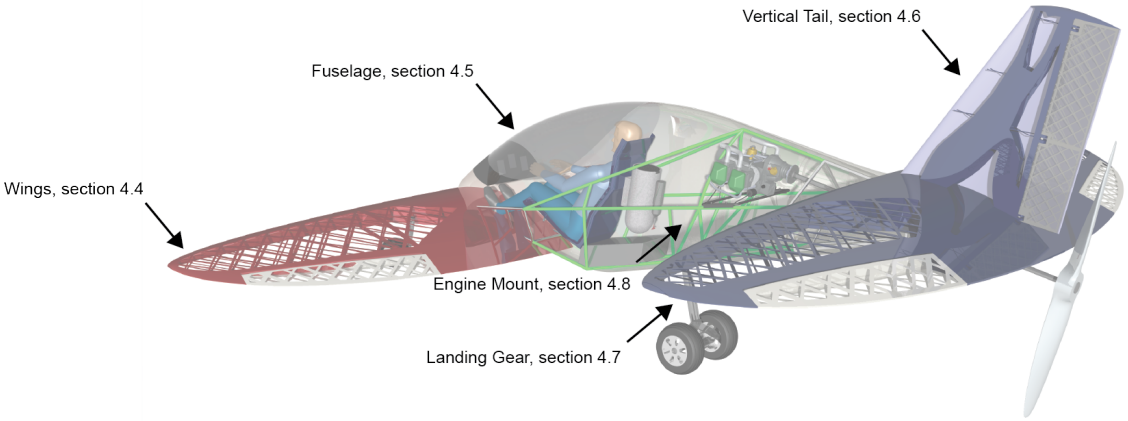

Figure 4.2: Render of the final design with references to the sections describing the detailed structural design of individual components.

Starting with high-strength metal parts, there are two major technologies which are used, Selective Laser Melting (SLM) and Direct Energy Deposition (DED). The differentiator in the application of these two methodologies is mainly the build volume, but also printable wall thicknesses and tolerances. While DED can manufacture parts up to $2.0 \times 1.5 \times 0.75\,m$, Selective Laser Melting is currently limited to build volumes of $0.27 \times 0.27 \times 0.42\,m$ [18, 19]. The latter are the build volumes as specified by *LayerWise*. However, the company is looking into scaling up its SLM build volume within the next year such that larger parts can be printed with this technology. This information was given during a factory visit in June 2014. Both technologies produce parts with material properties close to fully dense materials. A selection of materials is presented in Table 4.1.

Table 4.1: Material properties using Selective Laser Melting (SLM) and Direct Energy Deposition (DED) [20]

Property	Unit	Stainless steel 420 S29	AlSi10Mg	Ti-6Al-4V
Density, ρ	$[kg/m^3]$	7800	2710	4430
E-modulus, E	$[GPa]$	190	69.6	113
Yield strength, σ_y	$[MPa]$	340	163	786
Failure strength, σ_{ult}	$[MPa]$	622	324	869
Failure strain, $\varepsilon_{Failure}$	[%]	25	3.6	8

Direct Energy Deposition is an AM technique that sprays metal powder onto a surface and subsequently melts it using a high power laser. Material can also be added by melting a wire. The process is also suitable for hybrid material design because it can easily change the material that is fed. Compared to SLM, the DED process is less precise but allows for larger build volumes.

Selective Laser Melting is an AM method that belongs to the Power Bed Fusion (PBF) technologies. It builds up the object by sequently adding layers of powder, which are solidified using a laser. Processing requires in any case an inert gas environment. There is a variety of materials that can be processed. The advantage of this technology lies in its accuracy and achievable wall thicknesses. However, its build volume is currently rather limited.

The chosen design also consists of large scale components which can be made from low-strength materials such as polymers. Specifically, these components are the wing-tips, the control surfaces, the vertical tail and the fuselage structure. One major objective is to make these components out of a minimum amount of subelements. For this reason, Vat Polymerization is a suitable process: The *Materialise Mammoth* machine can print parts with a build volume of $2.1 \times 0.8 \times 0.7\,m$. However, according to *Materialise* the process can be scaled up easily if there is sufficient demand from industry. The most suitable materials offered by *Materialise* are the *Tusk Somos ®* for structural parts as well as the *WaterClear* for the canopy [21]. The attainable material properties, using the *Mammoth* machine are illustrated in Table 4.2.

Table 4.2: Material properties using the *Materialise Mammoth* Vat Polymerization respectively the *Fortus 900mc* FDM machine [21, 22].

Property	Unit	Tusk Somos ®	WaterClear	Polyphenylsulfone	ULTEM™9085
Machine		Mammoth	Mammoth	Fortus 900MC	Fortus 900MC
Density, ρ	$[kg/m^3]$	1200	1200	1280	1340
E-modulus, E	$[GPa]$	2.97	2.86	2.06	2.20
Yield strength, σ_y	$[MPa]$	60	-	-	-
Failure strength, σ_{ult}	$[MPa]$	-	55	55	72
Failure strain, $\varepsilon_{Failure}$	[%]	7.2	9	3	5.9
Heat deflection temperature at 1.81 MPa, ϕ	$[°C]$	53	42.5	189	153

Vat Polymerization (VP), also called Stereo-lithography, uses a photo-polymer resin in a container. The liquid resin is solidified by applying UV light, mostly by use of a laser, allowing the process to be fast and accurate. The main difficulty of the process is to find the adequate resin. The required characteristics appear contradicting since low viscosity and low shrinkage are required as well as high reactivity. Furthermore, resin curing properties have a significant effect on the attainable material properties. This characteristic limits the

There are some remarks that should be noted regarding the material properties presented in Table 4.2. First, manufactured parts are only cured to about 95 % when using VP. The time it takes for the parts to cure completely cannot be specified by *Materialise*, but is expected to take multiple months. If the material is used while not being fully cured its properties are highly temperature dependent. Next, according to *Materialise*, the *Mammoth* machines are mainly used for prototypes and non-structural parts and little experience is present with using this process for highly loaded components such as aircraft wings. Nevertheless, the achievable build volumes and material properties provide sufficient reason to use these materials in a demonstrator aircraft as is designed in this project. Furthermore, processing polymers is more sustainable as compared to metal-processes when considering energy consumption during production.

Next to VP, Fused Deposition Modeling (FDM) is used to manufacture polymer parts. In this process the material is heated and pressed through a nozzle in a semi-liquid state, creating a string of material which can be laid on a surface. Laying these strings of materials in an ordered fashion, a model is built. If necessary, a scaffolding material is used which can be removed easily after the part has been produced. The *Stratasys Fortus 900mc*, as used by *Materialise*, machine allows for a build volume of $0.91 \times 0.91 \times 0.61\,m$ while being able to process several materials [22]. The team's intention is to use this process for the fuel tank as it allows to manufacture chemical resistant materials as well

as for the engine casing. The specific materials that are used are Polyphenylsulfone (PPSU) for the fuel tank and *ULTEM™9085* for the engine casing. Both materials are very temperature resistant and can therefore also be used close to the engine. The properties are included in Table 4.2.

4.4 Vertical Tail

In the detailed design process of the vertical tail mainly the TO based design philosophy is employed. The reason for this is twofold: Firstly, it is a structure with clearly defined load cases which allows the team to gain experience in the TO software. Secondly, the design volume of the vertical is still rather small, allowing smaller element sizes in the FEM analysis which should result in a more accurate result. Therefore, even though it is normally not such an important structural part, more emphasis was put on the vertical tail in the detailed design phase. In the design process the TO is used as an inspiration or guideline for the final structural design which is subsequently fully redrawn in CAD software. Lastly, also the structural design of the rudder is investigated. This part is not optimised using TO, but is designed to benefit from AM in a more straightforward way.

The load cases for which the vertical tail is designed, are taken from the Federal Aviation Regulations (FAR) (FAR §23.441 [23]). From this document it follows that the vertical tail shall be designed for three distinct load cases:

Flight at the design maneuvering speed V_A and a sideslip angle of:

1. 22.5° together with the maximum rudder deflection in the relaxing state.
2. 0° together with the maximum rudder deflection.
3. 15° with no rudder deflection.

These three load cases are analysed using `XFOIL` with the NACA 64A015 airfoil combined with the rudder deflections. Also the force at the hinge line is determined from this analysis. Since the chord of the rudder is constant and the vertical tail is tapered, the rudder deflection point moves towards the tip. A 2D analysis is performed at different points along the span to obtain a pressure distribution and an estimation of the total hinge force. Since these are 2D analyses, aerodynamic effects of the finite wing are not taken into account. Therefore, drag is underestimated and the lift is overestimated. Due to this assumption, a safety factor of 1.5 is applied.

An analysis of the results shows that Load Case 2 and 3 introduce a higher load in every aspect as compared to Load Case 1; both, for the pressure distribution and the hinge force. This is most likely due to the fact that at 22.5° the tail has already stalled. Therefore, Load Case 1 is omitted from the further design of the vertical tail.

From the maximum loads, a simple sizing of the connection pins to the wing root is done. The sizing is based on rectangular beam cross-sections. Then, the connections itself are only used to define boundary conditions in the Topology Optimization, but they are not optimized themselves. The pins are also indicated in Figure 4.3. Furthermore, the build envelope of the *Materialise Mammoth* machine allows to print the vertical tail in a single, continuous part. Therefore, the vertical tail is designed for the *Tusk Somos ®* material using the *Materialise Mammoth* VP machine.

Before going into the detailed structural design, the design space for the vertical tail has to be set. In Section 3.2.1 the size of the rudder and location of the hinge line has already been determined. The rudder is removed from the vertical tail design space as seen in Figure 4.3. The position of the hinge points is determined from reference aircraft. Most small aircraft use three hinge points, one located at the root, one at the tip and one at the area centroid of the vertical tail [8]. This configuration is then modeled as a three point bending problem, from which the loads on the hinges are also determined, since these are necessary for the load cases of the Topology Optimization.

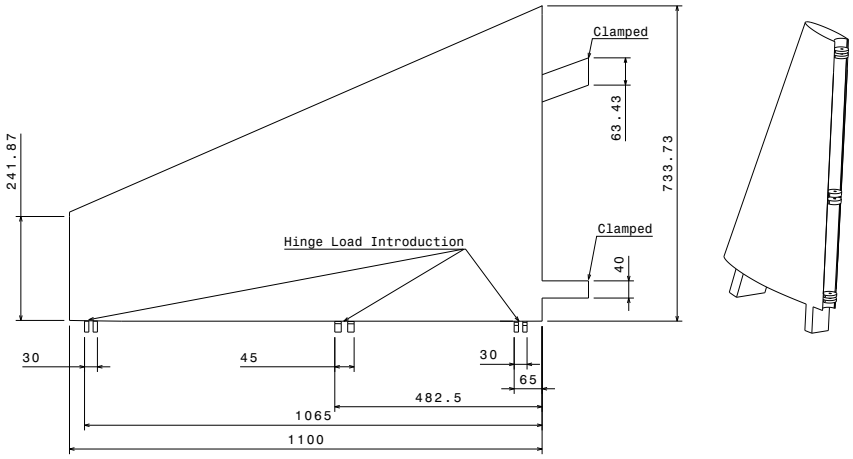

(a) Front view (b) Iso view

Figure 4.3: Vertical tail outer shape, dimensions in $[mm]$

The model as seen in Figure 4.3 is optimised for two distinct load cases using the TO software. An additional safety factor of 3 is applied on all loads to account for incorrect load introduction and fatigue. Furthermore, a symmetry condition is applied to the whole model in thickness direction, ensuring that the design can withstand loads for both negative and positive sideslip angles. This reduces the need for two extra load cases which are equal but opposite in direction. Only two boundary conditions are applied to the model, which are the clamped end surfaces of the connection pins, as indicated in Figure 4.3. The TO is also allowed to remove material at regions where pressure loads are applied. This way, it is ensured that elements of the skin can be removed as well, and the internal structure is easily visible. This does not mean that for instance the pressure load disappears on those elements which are removed. Instead, the pressure acts on the low density elements. The TO performs an optimisation on stiffness under a volume constraint, with the final mesh size being $\sim 310,000$ elements. The final result of the TO can be seen in Figure 4.4.

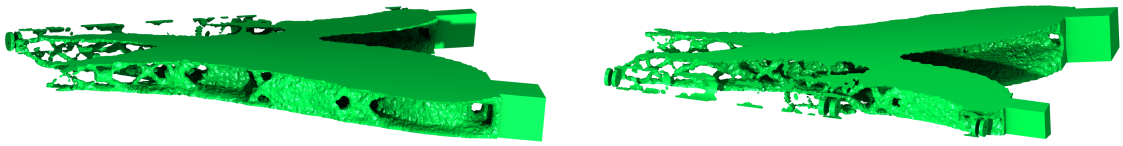

(a) 3D front view (b) 3D back view

Figure 4.4: Vertical tail Topology Optimization (TO) results (isosurface value = 0.2, volume = 17% of initial volume)

The output of the TO is a surface, in `.STL` format, which cannot be transformed to a solid in `CATIA`. Also, if the output would be directly used as the final design of the vertical tail, it would not have an airfoil shape and some hinges would not be connected to the final section. Therefore, the output of the TO has to be manually redrawn in `CATIA`. The internal structure of the redrawn vertical tail is overlayed with the final TO result as seen in Figure 4.5. The complex internal structure exposes one large problem of this design methodology: the amount of time required to redraw the CAD model on the basis of the TO model. The internal structure consists of highly complex structures which all have to be drawn separately increasing the amount of time spent on CAD enormously. The full complexity may be better grasped by looking at the technical drawing in Appendix E. The thicknesses

of all these trusses and spars approximate the Topology Optimization results as closely as possible.

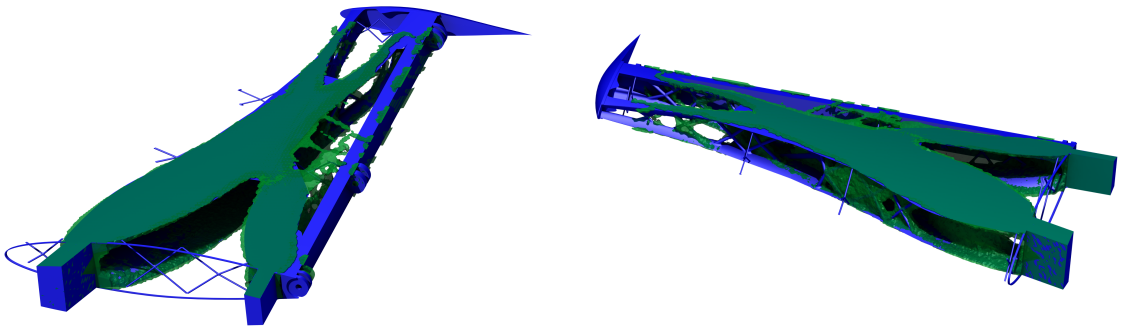

(a) Top view (b) Front view

Figure 4.5: Vertical tail final design overlayed with TO result. Green: Topology Optimization result; Blue: Final design.

For some parts however the TO result cannot be followed entirely. For instance, at some points the connection between the hinges and the rest of the internal structure is absent in the TO result. Furthermore, the vertical tail should also have an aerodynamic shape to follow the airfoil contour. For the vertical tail, it has been decided to use a 1 mm thick printed skin, which is still manufacturable using the *Materialise Mammoth* VP machine [21]. The skin is assumed to carry pressure loads only, while the resulting structure from the Topology Optimization carries all bending, normal and shear loads. Furthermore, combining the skin and the spars allows for printing the whole vertical tail in one part without the need for further assembly such as applying a foil. As such, the vertical tail becomes a true showcase for possible achievements with AM technologies.

Having such a thin skin, even though it is not highly loaded, requires some ribs in the vertical tail to ensure that the skin maintains the airfoil shape. Such a rib structure is optimised separately using TO for the cross-section at the second hinge point. The aerodynamic pressure load is applied to the model, as well as the load on the hinge. This rib is also optimised for Load Case 2 and 3 as used for the vertical tail. As boundary conditions, the top spar is clamped while the lower spar (see Figure 4.6) is given a symmetry constraint in span-wise direction (zero displacement in $z-$direction, together with zero rotation of the symmetry plane over $x-$ & $y-$axis). Again, the section is optimised for stiffness under a volume constraint, this time with a model of $\sim 103,000$ elements. The result shown in Figure 4.6(a), is generated with an isosurface value of 0.2. The volume of this iteration is 23% of the initial volume.

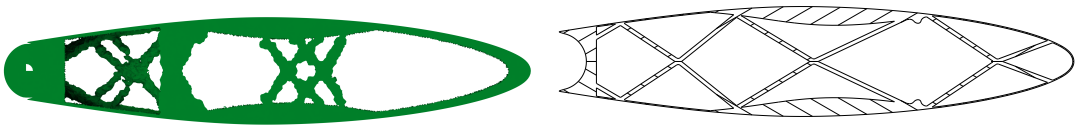

(a) TO result for rib optimisation

(b) Rib design as used in the final design. Clearly visible are the top & lower spar, connected via the truss members.

Figure 4.6: TO result versus final rib design

Figure 4.6(b) shows the final design for the rib at the second hinge location. In this case the TO is

used more as a guide for the location of the trusses. Also, a separate truss is added to the leading edge to ensure that the exact airfoil shape is maintained since that part is most critical for the aerodynamic performance. Such a truss is added at a total of four locations along the span of the vertical stabilizer (Figure 4.6). The actual thickness of the trusses is not derived from the TO, nor structurally sized. This should therefore be investigated in more detail in a further investigation.

Having such a detailed CAD model allows for making a more accurate weight estimation of the vertical tail. The weights of the different "parts" of the vertical tail can be found in Table 4.3, summing to a total weight of 9.27 kg. However, please note that this is a theoretical separation, since all these parts are actually one complete part which is printed in one go. The class II estimation of the final concept for the vertical tail is however 6.1 kg, meaning the current vertical tail design is still overweight. However, in a more detailed stage of the design process also the trusses can be made hollow to save considerable weight. Moreover, the thick spars can internally be more similar to a bone structure (trabecular structure) resulting in further weight savings. Lastly, a lattice structure can be incorporated for the skin, wrapped with a foil. This would result in large weight savings, but would require more assembly time, while now the vertical tail is printed and can basically be put on the aircraft straight away.

Table 4.3: Weight breakdown for vertical tail

Component Name	Weight [kg]
Skin	2.83
Trusses (Including ribs)	0.68
Spars	5.55
Cap	0.21
Total	**9.27**

To check whether the design can actually withstand all loads acting on it, a final FEM analysis is performed on the design. Both load cases are included in the analysis, where Load Case 2 is most critical, the result of which is shown in Figure 4.7. Overall, the vertical tail is still overdesigned, since the maximum stress in the structure is around 30 MPa while the yield stress for *Tusk Somos ®* is around 55 MPa. Therefore, the aforementioned weight savings should be possible without the structure failing. As an example, the results in Appendix C show that the spars at the root are still lightly loaded, providing an opportunity for large weight savings as these weigh 5.55 kg. Lastly, the FEM analysis shows that the skin at the root deforms heavily, thus additional reinforcements are needed in this area as well as in some other highly deformed parts of the skin.
Next to the structural design of the vertical tail, it has also been investigated what AM can offer for the rudder. Considering the rudder is lightly loaded and relatively small, also this part will be made from polymer. This part again has to be made using the *Materialise Mammoth* VP machine mostly because of the size limits. The rudder itself is not structurally sized, only a concept is selected for it. Only the part near the hinge rod is more highly loaded, but the rest of the rudder should only transfer aerodynamic pressure loads to that rod. Therefore, a lattice structure wrapped with a transparent foil should be sufficient as a structure for the rudder. An impression of such a design is shown in Figure 4.8.

Concluding, the vertical tail has been fully optimised using Topology Optimization, with the rudder being designed to take advantage of AM in a more straightforward way. It will be made from *Tusk Somos ®* using the *Materialise Mammoth* machine. AM allowed for making a very organic looking structure which cannot be efficiently manufactured using conventional manufacturing methods. However, fully optimising the whole tail proved to be a time consuming. The workflow between the TO and CAD needs to be improved a great deal in order to make this design philosophy an efficient

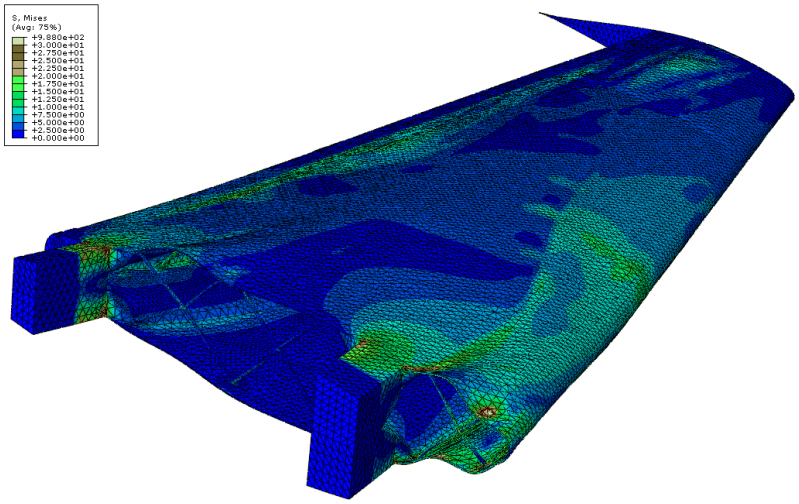

Figure 4.7: FEM analysis of the current vertical tail design for Load Case 3 (with safety factor 3). Deflections are multiplied by a factor of 4.0. Von Mises stress is indicated in $[MPa]$.

Figure 4.8: Impression of rudder design

one. Eventually, the current vertical tail is still overweight. Mostly this is because the design still has to be worked out in full detail. This would include making the trusses hollow and placing a bone structure in the thick spars.

4.5 Wings

The detailed wing design utilises both design philosophies that were described in Section 4.2. The rationale for this decision is the following: the large wing structure ($5.0\,m$ span $\times\, 1.14\,m$ root chord) cannot be printed in one part and therefore needs to be separated into multiple sections. Furthermore, it is unrealistic to numerically optimize the full wing structure in the given time frame. Still, since the wing structure, and especially its root section, is a heavily loaded component it is expected that large weight benefits can be drawn from an optimization cycle of the wing root. On the other hand, the outward wing structure is less loaded and thus, less improvements are expected from the application of Topology Optimization software. Therefore, these sections are developed based on classical design methodologies after which the results are fine-tuned to still draw benefits from the use of the AM technologies.

To design the individual wing sections, each of the two elliptical wings is split up in the following fashion: The wing root extends one meter in positive and negative spanwise direction and thus measures a span of two meters. This corresponds to the maximum build volume of DED manufactured parts. This AM technology is used because it enables to print such large scale parts while allowing for a wide range of metallic materials. Low strength materials such as polymers seem unsuitable for this component. The root section then also comprises integral connections to the fuselage structure as well as the landing gear in the front and the vertical tail in the rear. The remaining span that needs to be covered measures $1.5\,m$ for each half-wing. Throughout the structural analysis it turned out that polymers are suitable for this more lightly loaded wing section. Vat Polymerization using the *Tusk Somos ®* material is a suitable process for such large polymer components. However, the chord length in this section exceeds the build volume of the *Materialise Mammoth* machine which is described in Section 4.2. To still allow for printing in a single step, the control surfaces are fitted in such a way that the tip sections fit into the build volume of the *Mammoth* machine. A layout of the wing planform is indicated in Figure 4.9.

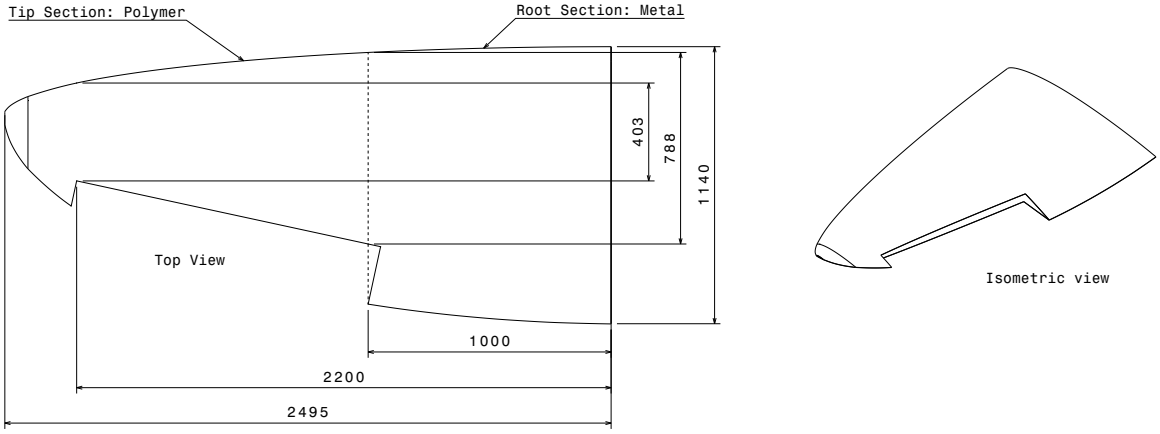

Figure 4.9: Wing planform layout, dimensions in $[mm]$

To define the boundary conditions for the topology optimization of the root sections, first the structural layout of the tip sections needs to be known. Based on inspiration of reference aircraft it is decided to follow a two-spar approach as is illustrated in Figure 4.10(a).

(a) Homebuilt aircraft wing structure [24]

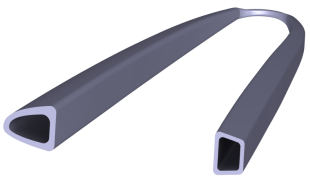

(b) GAW1 beam structure, tip-sections.

Figure 4.10: Inspiration and interpretation of an internal wing structure.

The front spar follows the elliptical shape of the wing with its geometrical center located at $0.1c$. The second spar runs in parallel with the hinge line of the control surfaces, at $0.72c \pm 0.02c$. While for the analysis both beams are modeled circular, the actual design of the front spar follows the airfoil contour at the leading edge and the rear spar is also extended to follow the airfoil contour. An

illustration can be seen in Figure 4.10(b). Further assumptions made during the sizing of the two beams are listed in the following:

- The two beams carry all loads acting on the corresponding wing section. While the front spar is designed to take up all lifting loads which are assumed to act at the quarter chord, the rear spar is designed to carry all loads resulting from control surface deflections.
- Normal forces in the beams result from symmetric bending. The inertias of the cross sections are based on circular models.
- Shear forces act through the shear center of the cross section, while additional torsion is added for the offset between the lifting force and the location of the spars. For the shear analysis the cross sections are further assumed to be thin-walled.
- Stresses resulting from torsion are again based on thin walled structures. However, for this analysis the actual leading edge shape is considered as this significantly increases the enclosed area.
- The load case that is considered is a $4g$ pitch up maneuver. Additionally a load factor of 1.5 is added for safety reasons plus an additional factor of 2 for the ambiguity in fatigue behavior of the material and manufacturing process.
- The von Mises stresses are computed for a planar stress state. That is, normal forces result from bending only, while shear stresses result from the sum of stresses due to shear and torsional loads.

The resulting cross sectional dimensions for front and rear spar are different for the two wings, as they feature different airfoils. The front wing comprises a NACA 2412 airfoil while the rear wing follows the shape of the GAW-1 airfoil. Further data on these is given in Section 3.3. For both airfoils, the spar dimensions are summarized in Table 4.4.

Table 4.4: Spar dimensions for wing tip sections.

Airfoil	Spanwise Position $[mm]$	Max. height Front $[mm]$	Wall thickness Front $[mm]$	Max. height Rear $[mm]$	Wall thickness Rear $[mm]$
NACA 2412	1000	106.0	35.0	74.0	15.0
	1400	94.0	18.1	72.0	15.0
	1800	78.0	16.7	60.0	10.0
	2200	51.0	13.4	36.5	10.0
	2400	29.0	10.1	22.5	8.0
GAW-1	1000	139.0	17.7	133.0	12.7
	1400	125.0	13.3	129.0	12.7
	1800	103.0	11.0	110.0	10.6
	2200	68.0	10.3	67.0	5.7
	2400	37.0	7.0	36.0	5.0

As the beams are designed to carry all loads, the airfoil skin only needs to withstand the pressure loads acting on it. It is suggested to connect the spars via a lattice structure which allows to span a foil over the airfoil surface. This way, the wing structure is most lightweight while being more accessible for inspection and installation of control systems and similar. The lattice structure however is not yet designed in detail and shall be part of a consecutive analysis. The render (Figure 4.11) includes an

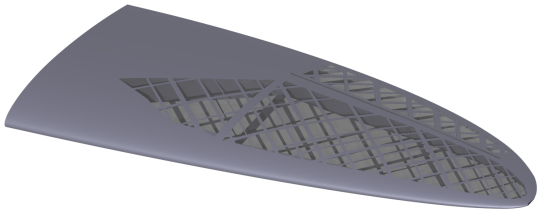

Figure 4.11: Artists impression of a lattice structure supporting the wing-skin.

artist's impression of such a design.

With the load carrying structure of the tip sections designed, the load transfer to the root section can be modeled in FEM software to initiate a Topology Optimization. Two separate analyses are run for the front respectively the rear root section. The defined design space can be seen in Figure 4.12.

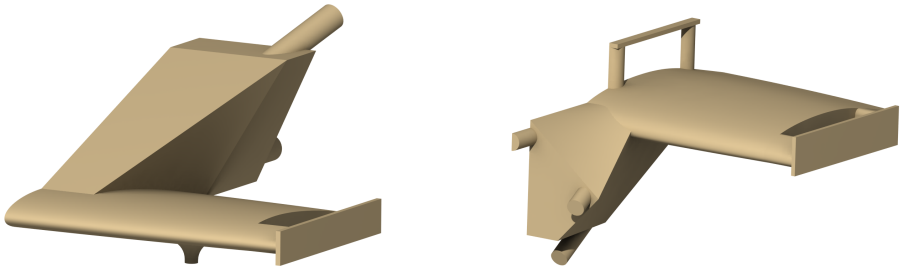

(a) Front wing. (b) Aft wing.

Figure 4.12: Design spaces for the two wing root sections.

Then, the following load cases are defined:

- A $4g$ pull-up maneuver. The load contribution of the tip section is modeled as a point load and a bending moment at $1.1\,m$ span at the quarter chord. For the application of this load an infinetly stiff plate is added to the structure. The lift contribution of the root section is modeled as a distributed pressure load obtained from `XFOIL`. Therefore aerodynamic effects due to the finite wing are neglected.
- A negative load of $2g$ (e.g. impact). The load contributions of the tip section and the root itself are modeled in the same way as for the previous load case.
- For the front root section a braking maneuver is modeled. It is assumed that $20\,\%$ of the aircraft weight is carried by one wheel only which reaches its maximum friction coefficient of $\mu = 1.0$ just before slipping [25].
- The previous load case is repeated at a $45°$ angle to model a cornering maneuver at high speed.
- For the rear wing the maximum load on the vertical tail is modeled which is obtained at a sideslip angle of $15°$ without rudder deflection.

Similar to the tip-sections, a load factor of 1.5 is applied in addition to a safety factor of 2 to cover the ambiguity in fatigue behavior. Considering the boundary conditions, the following constraints are applied:

- The symmetry plane has a displacement constraint in $z-$direction. Additionally rotation of the symmetry plane over $x-$ & $y-$axis are prohibited.

- The end surfaces of the extended fuselage struts are clamped.

An issue that arose during the optimisation is that the clamped fuselage strut surfaces seem to limit the displacement of the elements between the struts so much, that too much material is removed. For this reason, when redrawing the fuselage integration, the fuselage struts are continued and connected to the main load carrying wing structure. Further analysis and improvement shall be done in a consecutive analysis.

The material which is chosen for the root sections is the *AlSi10Mg* aluminum alloy. This is one of the commonly used alloys for the DED manufacturing process. Due to the short wingspan of the tandem configuration it is expected that steel will result a too heavy structure, while titanium would drive the costs to an unreasonably extent.

The results of the optimisation procedures are shown in Figure 4.13. In the same renders, the

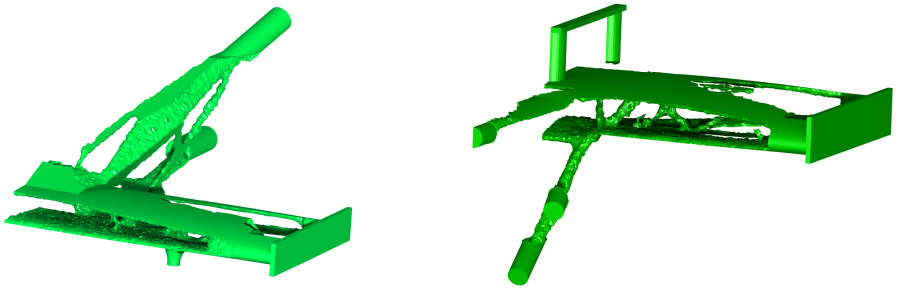

(a) Front wing. (b) Aft wing.

Figure 4.13: Optimized solutions for the two wing root sections.

interpretation and modification to the final design is added (Figure 4.14).

The result of the Topology Optimization is interpreted as such: For both wings the two spars from the tip-sections connect to one large hollow beam. For simplicity a constant wall thickness of 4 mm for the aft root section respectively 3 mm for the front root is applied. A closer approximation of the optimisation output can be worked out in a followup project.

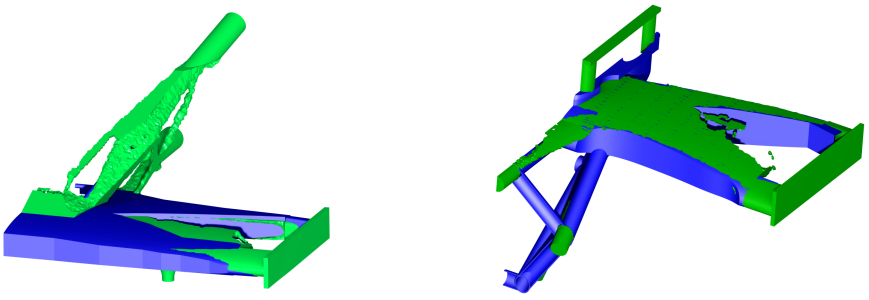

(a) Front wing. (b) Aft wing.

Figure 4.14: Overlay of optimisation results (light green) and simplified design solution (dark blue) for the two wing root sections.

A full weight estimation of the internal wing structure, based on the CAD files, yields a total wing weights of 53.16 kg for the NACA 2412 wing in the front and 49.98 kg for the GAW-1 wing in the rear. The difference in mass between the two wings can be explained by the greater thickness of the GAW-1 airfoil as compared to the NACA airfoil. This allows to create a greater inertia to resist the bending loads while using less material. Comparing the computed mass to the Class II weight estimation from Section 2.2, one finds that the wings as designed are 23.5 % heavier than predicted. This trend is also

observed for the vertical stabilizer, as described in Section 4.4. The reasons are similar and lie mainly in the large safety factors which are applied due to the uncertainties which are present in the material properties, especially its fatigue behavior. Additionally, it should be mentioned that the tip sections which are made from polymers could be made lighter by using high performance metals. However, this would drive the production costs unreasonably high. Detailed recommendations for future work are given in Section 8.2.

To conclude, the application of Additive Manufacturing technologies to the wing structure enabled the team to design a fully integrated wing root structure. Unfortunately, a conventional wing structure could not be developed in the given time frame to compare the performance of both structures. In future design activities, this design can be further refined and an optimisation of the full wing structure can be executed. Still, in the conventionally designed tip-sections, a set of AM features is introduced: The beams follow the airfoil shape and a lattice structure is integrated to span a foil which preserves the airfoil shape. Furthermore, the manufacturing process allows to create elliptical wing planforms which enhance aerodynamic performance.

On the other hand, the design also needs to be tailored to the limitations of AM technologies. The most obvious feature in this sense is the size limitation in build volume, forcing to split the wing structure in discrete sections. Therefore, special attention needs to be paid to joining these structures. Furthermore, each individual section represents a closed structure. This means that inspection for cracks becomes more difficult. The latter is one of the reasons to apply the high safety factors that have been used.

4.6 Fuselage

The fuselage design implements the more conventional design philosophy of the ones described in Section 4.2. Initially the design is calculated using conventional methods and geometries, after which adaptions are made that exploit the benefits of AM to improve the design. This section shows first the conventional design after which the adaptions and opportunities and challenges that AM offers are discussed. It should be noted that the fuselage is non pressurized. Therefore, no internal pressure forces were accounted for during design. It should be noted that the calculations have been done on a slightly simplified design of the truss structure. In the final design, the truss structure is reinforced to account for the loads from the landing gear.

General Layout and Conventional Sizing

An accurate estimation of the loads that act on the fuselage is required to design the structure. This estimation is usually based on a performance envelope from which a load distribution is created. The load distribution is constructed for $1g$ static conditions. Material properties for additively manufactured materials are however not defined and researched as well as most materials used in aircraft manufacturing. To make sure the design will withstand the loads, compensating factors for material properties, tolerances, general engineering safety factors and load factors are introduced during sizing of the individual components. From the location of each aircraft component a distributed load diagram was constructed. This load diagram can be seen in Figure 4.15. It should be noted that the location is measured from the leading edge of the front wing up until the end of the fuselage at 4.5 m. The first inputs of this calculation are the CG locations and results from the Class II weight estimations of each component shown in Section 2.2. These locations and weights have been continuously updated during the design process. The input for the final load distribution is shown in Table 4.5.

Table 4.5: Locations measured from leading edge of the front wing in longitudinal direction and masses of each component

Component	x-location $[m]$	Mass $[kg]$
Front wing	0.285	41.75
Rear wing	3.645	41.75
Fuselage	2.2	66.2
Engine	2.785	64
Front landing gear	0.285	20
Rear landing gear	2.435	8.6
IAE	0.75	17.9
Propeller	4.5	10
Nacelle	2.5	9.2
Front flight controls	1	3.2
Rear flight controls	4.3	4
Vertical tail	4	6.1
Furnishing	1.5	5.5
Fuel system	1.8	3
Fuel	1.8	44.7
Pilot	1.215	100

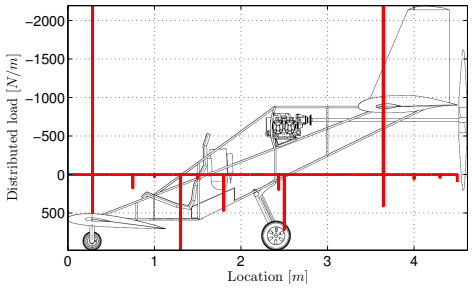

Figure 4.15: Distributed load diagram in longitudinal direction of fuselage

After construction of the load diagram, also shear and bending moment diagrams were generated. These are shown in Figure 4.16. They are used for determination of the fuselage design loads. The results are as expected for the applied loads: in the bending moment distribution sagging is shown between the main wings and the shear flow distribution shows opposing maximum values near the wings with a minimum near in the middle of the fuselage.

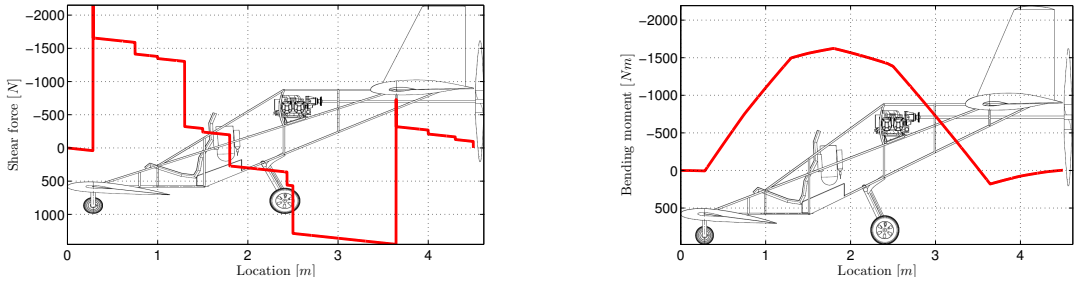

(a) Shear force diagram of fuselage

(b) Bending moment diagram of fuselage

Figure 4.16: Shear and bending moment diagrams of fuselage

From the load distribution diagrams in Figure 4.16 the applied loads for the sizing calculations are derived. The first assumption that is made is that all bending moments are absorbed only by the

tubular longerons which are modelled as booms. The shear force is absorbed by shear panels. These thin-walled shear panels are sized with a linear shear flow distribution on the bottom panels and a constant shear flow in the side panels. To prevent buckling and provide support for the shear panels, transverse beams are used. These are sized using maximum compressive and tensile forces that the shear panels introduce. All sizing calculations use the generated shear and bending moment with a general engineering safety factor of 1.5 in addition to a fatigue safety factor of 2 and a load factor of 4. The last assumption that should be mentioned is that all beams and skins in the same section have the same constant cross sectional properties. This limits structural optimization significantly however it is required due to time constraints. The final geometry of the fuselage load bearing structure, with the exception of the shear panels is shown in Figure 4.17.

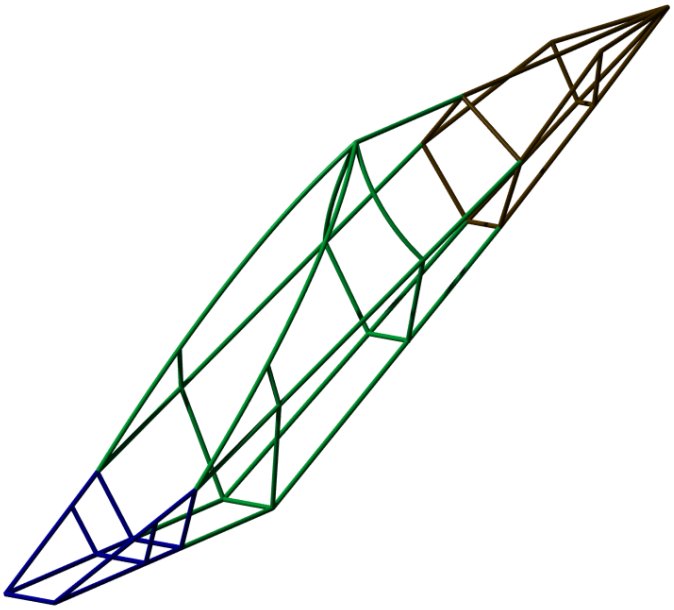

Figure 4.17: Render of fuselage truss structure

One of the driving design parameters of the fuselage is the maximum size of parts that can be printed. Based on this limitation the fuselage is divided into three sections. The front part of the fuselage along with the roots of the front wing is printed using Direct Energy Deposition (DED) from aluminum alloy AlSi10Mg. The rear section of the fuselage is also printed in aluminum alloy along with the roots of the rear wing and attachment of the vertical tail using DED. The middle section of the fuselage is printed from *Tusk Somos SolidGrey3000*, a high performance polymer by *Materialise* [21], using Vat Polymerization (VP). These material choices originate from the reasoning that preference is given to polymers due to the lower price and thicker cross sections that allow more leeway in printing tolerances. In case the specific properties of polymers did not suffice, metals are used. Figure 4.18 shows a side view of the fuselage with labels indicating different sections and joints between the sections. The larger the size of each section, the lower the amount of joints can be. Joints are a very critical location, thus, eliminating them as much as possible is desirable. The interface of the front and middle part is just right of joint 2. The interface of the middle and rear section is just left of joint 5. The joining of these sections is discussed in Section 4.9.

Tables 4.6 and 4.7 show the final size of each component that makes up the fuselage structure and the corresponding load. The section labels that have been used in calculations correspond to the ones

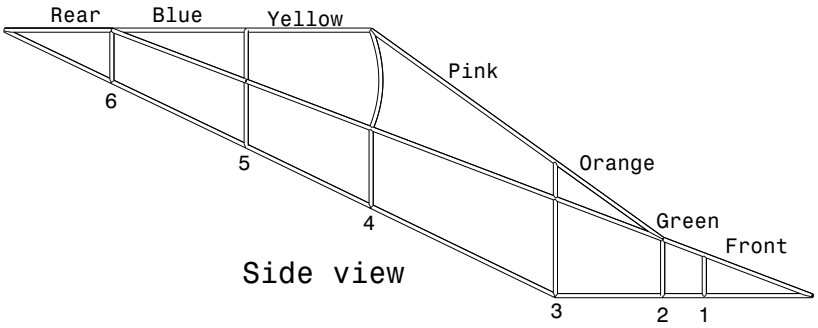

Figure 4.18: Side view of the fuselage structure with section and joint labels

indicated in Figure 4.18. The booms are numbered starting with the bottom left boom as seen from the front and traversing the cross section in a counterclockwise fashion. Skins and transverse beams are numbered starting with the bottom member as seen from the front and once again traversing the cross section in a counterclockwise manner.

Table 4.6: Longeron and skin properties

Component	Unit	Front	Orange	Green	Pink	Yellow	Blue	Rear
Shear force	$[kN]$	1.628	1.628	1.318	0.386	1.387	1.480	0.320
Bending moment	$[kNm]$	0.805	1078	1.440	1.498	1.292	0.745	0.180
Skin 1 - Thickness	$[mm]$	-	4	1.5	1	1	1	-
Skin 2 - Thickness	$[mm]$	-	6	3	1	2	2.5	-
Skin 3 - Thickness	$[mm]$	-	0	3	1	0	2.5	-
Skin 4 - Thickness	$[mm]$	-	6	0	0	0	2.5	-
Skin 5 - Thickness	$[mm]$	-	-	3	1	2	2.5	-
Skin 6 - Thickness	$[mm]$	-	-	3	1	-	-	-
Boom 1 - Radius	$[mm]$	25	25	35	25	30	20	8
Boom 1 - Thickness	$[mm]$	2	2	3	2	2	2	2
Boom 2 - Radius	$[mm]$	25	25	35	25	30	20	8
Boom 2 - Thickness	$[mm]$	2	2	3	2	2	2	2
Boom 3 - Radius	$[mm]$	25	25	35	25	30	20	8
Boom 3 - Thickness	$[mm]$	2	2	3	2	2	2	2
Boom 4 - Radius	$[mm]$	25	25	35	25	30	20	8
Boom 4 - Thickness	$[mm]$	2	2	3	2	2	2	2
Boom 5 - Radius	$[mm]$	-	-	35	25	30	20	8
Boom 5 - Thickness	$[mm]$	-	-	3	2	2	2	2
Boom 6 - Radius	$[mm]$	-	-	35	25	-	-	-
Boom 6 - Thickness	$[mm]$	-	-	3	2	-	-	-

AM Adaptions

The use of trusses enables relatively simple calculations. It is however a restricted design element that creates a load path which is far from ideal. AM techniques can be used to create trusses that have variable cross sections, thicknesses and longitudinally curved truss members. The benefits that arise due to this freedom of geometry can have a significant impact on the structure. The downside of these adaptations is that calculations become much more complicated. Sticking to standard engineering structural elements such as simple beams and skins enables engineers to thoroughly understand the structure and size individual parts. Complex organic geometries however require designers to, at least partially, let go of these standard elements.

Table 4.7: Transversal beam properties

Component	Unit	Joint 1	Joint 2	Joint 3	Joint 4	Joint 5	Joint 6
Beam 1 - Radius	$[mm]$	25	20	10	10	16	15
Beam 1 - Thickness	$[mm]$	5	5	2	2	5	5
Beam 2 - Radius	$[mm]$	25	20	10	10	16	15
Beam 2 - Thickness	$[mm]$	5	5	2	2	5	5
Beam 3 - Radius	$[mm]$	0	0	10	10	16	15
Beam 3 - Thickness	$[mm]$	0	0	2	2	5	5
Beam 4 - Radius	$[mm]$	25	20	0	10	16	15
Beam 4 - Thickness	$[mm]$	5	5	0	2	5	5
Beam 5 - Radius	$[mm]$	-	-	10	10	16	-
Beam 5 - Thickness	$[mm]$	-	-	2	2	5	-
Beam 6 - Radius	$[mm]$	-	-	10	-	-	-
Beam 6 - Thickness	$[mm]$	-	-	2	-	-	-

The joining of trusses is another area that could benefit from using AM techniques. The method of tensile triangles is a valuable tool in constructing edge fillets to reduce stress concentrations and optimize the load path in the structure. It uses the forces of each truss as input and through geometric fitting of triangles in a certain layout with consequent rounding creates an organic fillet between the members [26]. An example of this method is shown in Figure 4.19.

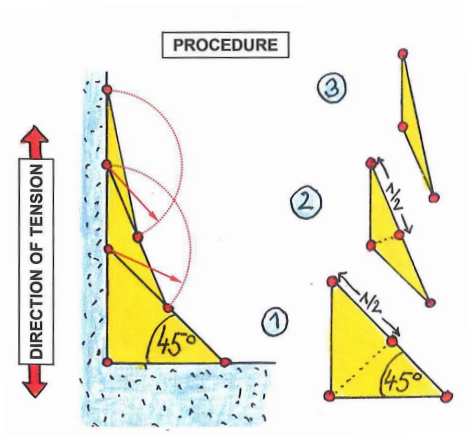

Figure 4.19: Example of tensile triangle methodology [26]

The shear panels have been designed using flat plates. Flat plates are however far from the ideal structure for carrying the shear loads that the fuselage is subjected to. Generally, in order to reduce weight in these plates cutouts are used. These cutouts are located in areas of low stress and subsequent stress concentrations accounted for. Furthermore, a TO analysis has shown that shear plates can be optimized in such a way that they consist of a mere lattice structure to carry the load. Figure 4.20 shows an example of such a panel. A panel of $100 \times 100 \times 5\,mm$ was subjected to a 10 MPa shear load and its geometry was optimized. It clearly shows the lattice structure and cutouts that make up the optimized geometry. It should be noted that the exact dimensions and locations of these cutouts are dependent on the element size of the mesh used for TO and load case that the panel is subjected to in the computational model. The final result should however remain a diagonal lattice structure. Using AM technology these kind of structures can be produced relatively easily and can result in large weight savings in aircraft structures.

Conventional internal load carrying structures tend to use straight elements and constant cross

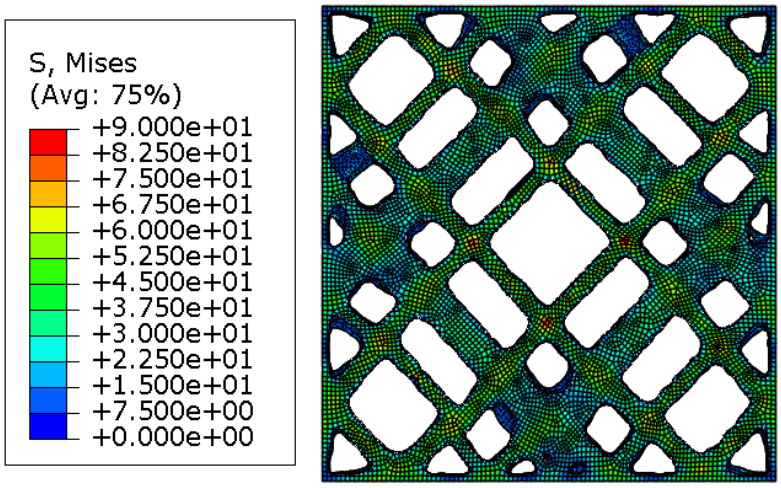

Figure 4.20: Optimized shear panel: internal Von Mises stresses in $[MPa]$

sectional parameters. Besides the structural geometrical advantages there is another reason for aircraft design to benefit from AM technology. This can be found in the fact that the aerodynamic outer skin can be integrated into the structural design of the aircraft. This enables designers to fulfill two functions, namely shaping the aerodynamic exterior and transferring load from one location to another using a single part. The combined use of curved beam members, optimized joints, lattice structure shear panels and a tight thin skin finish can enable the fuselage structure and aerodynamic shape to be printed together. Both the structural optimization and combining of functions of various components into a single part make AM a valuable manufacturing tool for fuselage design.

In conclusion, AM provides many opportunities for the design of the fuselage. It does however require engineers to adapt the way they design parts. Sticking to conventional engineering methods means that the design will end up the same as before, only with additional limitations that AM imposes. This is the case for many other parts as well, however due to the complex load and integral function that the fuselage fulfills both AM opportunities and conventional design disadvantages are amplified.

4.7 Landing Gear

The first step in the landing gear design is to determine the overall landing gear configuration. After that the structural design of the landing gear can commence, where the strut lengths and thicknesses are calculated. These two phases of the design will be discussed in the upcoming sections.

Landing Gear Configuration

The designed aircraft has a modified version of a conventional tail-gear configuration. This consists of two separated struts at the front of the aircraft, and one strut in the back. The only difference with the conventional tail-gear configuration is that there are two wheels in the back, to provide more stability. The top view of the landing gear configuration is visualised in Figure 4.21. This design is preferred because the shortest struts are required since the front struts are attached to the front wing and the main strut is attached to the fuselage. For steering, the struts wheel track should be big enough. This is only possible by connecting them to the front wing, or longer struts would be required. Steering is more elaborated in Section 5.2. The main landing gear takes the highest impact forces, and therefore this strut should be as short as possible. Therefore it is connected to the fuselage. The main configuration is discussed below.

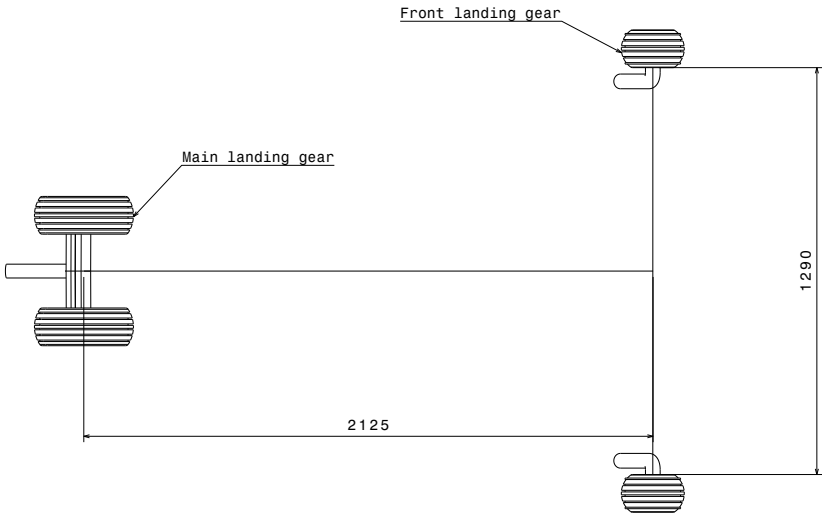

Figure 4.21: Top view of the landing gear configuration, dimensions in [mm]

Front Landing Gear

The front landing gear is directly attached to the front wing and attached to the wings at quarter chord. Since the aircraft should not tip over when turning or in large crosswinds, the wheel track had to be determined. This value is depending on the the height of the Center of Gravity and ground speed. According to calculations used in Sadraey [27], for this design the wheel track distance is calculated to be 1.29 m.

Main Landing Gear

The back or main landing gear position is determined by the location of the Center of Gravity and the position of the propeller. Since the bottom of the fuselage is at an angle, the closer the main landing gear is positioned to the front of the aircraft, the shorter the strut is. Nevertheless, the propeller should not hit the ground at take-off. This is the so-called clearance angle, decided to be 15° with an extra factor of safety of 20 cm.

Furthermore the aircraft should not tip back at landing. Therefore the position of the CG during landing (assuming a maximum approach angle of 15°) should still be between the front and main landing gear.

Taking these two requirements into account, the position of the main landing gear wheel base is determined to be at 2.125 m, measured from the leading edge of the front wing. As mentioned before, the main landing gear strut contains two wheels for stability reasons. When the aircraft hits the ground at maximum banking angle at approach (taken to be 12°) the CG should still be positioned between the two back wheels. Calculations show that the distance between the two wheels should be 40 cm. The main landing gear strut is placed perpendicular to the fuselage, since this covers the shortest distance to the required wheel base and fuselage.

Landing Gear Strut Design

The next step in the design process of the landing gear is the sizing of the struts. The landing gear should be able to withstand the impact forces at landing without buckling, but still be aerodynamic efficient. This can be possible with the advantages of Additive Manufacturing. The strut is designed to be a hollow circular tube, with an extra fairing in droplet shape, to improve aerodynamic properties. Due to the benefits of AM this fairing can be very thin and will not add much extra weight.

For safety reasons the forces the landing gear has to withstand are calculated for Maximum Take-off Weight with an impact force of $6g$ and an additional safety factor of 1.5. The struts are calculated to withstand all compressive loads while they should not buckle at impact. Since the aircraft will land at a certain angle also bending is taken into account. Every single strut is designed to withstand all loads in worst case scenario so the aircraft can land on any single wheel without failing.

To decide on the material that should been used for the landing gear, a trade-off between aluminum, stainless steel and titanium is performed. Using titanium would result in a 8% weight saving compared to stainless steel, but using stainless steel will save 37% on volume. This smaller volume will allow for a much lower production time. Therefore stainless steel is chosen to be the material for the landing gear.

The final dimensions for the landing gear are shown in Table 4.8.

Table 4.8: Strut sizes for the landing gear

Component	Radius $[mm]$	Thickness $[mm]$
Front strut	22	7
Back strut	40	10

The connection point of the two struts to the one large strut was chosen such that the overall weight of the struts was minimized. For the current layout the least material is needed. The total strut has a length of 0.56 m, consisting of a straight part of 0.435 m which it splits into two struts. The angle between the struts and the vertical axis is 57.62°. The landing gear strut can be visualised in Figure 4.22.

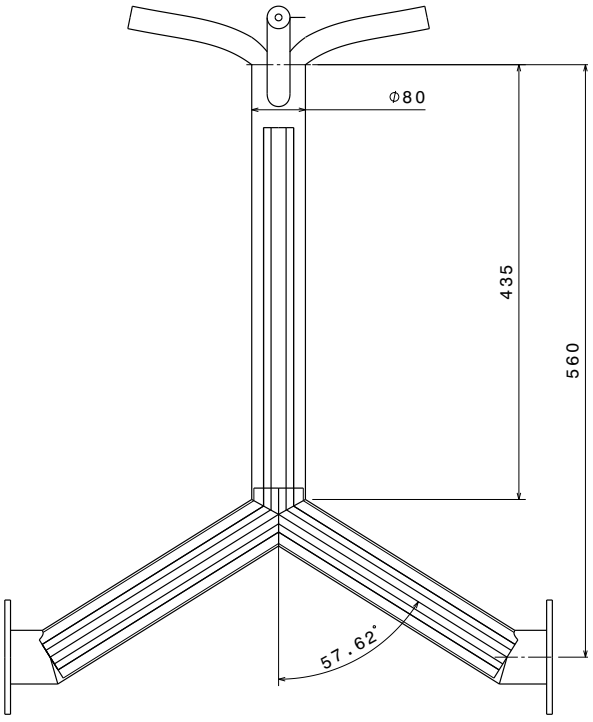

Figure 4.22: Front view of the main landing gear

The landing gear will be manufactured using Power Bed Fusion, Selective Laser Melting in particular. Using SLM will enable enough detail to print the fairing. Considering current size limitations at *LayerWise* it will be impossible to print the landing gear in one part but since the company is

planning to enlarge the build volume of this machine, as described in Section 4.3, it will be possible in the future.

Future Research

At this moment only the wheels absorb the impact shock so the pilot would be subjected to considerable g forces. Therefore some damping system should be investigated, preferably one that is possible to be made with Additive Manufacturing. A possible solution could be splitting the two struts of the main landing gear into two separate struts, connect them with a pin and place a spring in between the two such that the wheels can move to take up part of the impact.

4.8 Engine Mount

Aircraft engines often come with a predesigned engine mount. For this aircraft however, due to its engine position and in order to avoid multiple strut layers, the complete engine mount is designed. This design is inspired by the existing engine mount that comes with the *Rotax 912 iS* engine. In this section the engine mount requirements and design process are elaborated on.

Engine Mount Requirements and Positioning

The engine needs to be connected to other structural components to transfer the thrust that it produces to the rest of the aircraft. The selected engine has eight suspension points. These are symmetrically located with respect to the xz plane (in the aircraft's body axis). A minimum of four symmetrically located suspension points is required to mount the engine [17]. The engine is located relatively high in the fuselage, because the drive shaft of the engine is straight and the propeller needs sufficient ground clearance.

It was first investigated how the mount would be positioned if the existing mount would be used. Two different suspension point configurations were examined, the four points below and in front of the engine. Both encountered the same problems. For these configurations additional struts had to be designed connecting the mount to the fuselage. This would mean the total engine mount would consist of two large strut connections instead of one. Electing one of these configurations would take away the advantages of using the existing engine mount. The engine mount would be significantly larger, heavier and it would have to go through the same testing procedure as if the whole mount would be designed.

The final engine mount configuration also makes use of the bottom four suspension points. However, in this configuration the engine mount is positioned in line with the fuselage beams. Not only did the existing mount not fit properly on the fuselage but in order to connect the engine to the mount, the struts had to be enlarged and redesigned. Therefore a complete new engine mount was designed since the existing mount would not fit on the fuselage beams. This has several advantages over adjusting the existing mount. By designing a new engine mount, the mount can be printed and tested as one part. No additional joints are needed and the mount would only consist of a single strut system. These struts can then be sized according to the applied loads resulting in a more optimized design.

Engine Mount Design and Sizing

The mount position is fixed which leads to the strut design. Since the engine mount is constrained by the fuselage beams, the mount is designed in such a way that the engine mount to fuselage connection is as small as possible. Therefore the engine mount is placed right on top of the fuselage beams.

The connection between these two parts is through vibrational dampers. Besides these two large vibrational dampers there is also a damper attached to each suspension point of the engine for safety reasons. By using dampers at two different positions, it is assumed that all vibrations due to the engine can be neglected in the strut design. This means the struts are designed for a static loading case. Because of this assumption an extra safety factor of 1.5 is added.

Each strut is designed to resist the engine weight and thrust force acting on the engine. Solid and hollow circular struts are considered, each evaluated in titanium, steel and aluminum. For the hollow struts calculations for the wall thickness ranged from $2\,mm$ to $10\,mm$ in order obtain the strut radius. The strut length and angle followed from the mount position since it is constrained by the fuselage and the engine itself. Four different struts were examined resulting in four different load cases. Due to symmetry in the xz plane (in the aircraft's body axis), each load case represented two struts on the engine mount.

Additive manufacturing titanium delivers a reduction in costs, weight and carbon emissions both during manufacturing and use. Furthermore, titanium could withstand the applied loads while having the smallest diameter. Therefore the selected material for the engine mount is titanium. Note that this decision relies on the fact that the vibrations are neglected in the stress calculations. More in depth research on the fatigue performance of titanium is required [28].

All four strut dimensions are given in Table 4.9. The engine mount is then printed with Selective Laser Melting. Nowadays this printing technique is able to print metal up to $0.27 \times 0.27 \times 0.42\,m$ [18, 19] but the printing volume will significantly increase in the imminent future, as discussed in Section 4.3. Therefore it will be possible to print the engine mount in one go with SLM.

Table 4.9: Engine mount strut dimensions

Strut number	Length $[mm]$	Angle $[°]$	Radius $[mm]$	Wall thickness $[mm]$
Strut 1	49.7	50.7	3.4	6
Strut 2	117.8	75.8	4.1	7
Strut 3	190.1	11.7	5.2	7
Strut 4	218.4	31.5	3.5	5

4.9 Joints

In conventional structural design, joints are often critical parts since load transfer from one section to another often leads to peak stresses. The major restriction of many Additive Manufacturing methods is the size of which the components can be manufactured. This means that the aircraft has to be build up of multiple sections which are connected at certain transition planes. The joining methods are therefore a crucial aspect of the design. The freedom offered by AM allows for more complex joints than those used in conventional design. Geometrical interlocking is for instance one of the options.

In total there are three main joining areas: the wing roots to fuselage connections, the wing tip to wing root connections and finally the vertical tail to wing root connection. The proposed strategy for each of these joints will be discussed together with a qualitative trade off of the different options and some basic sizing calculations.

Wing Root to Fuselage Connections

The main loading cases for the wing root to fuselage joint are tension and compression. Since the wing root is integrated in the fuselage and therefore printed in one part, the bending loads of the wings are all transferred through the root relieving the fuselage of these major bending loads. Furthermore,

conventional joining techniques such as welding are not an option since the fuselage is made out of polymer and the wing root is manufactured in metal. This leads to two main joining methods to connect the wing root to fuselage connection: adhesive bonding and interlocking.

Adhesive bonding is a joining method that is used regularly in the aerospace industry. However, it is only used in non-critical load bearing structures. The reason for this is the uncertainty with respect to fatigue properties, the difficult inspection of the bond and in this case the difficulty in bonding a metal with a polymer. If adhesive bonding is used for this joint, the joint design should focus on creating sufficient bonding surface on the fuselage beam. This will minimize the stress concentrations in the bond and enable adhesive bonding as a joining method for the fuselage. Due to the use of AM this surface distribution can be designed in a more complex way. More surface can be created leading to a better result compared to conventional production techniques.

The final joining concept for this connection makes use of geometric interlocking and an elongated nut in order to hold the parts in place when the beam is loaded. The fuselage structure will slide into the wing root. Due to the geometry of the slide the beams are only able to move sideways. In order to lock the beams, the nut will be put in place constraining the beams in all directions. This nut, due to its large threaded surface, will take a portion of the load resulting in a distributed load transfer and a lower average stress. Another advantage of interlocking the two fuselage beams is the large surface created by the hooked end of the fuselage beams. Therefore the load is transferred more efficiently for both tension and compression. This system does however need more research. The dimensions of the thread should be determined in order to be sure the load is transferred properly. Not only should the threat withstand the loads but the polymer should not deform when the system is loaded. This is something which should be worked out in more detail in order to fully trust this joining method.

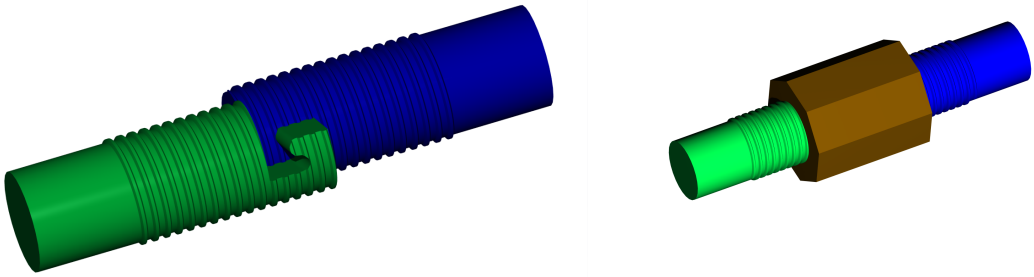

(a) Geometric interlocking slide system

(b) Fully assembled

Figure 4.23: Wing root to fuselage joint: geometrical interlocking system with an elongated nut

Wing Tip to Wing Root Connections

The main difference between the wing tip to wing root and wing root to fuselage connections is the primary load case. Where the fuselage structure is designed such that the beams are mostly in compression or tension, the wing tip to wing root connection will mostly be a bending problem. To make a structure bending resistant it is important to have a cross section with the highest possible moment of inertia, and thus the most material away from the centroid. In the case of a bending wing this means the most material near the upper and lower skin. This is also where the joint should act: as far away as possible from the centroid resulting in the lowest stresses.

The wings of sailplanes are often attached to the body using a single pin going vertically through the middle of the fuselage where the roots of the wings meet each other. This same system can also be used for this concept. Each wing tip section of the tandem aircraft carries approximately one eighth

of the weight of the aircraft. In cruise this results in a lifting force of approximately 600 N. When compared to the glider aircraft, which can easily weight 300 kg, it is found that each wing has to carry 1500 N and has a relatively large span resulting in high moments near the root. This therefore leads to the conclusion that a simple pin system should suffice. The simplicity of such system is also beneficial for the overall reliability of the design.

The most basic system could work as follows. The rectangular spar of the wing tip is elongated and can be slided into the rectangular spar of the root section. Once in place a pin can be put vertically through both spars locking them in place. To get a general idea of the required diameter of such a pin, a simplified analysis can be performed. It is assumed that the pin takes up all the bending loads. In reality this is however not the case as most of the load is transferred from the contact surfaces of the two spars which have been slided into one another. When it is assumed that the lift force acts at the center of area of the wing tip, the moment acting on the connection surface can be calculated. As the height of the inner rectangle of the spar is known, the shear load carried by the pin can also be determined. Assuming that the pin is made of the same aluminum as the wing root, namely *AlSi10Mg* which has a shear strength of 180 MPa, it is computed that the diameter of the pin should be 3.2 cm. This value is calculated assuming a 4g maneuver with a safety factor of 1.5 and another safety factor of 2 to account for fatigue uncertainties. In addition the pin is designed for 30% of the shear strength of the material. In total this means that the diameter of 3.2 cm is extremely over designed and is merely meant to show the feasibility of the usage of a pin system.

Even though the pin system is concluded to be feasible, it is not optimal and does not take full advantage of the benefits of AM. An additional suggestion for improvement of the joint is to make the upper and lower spars fork into each other and put a pin through horizontally. The benefit of such a system is that the pin does not have to carry the loads of the moment at a single point, but instead at every teeth of the fork. There are however also downsides to this system. For instance the load was initially mainly transferred directly via the skins of the beams that have been slided into each other and not via the pin. This disadvantage can be countered by continuing the flanges below the forked teeth as shown in Figure 4.24, which shows the bottom flange of the spars. Another downside might be the stress concentrations at the beginning of the teeth, yet there would also be stress concentrations at the initial suggestions near the single hole. It is suggested to do a more in depth analysis to make a weighted decision. A FEM analysis could be of value. Because of the simplicity of the vertical pin system, this joint will be used in the proposed final design.

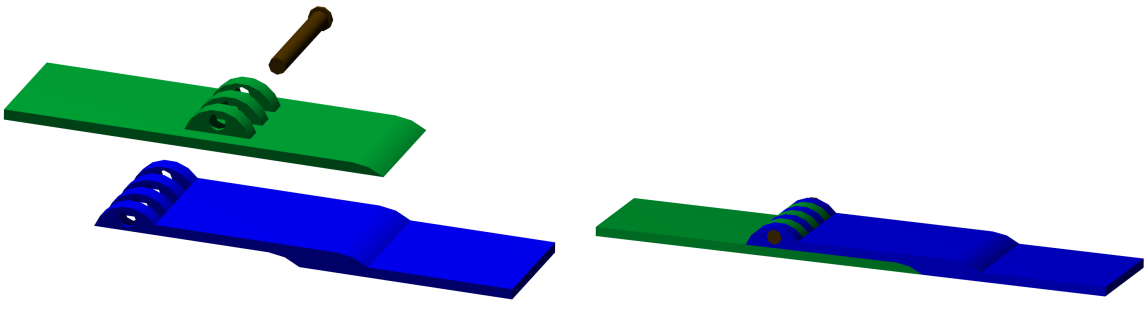

(a) Seperate parts (b) Assembled

Figure 4.24: Wing root to wing tip joint: bottom plate of the wing spar showing a teeth like pin joint

Vertical Tail to Wing Root Connection

The main load case of the vertical tail is bending. This makes the connection comparable to that of the wing tip to wing root. As such, also a pin connection is suggested. Initial calculations comparable

to those made in the previous section suggest a pin diameter of 2.3 cm. Again it is assumed that all loads are transferred through this pin.

Where the two spars of the wing tip have to slide into the two spars of the wing root, the vertical tail has a bit more freedom. Therefore it is proposed to implement a slide system where the tail slides in place along the direction of the fuselage. Such a slide is shown in Figure 4.25. The advantages of such a system is that a lot of of the load is directly transferred by the horizontal contact surfaces which lowers the stresses near the hole of the pin. Since the vertical tail is manufactured from the *Tusk Somos ®* polymer it is advantageous to distribute the load over as much area as possible such that the stresses stay well below the yield stress of 60 MPa.

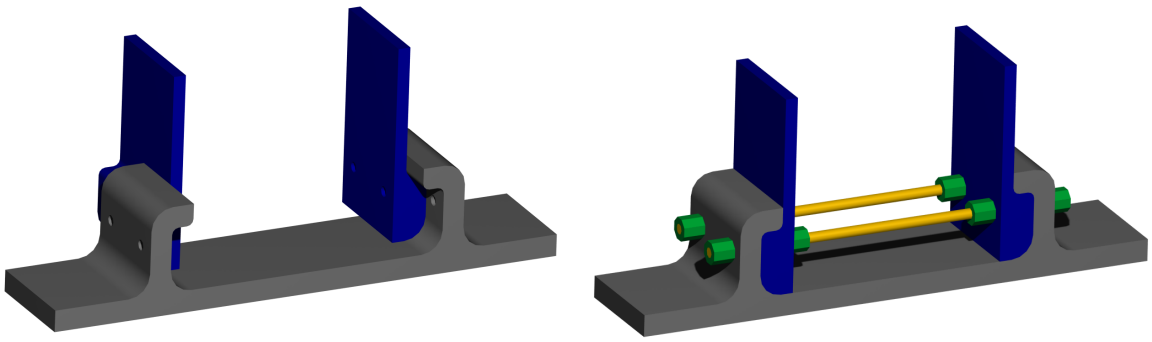

(a) Slide system

(b) Fully assembled

Figure 4.25: Vertical tail to wing root joint: combination of a slide and pin joint

Chapter 5

Subsystem Design

In addition to a strong structural design, any aircraft needs certain parts and components to help the pilot maneuver the aircraft on ground and in the air. Such parts first need to be located in specific locations since their placement can affect the overall CG location. Hence the first section of this chapter describes the internal layout of the aircraft. Following this section, the ground barking system is presented. Finally the electrical system and the flight control instruments are detailed in the last section. The internal layout of the aircraft is depicted in Figure 5.1 in which the corresponding sections are referred to.

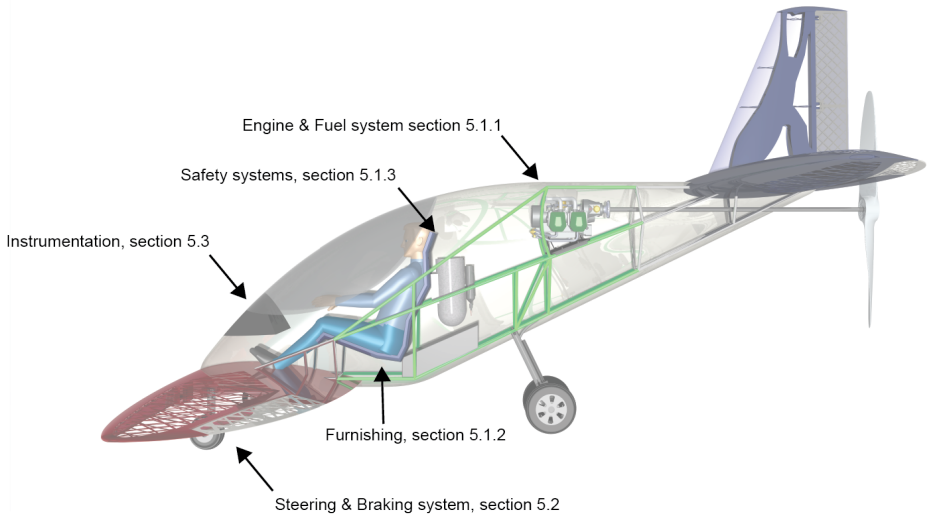

Figure 5.1: Render of the final design with references to the sections describing the internal layout

5.1 Internal Layout

Apart from the structural and aerodynamic design, a number of subsystems has to be developed to complete the entire aircraft. Since this is not the focus of this feasibility study, they will only be discussed briefly. The focus will lay on the positioning of the subsystems as this has an effect on the center of gravity of the overall aircraft. Furthermore the basic requirements of the systems are described, as well as the manufacturing method when applicable.

5.1.1 Engine & Fuel System

The engine placement is constrained by propeller clearance and dimensions of the truss structure. Because of the large mass of the engine, it is placed as much forward as possible. It was however

concluded that a straight propshaft should be used to keep the mechanical system as simple as possible. Therefore the engine is placed in line with the propeller, as far forward as possible as the fuselage skin allows for. The engine itself (Rotax 912 iS [29]) was already decided upon in the conceptual design phase, as discussed in the Midterm Report [3]. Since this engine is an off-the-shelf component, it will not be further discussed in this report. The positioning and mounting points are used to design the engine mount, connecting the engine to the longerons. The propshaft is a straight shaft, connecting the crankshaft pulley to the propeller. At the aft of the fuselage a needle bearing supports the shaft and carries the propeller. The entire propulsion system, engine-propshaft-propeller will therefore be carried by the needle bearing and the engine mount.

The fuel tank has a large weight contribution but also changes in weight significantly over the course of flight. Therefore it is beneficial to place this weight close to the center of gravity. The center of gravity of the fuel tank is located at 1.7 m. It is placed close to the bottom of the truss structure to leave enough room for the parachute system. This results in a fuel tank that is located partly under the seat. Therefore this side of the fuel tank is combined with the support structure of the seat. . The volume is 70 litres. The required volume is 56 litres, therefore 70 litres will be sufficient to account for possible expansion of the fuel due to higher temperatures. From this side on, the fuel tank runs along the longerons following the bottom side of the fuselage. The fuel tank will be created using Fused Deposition Modeling (FDM). The Polyphenylsulfone (PPSU) material is resistant to chemicals as well as temperature resistant and flame retardant. The entire fuel tank can be printed in one run, since it will fit in the *Fortus 900mc* and the *Maxum* machines from *Materialise* [22]. The fuel pump, an off-the-shelf component, will be fitted inside the fuel tank, with the fuel lines running along the trusses towards the engine.

5.1.2 Furnishing

After the engine location was determined, the pilot was positioned in the aircraft. Again, the pilot was placed as much forward as possible, not only for the center of gravity, but also for visibility. The feet of the pilot are placed almost all the way in front of the fuselage, leaving some room for flight controls. The pilot is in a semi-straight up position to provide more comfort while allowing the fuselage to keep an aerodynamic shape. This places the pilot's center of gravity on 1.2 m. The seat is designed to run from the knee to the head. The design of the chair will be completely customized to the body of the pilot. A longer pilot can still have head support and a thinner pilot will still have a seat that fits tight. The seat is connected to the truss structure at the joint where the upper leg is, as well as the joint at the waist of the pilot and the connection to the fuel tank. The pilot seat will be created in the *Materialise Mammoth* Vat Polymerization machine using the Tusk Somos ®. This is due to the large size of the seat, as well as the higher strength material.

The cockpit dimensions are 1.1 m in height, 0.3 m in width at the pilot's feet and 0.6 m in width at the pilot's waist. These widths are constrained by the truss structure, of which the design is, amongst others, based on AMA-Con.-Oper.-1-2. The height of the cockpit is designed to meet AMA-Con.-Oper.-1-3. The cockpit depth is 1.56 m and therefore also meets AMA-Con.-Oper.-1-4. With this, all driving requirements regarding the cockpit dimensions are met.

5.1.3 Safety Systems

Due to the fact that this aircraft is an experimental aircraft, it will be equipped with a number of safety systems. The safety systems that are present are a parachute system, the firewall and an engine casing.

The first important safety system is a parachute system. A vertical launch system was chosen such

that the parachute will not be damaged by the push propeller when deployed. The selected parachute is the so called BRS 1350 VLS. This parachute is able to recover an aircraft up to 612 kg and operate at a maximum speed of 222 km/h [30]. The parachute is placed at the back of the pilot seat as that is where the Center of Gravity is located. This will cause the aircraft to come down fairly horizontally. It is connected to the back of the pilot seat, which is connected to the vertical trusses at the pilot's back. A hatch on the top of the fuselage, immediately behind the canopy, will open to allow the ballistic parachute system to shoot through. Keeping the parachute system within the aircraft will not spoil any aerodynamic performance.

A second important safety system is a firewall that separates the pilot from the engine and fuel tank. In case of fire, the pilot and parachute system will be preserved from catching fire. According to Experimental Aircraft Info [31], the firewall can be a titanium plate with a thickness of 0.4 mm.

An engine casing is designed which covers the engine, protecting other structures in the aircraft of the heat that it generates. The engine casing is made of Ultem™[1]. This material can be used by Fused Deposition Modeling methods and withstands temperatures up to 153°C [32, 33]. For additional insulation two sheets of Ultem™ are used for the casing with a section of air in between. A sketch of the engine casing is made in Figure 5.2.

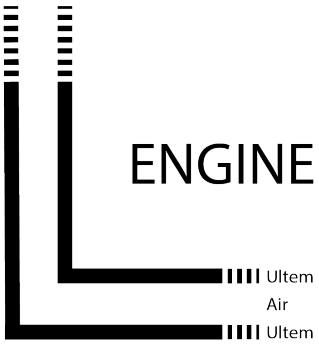

Figure 5.2: Sketch of the engine casing

5.2 Steering & Braking System

In the conceptual design phase it was decided to use hydraulic disc brakes for braking. To use the brakes at their best, the brakes should be placed at the main landing gear. The main landing gear carries the most of the weight, so braking becomes more efficient.

For steering purposes, differential braking is used. Using cables and pulleys would result in a more heavy design. The differential brakes are placed on the front wheels. These front wheels are the wheels with the most space between, making it easier to turn the aircraft. The weight distribution (20% of the weight on the front wheels) makes it possible to use the differential braking considering that commercial aircraft have about 5% - 20% of their weight on the front wheel (used for steering)[27]. The pilot can control the differential brakes with his toes, these toe brakes are installed on top of the pedals. The landing gear topview can be found in Figure 4.21. The actual sizing of the brakes should be done in a further more detailed design.

5.3 Electrical Systems, Data Acquisition & Instrumentation

To finalise the subsystem design a layout of the electrical systems is provided. This layout provides an overview of the required electrical systems and shows how these are connected. Also a data block

[1] Ultem 9085 is a trademark of SABIC Innovative Plastics IP BV.

diagram is discussed which will, among other things, show the data acquisition from sensors that monitor and store data on the structural integrity of the aircraft.

Electrical Systems

In the electrical diagram two main circuits can be distinguished: the aircraft circuit indicated by blue lines in Figure 5.3 and the electronic Engine Management System (EMS) in red, yellow and green. In dynamic, engine running, conditions the two circuits are connected to each other through the fuse box. The EMS circuit connects the Human Interface Connectors (HIC), Engine Control Unit (ECU), fuse box, internal alternators (A & B) and the engine (start relais, for starting the engine). The Aircraft circuit on the other hand connects the battery (Main and Backup), fuse box, internal alternators (A & B) and the external alternator.

The only requirement for the size of the battery is that it needs to be adequate for the essential flight equipment. The minimum voltage on the ECU on start-up has to be $9V$, also in cold weather conditions.

The fuse box connects the two internal alternators (A & B). If alternator A fails, alternator B takes over its functions. It means that the battery is no longer charged and there is no voltage provided for the on-board instruments.

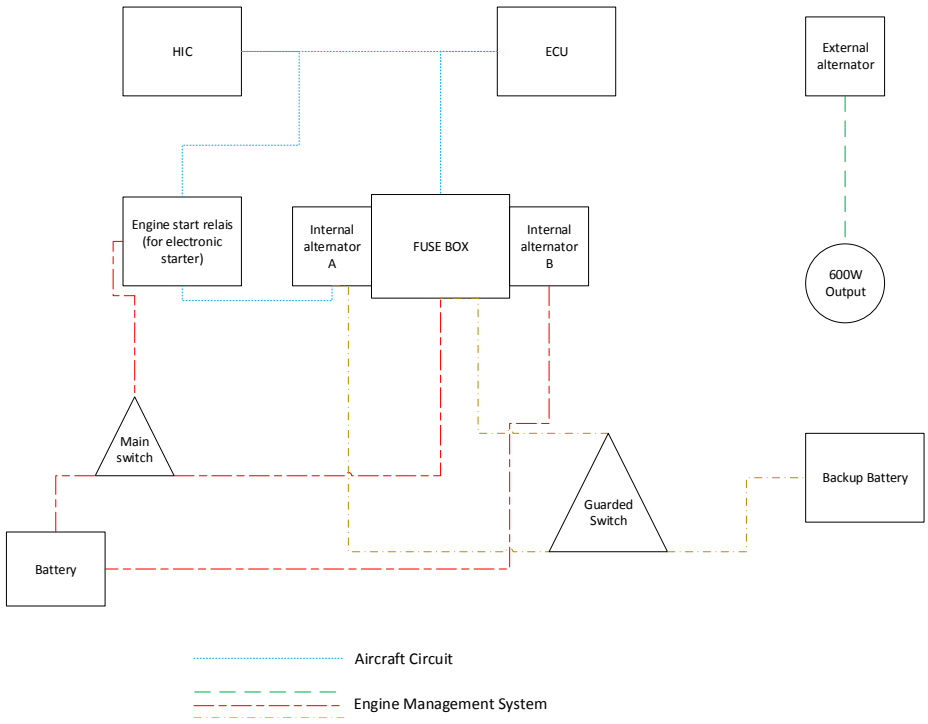

Figure 5.3: Electrical block diagram

- Alternator A: electronic engine components: ignition, injections and sensors.
- Alternator B: start engine, charge the aircraft battery. Also while the engine is running, it can be used for the on-board instruments.

The HIC connects the cockpit (Electronic Flight Instrument System) with the engine and other sensors on the aircraft. The external alternator provides the power for extra equipment in the aircraft,

for example the data acquisition system for the strain gauges. This alternator delivers a max output of $600W$ DC at 6000RPM and an output voltage of $14.2V - 14.8V$.

Data Acquisition & Instrumentation

The data acquisition can be divided into two parts, the first part is the flight data acquisition while the second part is the data acquisition for the experimental part on the aircraft (measuring strain, stress, etc.). The sensors for each part are connected to the same data acquisition system.

The sensors needed and used for the flight data acquisition are also used for the Electronic Flight Instrument System (EFIS). The EFIS consists of three LCD screens: one screen for the Primary Flight Display (PFD), another screen for the Multi-Function Display (MFD) and a final screen for the Engine Indicating and Crew Alerting System (EICAS). The screen for the EICAS can also be omitted and the EICAS can be shown on the MFD. For the MFD, the same sensors as for the PFD should be connected together with some other necessary and useful sensors. The MFD can be used as a back-up if the PFD fails. The following needed data and their sensors are needed at least:

- Attitude of the aircraft: Microelectronic sensors are used for this. They calculate the pitch, roll and yaw movements away from a known reference attitude.
- Aircraft heading: This is done by magnetic directions-sensing, a magnetometer or a magnetic flux valve.
- Altitude and airspeed: Sensors that measure static and ram air pressure are used. An Air Data Computer (ADC) combines those air pressure and temperature sensors with a computer processor. From this the pressure altitude, indicated airspeed, vertical speed and true airspeed are calculated.
- Navigation receivers: The onboard navigation should receive the following signals: Instrument Landing System (ILS), Global Positioning System (GPS), Very High Frequency (VHF) and VHF Omni Directional Radio Range (VOR).
- Weather data: onboard software receives information from the Stormscope/Strikefinder signals.

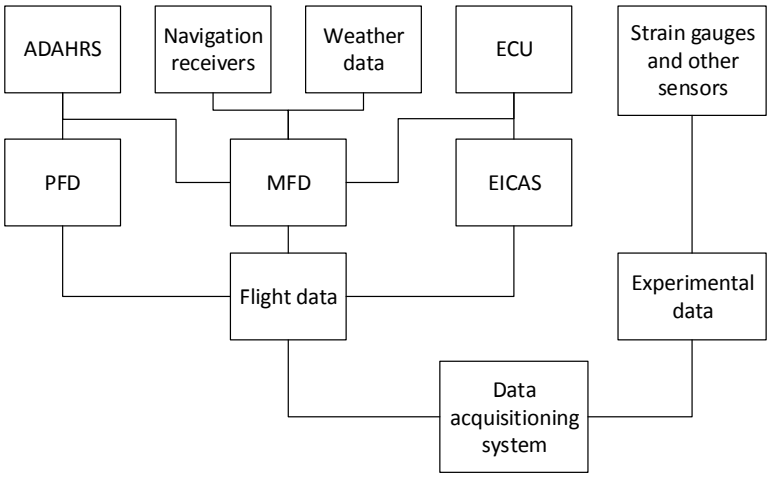

Figure 5.4: Data block diagram

The attitude, heading, altitude and airspeed of the aircraft are combined in the Air Data Attitude Heading Reference System (ADAHRS). The sensors and computer which processes the sensors input

are all included in this system. The ADAHRS is connected to both the PFD and MFD while the navigation receivers and weather data are also connected to the MFD. For the EICAS, the ECU (which is connected to the sensors in the engine) should also be connected with the EICAS LCD screen or with the MFD screen.

For the experimental data acquisition part, the sensors needed to measure strain, stress, torque, et cetera are place on the most critical parts of the aircraft that have been Additively Manufactured. An example for this is to put a strain gauge on locations in the fuselage structure and wings. After the flight it will be possible to evaluate the data, draw conclusions and make recommendations for further design.

Chapter 6

Manufacturing, Assembly & Operations

Considering this aircraft is a unique project with a design as final result that most likely will only be produced once, the exact production plan and efficiency of the production process is less important. The most important part of the production phase is how and where the parts will be manufactured and once they arrive, how they will be assembled. The post-processing of the produced parts is quite an important aspect for this aircraft.

6.1 Production Plan

Additive Manufacturing allows for manufacturing complex parts in one step, reducing the assembly time of these parts. However, once they are printed they might still need post-processing and of course still need to be assembled into the final aircraft. This section explains how to go from printed part to the final product.

Throughout the design different manufacturing processes with different materials are used. All of these have different production locations and need different levels of after-treatment and different activities before they can be assembled. SLM is used for the landing gear and the engine mount, these parts will therefore be printed at *LayerWise* in Leuven, Belgium. The main reason for this is that during a visit to their headquarters in Leuven it was mentioned that they would scale up the maximum build volume of their machine tremendously, allowing for the landing and engine mount to be printed in one piece. No other companies were found that can print that large at the moment, therefore *LayerWise* will be the production facility for these parts. The SLM process has a very high surface finish removing the need for post-processing[18]. Considering that in their process they can reach up to 97% of the material properties (such as Young's modulus) of the bulk material, no heat treatment is deemed necessary. The overhang angles in these parts are very small, hence no support structures have to be removed afterwards.

Direct Energy Deposition will be used for the manufacturing of the wing root sections. Current market leader in DED is *DM3D Technology LLC*, which can currently print parts up to a few meters in size [34, 35]. The material properties of the printed part are lower than for SLM, therefore a form of heat-treatment, such as HIP, is required for a highly loaded part. The surface finish of these parts is also lower than the surface finish of SLM. Considering that this part will directly determine the contour of the airfoil of the wing, the surface finish will to be improved during the post-processing to make sure the aerodynamic performance is not negativey influenced. Lastly, the required support structure is removed from the final product.

The most widely used manufacturing process in this design is Vat Polymerization or Stereolithography. To manufacture all of these parts, the *Materialise Mammoth* machine will be used which is located at *Materialise*'s headquarters in Leuven, Belgium. Due to both the high complexity and

large overhang angles (depending on the printing direction), support structures for these parts are necessary. These have to be removed afterwards, therefore some form of post-processing is required. However, the largest after-treatment for this process is the required curing. When the parts come out of the *Mammoth* machine they are only 95% cured (as explained during the excursion to *Materialise*). The other 5% takes another few months to cure under normal circumstances. Since these parts will be used as structural components, they have to be almost 100% cured to prevent this problem from becoming a liability. These parts will therefore be printed and stored until they are fully cured. This process will have to be discussed with *Materialise* to see if this process can be sped up under for instance the exposure of UV light. The long curing process of these parts will therefore require them to be printed long before the other parts are printed.

The aircraft will be fully assembled in a hangar near Lelystad Airport to keep the transport of the full aircraft to a minimum. However, as this is an experimental aircraft with novel manufacturing techniques, it is required to test these parts first in adequate testing facilities. Therefore, all parts will first be shipped to Delft University of Technology. Only after all tests are conducted, will they be shipped to Lelystad. For all parts manufactured using VP or SLM the logistic effort is minimal as the road transport for these parts can easily be arranged. The wing-root sections do require some more effort, since *DM3D Technology* is located in Michigan, USA. The easiest way to ship these parts is most likely through container transport by road and water. These parts can then be picked up in the harbor of Rotterdam after which they can be tested in Delft. Due to the long curing time for the parts produced using VP, the longer transport time the DED manufactured parts need is less of a problem.

Once the parts have arrived in Lelystad, the actual assembly will start, the middle part of the fuselage is used as a base to which all other parts shall be attached. An outline of the Assembly & Integration plan can be found in Figure 6.1. The actions which are indicated as parallel activities can of course also be done after one another depending on the size of the assembly crew, but this gives them some freedom in order of assembly. The assembly plan is mostly based on accessibility of all parts, which is most important for the control actuation system. After the fuselage and wing root sections are integrated with the control actuation system, the assembly crew will have to check if the control actuation system works as intended using dummy controls and control surfaces. Only once all other internals are added and the other major structural parts are assembled, external features such as the wing foil and shear/skin panels for the fuselage are added.

6.2 Operations & Logistics Concept

Once the aircraft is assembled, the logistical aspect of the project is trivial, as it will always be operated from the same airport and is stored in a hangar near that airport. More interesting, is the operational aspect of this experimental design project. Of course, a ground crew is required to operate the aircraft. However, in this case these people will have to be highly skilled technicians. The accessibility and inspectability of the complex parts is not as simple as in a conventional aircraft. Finding cracks in the parts can therefore be a meticulous exercise requiring a high attention to detail and experience in aircraft maintenance. This might even be performed by the scientific staff associated with the project, since this is an experimental aircraft with high academic value. An investigation of for instance crack growth in AM parts can be based off the aircraft.

During the flight experimental data is obtained on some of the aircrafts components. As already explained in Section 5.3 experimental data is obtained this may include, but is not limited to, strains

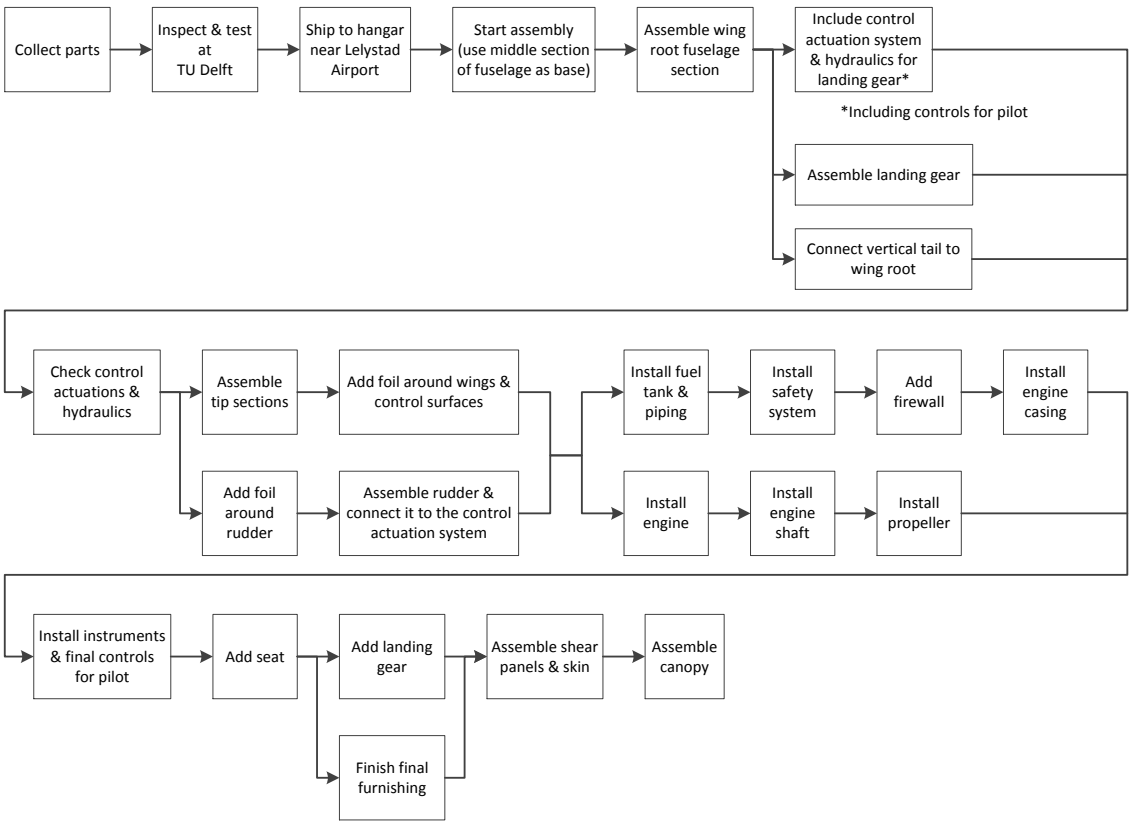

Figure 6.1: Assembly & integration plan

and stresses in certain highly loaded parts of the aircraft. The data from these strain gauges is to be analysed after the flights and is to be matched to the flight data to see which loads the stresses and strains correspond to. Scientific staff or students will need to perform these activities to take full advantage of the research opportunities this experimental aircraft has to offer.

Chapter 7

Design Evaluation

This chapter investigates the performance of the tandem aircraft with respect to a large array of different parameters. First, it is checked whether the aircraft respects the requirements set by the problem constraints and team. This is summarized in a compliance matrix. The results of a CFD analysis are also presented and recommendations are given to improve the stability and controllability of the aircraft. The case study that was performed by the team is discussed and the conclusions drawn from it are given. This chapter also gives an overview of the Reliability, Availability, Maintainability and Safety (RAMS) characteristics and risk associated with the aircraft. Lastly, the cost and market analysis together with the sensitivity and sustainability analysis is also elaborated on.

7.1 Performance Analysis

The performance analysis is conducted to assess the primary functions of the design and to what extent they comply with requirements that the design is subjected to. In Appendix A the full list of requirements can be found. Before demonstrating compliance of individual requirements it can be shown that driving design parameters naturally imply compliance with some of them. In the detailed structural design safety factors in accordance with the requirements have been used. Therefore Req. AMA-Tech.-Struct.-Loads-1 (Landing gear load factor), AMA-Tech.-Struct.-Loads-2 (Positive load factor) and AMA-Tech.-Struct.-Loads-3 (Negative load factor) are satisfied. Figure 7.1 shows the maneuvering and gust diagrams that were created. These show that Req. AMA-Tech.-Struct.-Loads-4 (Gusts, extended) − note that the aircraft does not feature any high lift devices − and AMA-Tech.-Struct.-Loads-5 (Gusts, retracted) are also fulfilled by not exceeding the maximum load factors that were used for the design for the given gusts. Also Req. AMA-Con.-FAA-1-4 (Two seater aircraft) until Req. AMA-Con.-FAA-1-9 (Non-pressurized cabin) are fulfilled by driving design parameters.

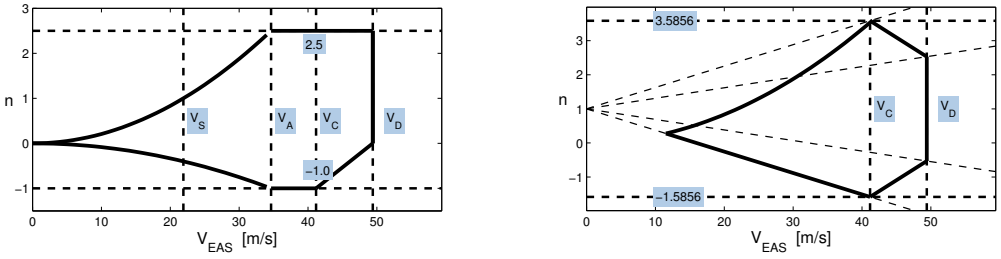

(a) Maneuvering diagram

(b) Gust diagram

Figure 7.1: Maneuvering and gust diagrams

The complete set of performance requirements is particularly important and are therefore individually evaluated.

Req. AMA-Tech.-Perf.-End.-1 (Endurance) covers arguably the most important performance specification. It is explicitly mentioned in the mission statement and is therefore one of the driving design parameters. The final concept is determined to definitely be able to loiter for two hours. The MTOW of the Class II weight estimation along with the fuel fraction determined in the Class I weight estimation gives a total fuel weight of 44.6 kg. Because simulations and calculations in the final design show that the inputs for both weight estimations are very accurate, the fuel weight also complies with the requirements. The fuel tank that is included in the final design has a capacity of 70 l or 56 kg and therefore is sufficiently large.

Req. AMA-Tech.-Perf.-End.-2 (Design airspeed) covers the airspeed of 85 kts. The entire aerodynamic design is based on this loiter speed and shown in Section 3.4. Therefore, this requirement is also met. Req. AMA-Tech.-Perf.-End.-3 (Design altitude) is also used in every aerodynamic calculation and can therefore be regarded as being met.

Req. AMA-Tech.-Perf.-Climb-1 (Climb rate) is also a driving parameter on which the design point of the Class I weight estimation shown in Figure 2.3 in Section 2.2 is based. Because the design point has not changed and both aerodynamic design, propeller and engine selection and maximum part weights are based on this point the requirement is also met. These initial calculations have also shown that the Req. AMA-Tech.-Perf.-Man.-1 (Maneuvering) is more critical than the climb requirement. The ability to pull a 2.5g pitch-up maneuver drives the power-loading value down more than the maneuvering as is shown in the Midterm Report [3]. By the same reasoning however by using a design point that satisfies Req. AMA-Tech.-Perf.-Man.-1 (Maneuvring), also Req. AMA-Tech.-Perf.-Climb-1 (Climb rate) is met.

For Req. AMA-Tech.-Perf.-FD-2 (Longitudinal static stability) until Req. AMA-Tech.-Perf.-FD-5 (Convergent Dutch Roll) it is important to mention that only static conditions are evaluated. Dynamic behaviour modelling requires specific control derivative values. These are however not straight forward to determine. Extensive aerodynamic analysis could provide them, however, this is not in the scope of the project. The aircraft is designed to be statically longitudinally stable as explained in Section 3.1. However, several other analysis methods show that the static longitudinal stability might be problem. However, due to the ambuigity in the results and the thorough design for static longitudinal stability, AMA-Tech.-Perf.-FD-2 (Longitudinal static stability) is still considered met. Static lateral stability is not investigated at the moment, therefore no conclusion can be drawn on the compliance to that requirement. Trimming the aircraft is investigated extensively for the loitering phase, while the controllability for landing and take-off is investigated for sizing the elevator. Therefore, also Req. AMA-Tech.-Perf.-FD-1 is considered met.

When evaluating operational requirements it can be concluded right away that these again were used as input for preliminary design point as shown in Figure 2.3 in Section 2.2. The values used for pilot weight, take-off and landing distance and cockpit size originate from these and are met. Based on the information as presented in Section 5.1, Section 2.2 and specifically the conclusions from Figure 2.3 these requirements have all been met.

In order to comply with FAA regulations, these requirements also play an important role in the design. In Section 8.1 it can be found that even though chances are slim that the aircraft is able to fly under LSA regulations, it can however fly as an experimental aircraft, as will be discussed in Section 8.1. For MTOW the weight estimations of Section 2.2 have shown that the final design stays more than 150 kg under the maximum allowed mass as stated in Req. AMA-Con.-FAA-1-1 (MTOW limit). FAA

regulations also limit stalling speed and maximum speed. The stall speed is currently 2.5 kts higher than is needed to meet Req. AMA-Con.-FAA-1-2 (Stall speed). However, it might be worthwhile to use the control surfaces for additional lift since they are quite large. The FAA should however be consulted to see whether this is allowed. The only drawback is therefore whether or not the FAA allows it, but since the outlook is positive, also Req. AMA-Con.-FAA-1-2 is considered met. Furthermore, preliminary calculations have shown that, based on CFD data for loiter conditions, a theoretical maximum velocity of 128.9 kts CAS can be achieved. This only just exceeds the regulations. Taking into account that the CFD computations do not include landing gear and wheels and the Reynolds number is slightly off for these conditions the theoretical maximum decreases. Furthermore, in case the actual maximum velocity turns out too high it is very simple to limit the maximum RPM of the engine.

The last two requirement categories that are evaluated are sustainability, Req. AMA-Con.-Sust.-1, and operational lifetime, Req. AMA-Con.-Sust.-2. In Section 7.11 it is explained that is is difficult to quantify the carbon footprint of the final concept. Variables like the origin of the energy used for production, transport distance and number of flights make it impossible to definitively quantify its sustainability. Various aspects show both better and worse results in comparison to conventional LSA aircraft, however for development of a single aircraft this requirement is not considered met. It is however important to note that the aircraft structure has been designed for at least 20 flights, therefore Req. AMA-Con.-Sust.-2 is considered met.

Concluding the performance analysis, one could state that nearly all requirements are met. The ones that cannot be definitively classified as being met, mostly need further investigation research. An example of such a requirement is is the dynamic flight behaviour. The only requirements that have not been met, or are not likely to be met if the necessary modelling production and testing was conducted, are Req. AMA-Con.-Sust.-1 (Sustainability) and AMA-Con.-FAA-1 (Light sport aircraft). Naturally, for a feasibility study subject this requirement is something that should be implemented in the design, however competing with larger scale production is simply unrealistic. Also it should be noted that certification in the LSA category is a target, rather than a hard requirement. Even though all top-level requirements to be certifiable in the LSA category are met (Req. AMA-Con.-FAA-1-1 through AMA-Con.-FAA-1-9), overall certification in the LSA category – which requires meeting an additional 1200 requirements, as explained in Section 8.1 – is not realistic. Flying under an experimental aircraft catagory certificate is a more realistic alternative, as that “only” requires meeting 600 additional requirements. A complete overview of all requirements and sections in which the justification is treated can be found in Section 7.4.

7.2 Aerodynamic Analysis

The final aerodynamic design is evaluated to see whether it meets all requirements and whether there are any issues associated with it. As already explained in Section 3.4, the aircraft has two elliptical wings with the front wing underneath the fuselage, while the aft wing is positioned in a high wing configuration to move it out of the wake of the front wing. However, a high risk is associated with that configuration due to the blanketing effect. This phenomenon occurs when the aft wing is fully covered by the wake of the front wing, when that wing has stalled. Recovering from such a flight condition proves to be difficult, since both wings lose most of their lift. To prevent that from happening, several warning systems, as explained in Section 3.4, could be installed to let the root section of the front wing stall first. This warns the pilot such that corrective action can be undertaken. These warning systems are a stall strip on the root section of the front wing and vortex generators on the tip sections of that wing. In the evaluation of the design it has therefore also been investigated whether blanketing

is indeed such a high risk to decide whether these warning systems are even needed.

This design is evaluated extensively using the `OpenFOAM` CFD analysis program. Readers who are particularly interested in the details of these CFD computations are advised to consult Appendix D. CFD computations are performed for various angles of attack in intervals of 2.5°. This relatively large step size is required to limit the computational demands, since the performed computations already took a cluster of 40 quadcore computers two full days to solve. For the same reason the landing gear and propeller are also omitted from the model. The result of these computations is presented in Figure 7.2, where the `XFLR5` result is used as a reference.

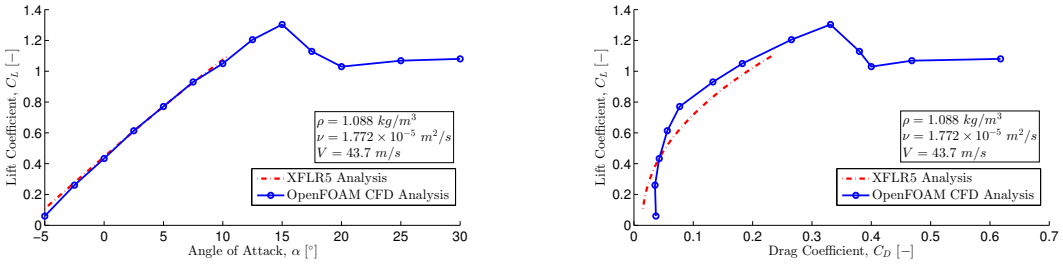

(a) C_L - α (b) C_L - C_D

Figure 7.2: Lift and drag polars for final aircraft design from CFD results

At $\alpha = 2.5°$ the aircraft has sufficient lift for sustained flight. At that angle of attack the L/D is 10.8, which is very close to the initial estimation of $L/D = 11$, used in the conceptual design phase for all initial sizing of the aircraft. Therefore, no design iterations with respect to the L/D ratio of the aircraft are required. Flying at $\alpha = 2.5°$ is actually better than at $\alpha = 0°$, since then the fuselage has zero lift, while at $\alpha = 0°$ it produces downforce and therefore generates more drag.

The maximum lift coefficient, however, is lower than what was estimated in the conceptual design phase. A $C_{L_{max}}$ of 1.54 is required to meet Req. AMA-Con.-FAA-1-2, while the CFD results show that the actual $C_{L_{max}}$ is 1.34 yielding a stall speed (V_S) of 47.5 kts. As such, the design should be altered slightly to increase $C_{L_{max}}$ otherwise the aircraft cannot be certified in the LSA category. The difference is however reasonably small, and an innovative solution using the control surfaces might be employed. These surfaces are quite large and can be used to increase $C_{L_{max}}$, by deflecting both ailerons and elevators to a new trim condition. Because the control surfaces do not count as lift-enhancing devices and only small deflections are required for the actual control of the aircraft, this may present a viable option. The FAA should be contacted on this matter to see whether this is allowed. Another option to increase $C_{L_{max}}$ would be to add leading edge slots which delay flow separation at the leading edge, increasing $C_{L_{max}}$. For the moment it is assumed that the solution using the control surfaces is allowed and therefore Req. AMA-Con.-FAA-1-2 is considered met.

From the controllability analysis of the aircraft it was found that the front wing needs to account for 55% of the lift, while the back wing should account for 45% of the lift. The CFD analysis shows that the front wing accounts for 58% with the back wing accounting for 40% of the lift - the rest is accounted for by the fuselage. However, the moment coefficient is very close to zero, which is beneficial as the elevator is then not required in the loitering stage, minimizing the drag during that phase. For the overall stability, the CFD results show some areas which require more work. $\partial C_m/\partial\alpha$ is slightly positive, indicating an unstable aircraft. This can be solved by adding more ballast to move the CG forward or by moveing the aft wing more backward. At high angles of attack C_m is however quite negative since the front wing stalls first while the back wing is not stalling yet.

At those high angles of attack, the blanketing effect has been identified as a high risk. One of

the main reasons for performing an extensive CFD analysis of the aircraft was to investigate whether blanketing was indeed a problem for this aircraft. The aforementioned mitigation strategies are therefore not applied to the CFD model to investigate whether they are actually needed. Firstly, it is checked which part of the front wing stalls first, since it was identified that the root section of the wing had to stall first to serve as a warning to the pilot. At 12.5° the first flow separation occurs at the front wing (indicated by the low velocities in Figure 7.3(a)), while at the back the flow is still fully attached. Thus, the tip section stalls before the root section and the warning systems are indeed required to let the root section stall first.

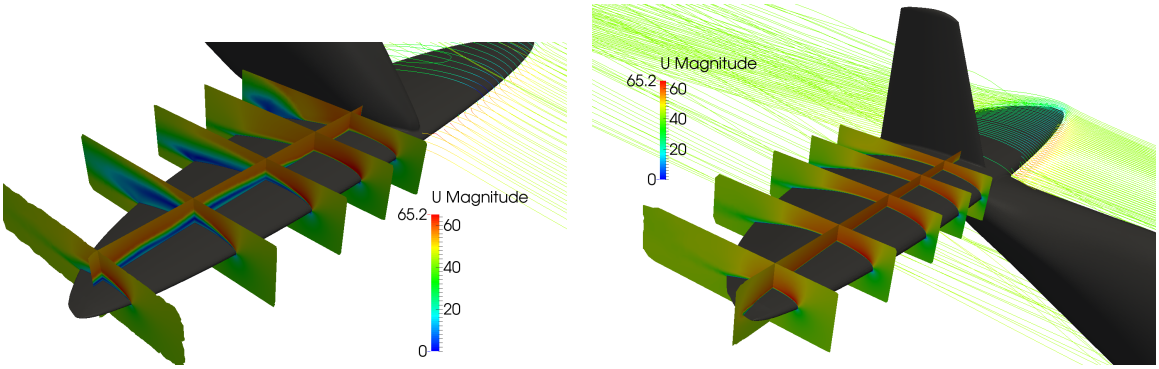

(a) Front wing (b) Aft wing

Figure 7.3: CFD flow separation visualisation at $\alpha = 12.5°$. Velocity magnitude is indicated in $[m/s]$.

The question remains whether the blanketing is indeed such a large problem for the aircraft. Therefore, the wake of the front wing is compared for $\alpha = 20°$ and $\alpha = 25°$ in Figure 7.4. At $\alpha = 20°$ the front wing is almost fully stalled, but the wake of the front wing does not yet hit the back wing but instead moves underneath it. Under those conditions, the back wing is not yet stalled. At $\alpha = 25°$, however, the back wing is fully in the wake of the front wing, causing it to stall as well. Therefore, it seems the blanketing effect only occurs at higher angles of attack than $\alpha = 20°$, which is already 5° more than the angle of attack for $C_{L_{max}}$. Thus, in normal flight conditions the blanketing effect is no problem at all. The warning systems might be employed as an extra safety feature to make sure the aircraft never flies at $\alpha = 25°$. However, considering the aft wing generates much more lift at high angles of attack (when the front wing starts stalling), thereby generating a large nose down moment, such a flight condition will never be reached and the extra warning systems would not be needed.

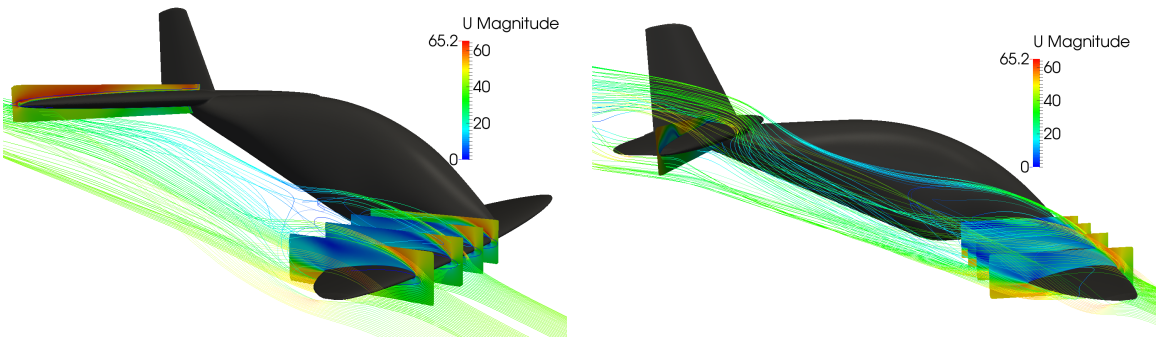

(a) $\alpha = 20°$ (b) $\alpha = 25°$

Figure 7.4: CFD comparison of blanketing effect at high angles of attack

Concluding, the L/D ratio of the aircraft is very close the value used for all preliminary sizing of the aircraft and requires no further design changes. The $C_{L_{max}}$ of the aircraft is however lower than anticipated, which might require an investigation into leading edge slots or into whether the FAA allows for using the control surfaces to meet the stall speed requirement. Furthermore, the stability of the aircraft should be investigated in more detail and it might require significant changes to the design. On the other hand, the blanketing effect is less of a problem than anticipated which might even eliminate the need for safety systems to warn the pilot at high angles of attack.

7.3 Stability & Controllability Analysis

The stability and controllability design parameters of the tandem aircraft are explained in Section 3.1 and Section 3.2 respectively. The following section evaluates the stability and controllability performance of the aircraft and proposes alternatives to improve them. Furthermore, the ground stability and the eventual amount of ballast required for stability are also explained in this section. Finally the stick forces and displacements calculations are elaborated on in this section.

Further Stability Analysis

The aircraft has been designed to be both statically stable and controllable during flight, as explained in Section 3.1. However longitudinal and lateral stability has not been checked thoroughly. This would require a much more in-depth analysis and thus has not been developed in this report due to time constraints and questionable relevance to the scope of the project. It is however touched upon in the CFD results as discussed in Section 7.2. On the other hand, the ground stability of the aircraft has be investigated. Indeed, knowing whether the aircraft does or does not tip over when it is stored in a hangar should be known. This resulted in the creation of a aircraft loading diagram and it can be seen in Figure 7.5.

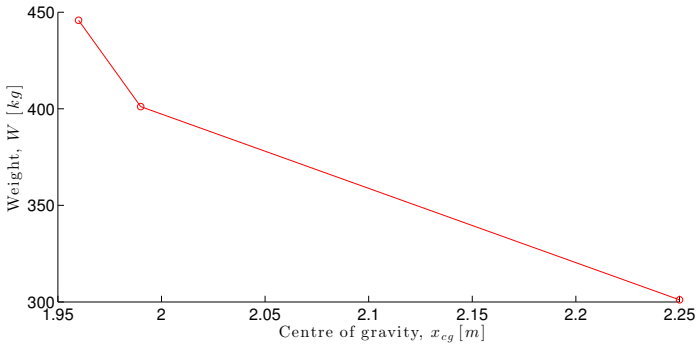

Figure 7.5: Aircraft loading diagram

From Figure 7.5 the most aft CG location is 2.25 m from the nose, hence more forward then the rear landing gear located at 2.41 m from the nose. Hence the aircraft will not tip backwards when the pilot gets out of the cockpit.

Ballast

In the Class II weight estimation it was assumed that the pilot's weight was 100 kg. To allow lighter pilots to use the aircraft it is necessary to use ballast to keep the aircraft stable and controllable. Ballast is extra weight that is placed in the nose of the aircraft with the purpose of moving the CG forwards. The CG of the ballast was chosen to be at 0.1 m of the nose: this was the most forward

location possible. Hence the weight of ballast to move the CG forward can be kept to a minimum. Knowing the CG of the ballast as well as the weight of the pilot and the desired aircraft's CG location, the weight of the ballast can be calculated. The ballast weight is calculated for an empty fuel tank, thus the most aft CG location. In Table 7.1 it is possible to see the amount of ballast required depending on the weight of the pilot.

Table 7.1: Ballast weights

Pilot mass $[kg]$	Ballast mass $[kg]$	Number of steel blocks
100	9.7	5
95	11.7	6
90	13.7	7
85	15.7	8
80	17.6	9
75	19.6	10
70	21.6	11
65	23.5	12
60	25.6	13

Next the material used for the ballast needed to be determined. Since the volume available in the nose is limited, using sand or water would not fit due to their low density. However, if steel is used the volume of ballast can be limited to a small size, thus steel was chosen as the material for ballast. Finally the amount of steel blocks of 2 kg required for ballast is also listed in Table 7.1.

Possible Improvements

More investigation into the static stability characteristics should be undertaken, since some analyses point to an unstable aircraft. Several mitigation strategies to make the aircraft more stable are therefore investigated. One of them could be to reduce the amount of ballast needed. This could be achieved by sweeping the front wing forwards. In addition to moving the CG slightly forwards, forward swept wings would make their root section stall first and giving the aircraft a more aggressive look [8]. If the root section of the wing stalls first, the aircraft will be safer and the use of stall strips would no longer be required. The reason forward swept wings were not chosen is mostly a structural reason: the root section needs to be stronger than that of an un-swept wing due to the added moment and an AM would need to be greatly over-designed. The location of the control surfaces could also be revised since their location was dictated by AM size limitation. In addition, applying dihedral to the front wing and anhedral to the back wing could improve the lateral stability of the aircraft. Finally, the use of fly-by-wire for actuating these surfaces could greatly improve the ailerons and elevators efficiency since it would then be possible to move all four surfaces at the same time and in the desired way.

Critical Stick Deflection and Stick Force Case

To find the critical load factor for which the stick force and stick deflection are highest, this load factor is checked per maneuver. It was found that the maneuver with the highest load factor is the $2.5g$ pull-up maneuver. For this critical maneuver the stick force and the stick deflection are calculated. To do so the previously designed elevator and its values are used, as discussed in Section 3.2.

From the stick deflection calculation taken from [36] a deflection of $0.7661°$ per g is found. The result is a deflection of $1.9152°$ at a $2.5g$ pull-up maneuver. A note has to be made that this calculation is done with an old and negative value of $C_{L_{\delta_e}}$ whereas the most recent iteration of this value is positive.

To find the stick force a different method was used, this method was discussed in a course taught by Virginia Tech [37]. The method uses the $dC_h/d\alpha$ and $dC_h/d\delta_e$. It was found that the influence of $dC_h/d\alpha$ is relatively small with respect to the influence of $dC_h/d\delta_e$.

To gain knowledge about what order of size these values should be, `XFOIL` was used to estimate the $dC_h/d\alpha$ and $dC_h/d\delta_e$ at different angles of attack and for different elevator angles assuming a linear relation. This resulted in an estimated $dC_h/d\alpha$ of -0.0176 and an estimated value of $dC_h/d\delta_e$ of $-3.452 \cdot 10^{-4}$. The stick force per g is then found to be $-0.136\,N$ for these estimated values.

The deflection per g is compared to the results in [36], where it is stated that the stick force per g should be around 4 N/g, therefore the found value can be considered incorrect. One of the culprits is an error in the dC_m/dq as in the calculation this coefficient is estimated to be 0.5685. In [36] this coefficient can be found for different aircraft, in all cases this values is more negative than -5. Changing this value does not influence the final result greatly, and a different more significant error is suspected to be the flaw in this calculation. The error in the stick forces per g is significant and research in this direction is recommended in future work. As stated earlier, this calculation is done with an old and negative value of $C_{L_{\delta_e}}$. The newest value which is positive was not taken into account, therefore the consequences of this change should be taken in account in future research.

7.4 Compliance Matrix

In this part all requirements are evaluated, that is done in the compliance matrix. The Compliance Matrix is split up into two parts: first the hard requirements are evaluated, these can be found in Table 7.2, and the targets are assessed in Table 7.3. All requirements themselves can be found in Appendix A. The requirements that have been met are indicated with green. Requirements that cannot be definitively be classified as being met are left open by using a yellow tag and question mark. These are however, after appropriate research and calculations, expected to also be met. Only two requirements are not met, namely sustainability and certification in the LSA category. These are indicated using a red color. All reasoning has been very briefly discussed in Section 7.1 but for more information the reasoning can be found in the sections stated in the rightmost column.

7.5 Performed Verification & Validation Activities

Parts of the design relied heavily on certain software packages. Mainly the Topology Optimization software had a great influence on the structural design process. To properly understand the limitations and accuracy of the results provided by the software a case study was performed. The goals of this case study are discussed as well as the approach and results.

The ultimate goal of validating the TO software would be to determine whether the results are indeed the most weight optimal structures. To properly perform such a test would require extensive testing of multiple models which iteratively converge to an optimal structure. Also the interpretation of *optimal* should be carefully defined. For instance peak stress or failure load per unit weight might not be entirely applicable as the software optimizes for total strain energy. In the interest of time such an extensive and iterative validation process is not desirable. Instead it is chosen to look into a single output of the software and see whether the software has correctly computed the general stress lay-out and certain deflections. This approach can also provide insights in the effect of a highly anisotropic manufacturing method which can be of value throughout the entire structural sizing process.

To test the limits of the software it was decided to create a model that was loaded in both shear, torque and bending. A cantilever beam that is loaded slightly off center was chosen. The test

Table 7.2: Compliance matrix for hard requirements

Requirement	Met	Rationale
AMA-Tech.-Perf.-End.-1 (Endurance)	✓	Section 7.1
AMA-Tech.-Perf.-Man.-1 (Maneuvering)	✓	Section 3.2
AMA-Tech.-Perf.-FD-1 (Controllability)	✓	Section 3.2
AMA-Tech.-Perf.-FD-2 (Longitudinal static stability)	✓	Sections 3.1 and 7.3
AMA-Tech.-Perf.-FD-3 (Longitudinal dynamic stability)	?	Sections 3.1 and 7.3
AMA-Tech.-Perf.-FD-4 (Lateral static stability)	?	Sections 3.1 and 7.3
AMA-Tech.-Perf.-FD-5 (Convergent Dutch Roll)	?	Sections 3.1 and 7.3
AMA-Tech.-Manu.-1 (AM techniques)	✓	Section 6.1
AMA-Tech.-Manu.-2 (AM techniques)	?	Sections 6.1 and 7.1
AMA-Tech.-Manu.-3 (AM techniques)	?	Section 3.2
AMA-Tech.-Struct.-Loads-1 (Landing gear load factor)	✓	Section 4.7
AMA-Tech.-Struct.-Loads-2 (Positive load factor)	✓	Chapter 4
AMA-Tech.-Struct.-Loads-3 (Negative load factor)	✓	Chapter 4
AMA-Tech.-Struct.-Loads-4 (Gusts, extended)	✓	Section 7.1
AMA-Tech.-Struct.-Loads-5 (Gusts, retracted)	✓	Section 7.1
AMA-Con.-Sched.-1 (Schedule)	✓	Section 8.2
AMA-Con.-FAA-1-1 (Maximum take-off weight)	✓	Section 2.2
AMA-Con.-FAA-1-2 (Stall speed)	✓	Section 7.2, but FAA should be contacted on the solution
AMA-Con.-FAA-1-3 (Maximum airspeed)	✓	Sections 7.1 and 7.2
AMA-Con.-FAA-1-4 (Two seater aircraft)	✓	Design
AMA-Con.-FAA-1-5 (Single engine)	✓	Section 4.8
AMA-Con.-FAA-1-8 (Fixed landing gear)	✓	Section 4.7
AMA-Con.-FAA-1-7 (Fixed propeller)	✓	Section 3.5
AMA-Con.-FAA-1-9 (Non-pressurized cabin)	✓	Section 4.6
AMA-Con.-FAA-2 (Airworthiness certificate)	?	Section 8.1
AMA-Con.-Oper.-1 (Single seat aircraft)	✓	Design
AMA-Con.-Oper.-1-1 (Payload weight)	✓	Section 2.2
AMA-Con.-Oper.-2 (Operative from Lelystad)	✓	Section 2.2
AMA-Con.-Oper.-2-1 (Take-Off length)	✓	Section 3.5
AMA-Con.-Oper.-2-2 (Landing length)	✓	Section 5.1

Table 7.3: Compliance matrix for targets

Requirement	Met	Rationale
AMA-Tech.-Perf.-End.-2 (Design airspeed)	✓	Section 3.4
AMA-Tech.-Perf.-End.-3 (Design altitude)	✓	Section 3.4
AMA-Tech.-Perf.-Climb-1 (Climb rate)	✓	Section 2.2
AMA-Tech.-Struct.-Maint.-1 (Maintenance)	✓	Section 7.6
AMA-Con.-FAA-1 (Light sport aircraft)	X	Section 8.1
AMA-Con.-FAA-1-6 (Reciprocating engine)	✓	Section 4.8
AMA-Con.-Sust.-1 (Sustainability)	X	Section 7.11
AMA-Con.-Sust.-2 (Operational lifetime)	✓	Section 8.2

specimen was printed with a *Builder 3D* desktop printer which prints PLA and which has size limits of $20\,cm \times 22\,cm \times 16\,cm$. This resulted in model final dimensions of $122\,mm \times 102\, \times mm$ for the base and a height of $160\,mm$, where the model was printed from the base up. This beam was loaded by adding weights on a pin which is connected through a hole near the tip of the model. During the

loading the stresses were determined using a Direct Image Correlation (DIC) system. This system consists of two cameras pointed at the specimen from a different angle. The specimen has previously been prepared such that there are many dots with an approximate size of 0.5 mm on the surface. The two cameras measure the displacement of these dots and thus the strain of the surface of the model.

Figures 7.6(a) and 7.6(b) show the surface displacement of the model for a load at the tip of 205 N. Most notable from these figures is how well they correspond to the ideal case of a bending cantilever beam: negative displacements in the x direction above the centroid line and positive displacements below. Also the displacement in y direction appears to be as expected: all negative values that increase in magnitude towards the tip. It should be noted that the actual values found in the figure are well below the noise levels of the Direct Image Correlation system. The values should therefore not be trusted, yet the displacement distribution correctly represents the actual displacements. The test specimen failed at a load of 606 N. It sheared along one of the printed layers near the base of the model.

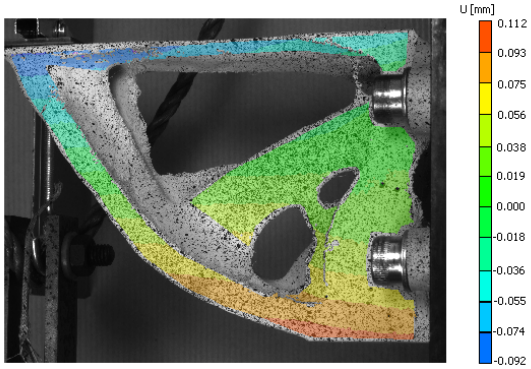

(a) Test setup result displacement in x

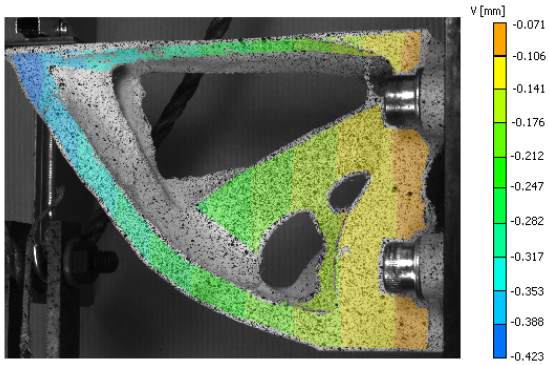

(b) Test setup Result Displacement in y

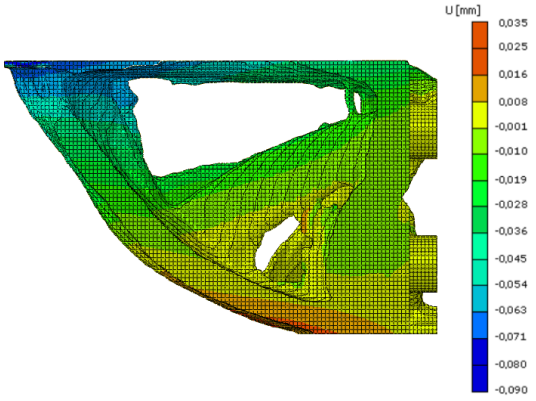

(c) TO software result displacement in x

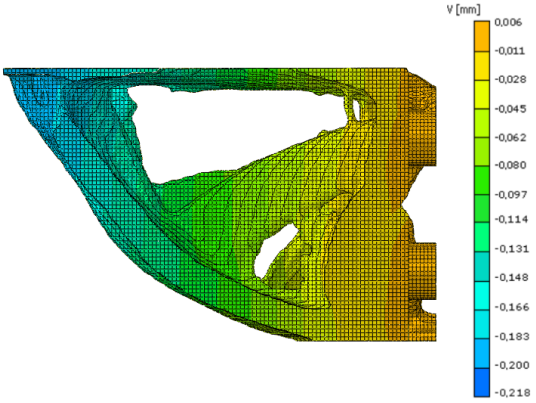

(d) TO software result displacement in y

Figure 7.6: Skin displacement in x and y direction for a load of 200 N for both test and simulation results. Positive to the right and upwards

The Topology Optimization simulation ran with a load of 200 N. The displacements of the final model according to the FEM used in the TO simulation are shown in Figures 7.6(c) and 7.6(d). When the displacement distributions of the test and simulation are compared it can be concluded that they are quite similar. This appears to be slightly more so for the y deflections than for the x deflections. The actual values are not entirely comparable but they are in the same range.

Figure 7.7 shows the strains obtained from the DIC output and the TO software output. As it requires post processing from DIC system to obtain these values it was expected that these were

less similar to the software output. This is correct for the distributions but the actual values are surprisingly comparable. The locations of the peak strains are in the same region for both results. It also becomes clear that the highest strains, and thus stresses, are indeed near the base of the specimen where it eventually failed.

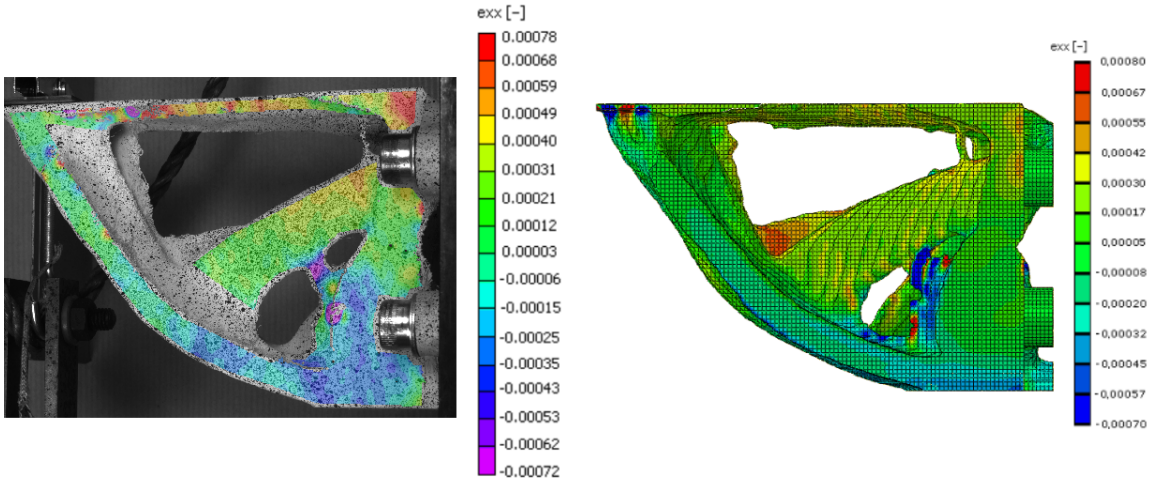

(a) Test setup ε_{xx} (b) TO software ε_{xx}

Figure 7.7: Strain for a load of 200 N according to both the test setup and the TO software.

In conclusion it was found that the results obtained by the TO software showed the correct displacement distributions. The main important regions are those with the peak stresses and these were at the correct locations. Another conclusion that was also drawn during the execution of this case study was that it is very difficult to directly use the output from TO software for further analysis. No usable method for doing a new FEM analysis on the resulting geometry of the Topology Optimization was found. This meant that the displacements and strains from the initial Topology Optimization with a load of 200 N had to be used instead of a new FEM with a load of 500 N for which the DIC system might have provided more accurate results. Finally, it was confirmed that the anisotropy due to the layer wise build up of the model was indeed the reason for failure. The anisotropic properties could however not be determined as the stresses at this load could not be calculated with a FEM analysis for reasons previously discussed.

A recommendation for further research is to design the same load carrying structure with the same restrictions and the same mass using conventional structural sizing methods. Stress distributions and failure loads for this model could provide further insights on the benefits of Topology Optimization. A point that could greatly increase the value of TO software is the establishment of a clear workflow that allows the output geometry to be used for follow-up analysis or development.

7.6 Reliability, Availability, Maintainability & Safety Characteristics

During a design process it should constantly be validated whether the results still meet the requirements derived from the customer's demands. In the case of aircraft development the reliability and safety of a system are of particular interest. During operation of the aircraft this reliability and safety is ensured by regular maintenance. Finally the extent to which a product will be operated depends strongly on its availability. An analysis on these four aspects, reliability, availability, maintainability & safety, is performed to ensure that these facets are sufficiently considered in the design.

Reliability

"Reliability is the probability that a system will perform in a satisfactory manner for a given period of time when used under specified operating conditions", as stated in [38]. As the aircraft that is being designed is mainly a proof of concept the demands on its performance are not particularly high. The main requirement is that the aircraft safely performs a flight. The use of AM in the structural design is the distinguishing factor when compared to other aircraft. The analysis on safety, and thus reliability, of the aircraft will thus focus on the additively manufactured structures.

During detailed structural design, discussed in Chapter 4, a number of safety factors is used. In general these are the standard engineering safety factor of 1.5 and the safety factor of 2 due to uncertainties of the effects of AM, especially with respect to fatigue. When the forces acting on a structure were not clearly defined another safety factor, often of 2, is used. Finally the structure is designed for a factor of the yield strength of the material. This factor varies per part.

Often in critical parts of a design a redundancy philosophy is applied. This method of design was used in the engine mount design where the struts were designed such that when one fails, for instance due to vibrational loads, the mount itself could still hold the engine in place. Redundancy is however not taken into account for the design of other parts. This methodology is especially difficult to use for topology optimized parts. The TO software presents the optimal material distribution without taking the possibility of failure of a certain beam into account. During the redrawing of these parts certain thicknesses were exaggerated to employ some form of redundancy.

The design thus incorporates safety factors and redundancy strategies. Before the aircraft can be deployed a testing stage should be performed to prove the reliability of the system. Different sub components can be tested to see whether they can carry the maximum loads. An example is to subject the wing root to a bending test. Subsequently a system test can be performed that tests whether the system as a whole functions as required. For example the bending test can be expanded to incorporate the wing tip and fuselage. This also tests whether the joints can withstand the required loads.

In conclusion the reliability of the system is secured by using substantial safety factors and by somewhat amplify the TO output. Additional practical evaluation of the structure is required to make the design as reliable as possible.

Availability

"Availability is the degree, percent, or probability that a system will be ready or available when required for use", as stated in [38]. As the aircraft is considered a feasibility study its availability is not an important factor.

On a more general note the availability of additively manufactured aircraft can be discussed. The main point in this regard is the relatively short production process. Only AM facilities with the required build volumes are needed to manufacture the most substantial part of the design. The assembly of these components is relatively simple. Up until now the availability of AM facilities is somewhat limited. When the number of AM facilities grows, so will the availability of fully additively manufactured aircraft.

Maintainability

"Maintainability is the ease, accuracy, safety, and economy in the performance of maintenance actions", as stated in [38]. A design with good maintainability requires good inspectability. This means that there should be sufficient empty space for someone to inspect the internal structure. The inspectability of the system differs significantly per part. The parts that were topology optimized often consist of organic looking structures with beams and spars running trough the internal structure. Such complex

structures make it difficult to inspect parts. Other parts, such as the wing tip, are very inspectable as AM allows for manufacturing of open structures which can still efficiently carry loads. Furthermore, the major joints are removable with complies with AMA-Tech.-Struct.-Maint.-1.

When inspections have revealed failure the part should be repaired or replaced. As the designed aircraft is assembled from a number of discrete parts it is relatively easy to replace a part. In the current design these separate parts are still quite large. This results in significant costs in case of replacement. For subsequent aircraft design more emphasise could be put on creating smaller components. This reduces maintenance costs but will most probably result in a less efficient aircraft as more joints are required. Therefore an in-depth trade-off is required.

Safety

"Safety is the freedom from hazards to human and equipment", as given in [38]. The research on the experimental aircraft focuses on a key aspect of aircraft design, namely its manufacturing. Since some uncertainties still exist on how AM manufactured parts will behave during operation, safety systems are required to guarantee the pilot's well-being. The main safety systems that have been installed are the firewall, the engine casing and the parachute system. All of these systems have been discussed in Section 5.1.3 and their application will only be summarized here.

First of all the engine casing; this casing traps the heat that is expelled by the engine. If such a system were not used, the peak temperatures might cause the polymer fuselage to melt. Secondly, a firewall is installed. This is a metal plate that separates the pilot and the parachute system from the back of the aircraft where the fuel tank and engine are installed. The firewall shields the pilot from the heat in case of an engine fire. This heat would greatly damage the fuselage structure which might fail. For such extreme situations the third and final safety system will be build in: the crash parachute. This parachute can be deployed when the pilot has fully lost control, such as after serious structural failure. To safely operate the parachute sufficient height is required. This means that the pilot should try to reach this minimum height as soon as possible and only descend when all the on board measuring systems indicate that the structural integrity of the aircraft is well within safety limits. The combination of these safety systems should assure the pilot's safe return from the flight of this experimental aircraft.

7.7 Risk Analysis

In the Baseline Report [2] and the Midterm Report [3], the six major categories for risk where discussed and explained. These categories are: Team (1), Design (2), Materials (3), Certification (4), Flight and Stability (5) & Controllability risks (6). The purpose of such a risk map is to identify the risks and to mitigate them as much as possible. In this section, the changes made in comparison to the risk map of the Baseline Report are explained and additionally some extra important risks are added.

Risk Map

The adjustments and additions in the table ranking are made during the progress of the DSE and are shown in Table 7.4, they are bold.

7. Design Evaluation

1a. Overestimate knowledge/capabilities

1b. Underestimate schedule

1c. Miscommunication

1d. No experience

1e. Productivity

1f. Topology Optimization

1g. Maintenance

2a. Replication

2b. Scalability

2c. Joints

2d. Applied forces/stresses

3a. Material imperfections/failure

3b. Material properties

4a. No Airworthiness-certificate

4b. No LSA-certificate

5a. Material failure

5b. Propulsion failure

5c. Control systems failure

5d. No test pilot

5e. Human (pilot) error

5f. Vibrations engine

6a. Overall stability/Controllability

6b. Stall/Spin

Newly added and updated risks are 1f, 1g, 3b, 5f, 6a and 6b. The Topology Optimization risk (1f) contains different parts: obtaining the software license, validations of the result, the time constraints per object (difficult to predict the time it takes per object), boundary conditions (correctness) and the mesh dependency (using a different mesh gives different results). The maintenance risk (1g) is the risk if something fails or should be replaced and it cannot be replaced or fixed because it is not reachable. Material properties (3b) were already in the table, but it has a higher probability in comparison with the Baseline and Midterm Report. This because of the unpredictability of the fatigue resistance and the time to cure the material after it has been manufactured (no data available over the curing time of the internal material in the case of VP). Also the vibration of the engine is a risk which influences the design of the engine mount. The engine mount and the interaction of the engine mount and the fuselage should be tested thoroughly before flying. Overall Stability/Controllability and Stall/Spin risk are also put higher on the probability axis. It appeared to be more difficult than predicted to design the overall Stability/ Controllability of the aircraft. Because the tail is located in the wake of the aft wing, it becomes more difficult to recover from spin. Therefore, the Stall/Spin risk is put higher on the probability axis as well.

Probability					
	Very high		**5f**	2b	
	High		2a		2c, **3b**, **6b**
	Moderate	4b	1c	1d, **6a**	2d, 3a, 5a
	Low		1b, **1g**, **1f**	5e	5c
	Very low		5d	1a, 1e,	4a, 5b
		Negligible	Marginal	Critical	Catastrophic
		Consequence			

Table 7.4: Total risk map

Risk Mitigation

The risk mitigation for the Material Properties, Stall/Spin risk, overall Stability/Controllability are already given in the Baseline Report [2] and the Midterm Report [3]. To mitigate the vibrations of the engine, vibrational dampers can be used between the engine mount and the engine and also between the engine mount and the fuselage. Using a vibrational damper, the amount of vibrations of the engine can be neglected.

7.8 Cost Analysis

The total cost of the aircraft comprises two main parts, the first part is the Additive Manufacturing (AM) part (costs to build the aircraft) and the second part the cost of the off-the-shelf components. The off-the-shelf components are the data acquisition system, electrical systems, engine, flight instrument systems, wheels & brakes, parachute system, etc. The engine alone will cost €19,000. When all the other components are included a total price above €100,000 for the off-the-shelf components is very well possible.

To make a cost analysis for the AM part, the direct cost and indirect cost should be defined and calculated. The direct cost is defined as *"A price that can be completely attributed to the production of specific goods or services"* [39]. So the direct costs are the raw material costs times the mass of deposited material (inclusive support structures) and the energy consumption times the energy price.

The indirect cost is defined as *"A cost or expense that is not directly traceable to a department, product, activity, customer, etc"*[40]. Meaning that the indirect cost comprises the rent/building costs, administration overhead costs, production labor (technicians, employer contribution) and machine costs (purchase, maintenance, etc.). An estimation for the indirect cost per machine hour is about €30 , while the energy price is around 0.021 €/MJ [41].

For example for the landing gear, the three struts together consist of 2,800 cm^3. So it would take 280 hours to only print the landing gear (taking no support structures into account). This would weigh around 22 kg (stainless steel has a density of 7,800 kg/m^3) costing around €1,000 for only materials cost [42]. The indirect cost will be around €8,400 (€30 per machine hour times 280 hours). So excluding the energy costs (no info available on energy consumption per hour) and the support structure material, the landing gear will cost €9,400.

Another example is the engine mount made out of titanium, it has a volume of 2,000 cm^3. With a built rate of 10 cm^3, it results in 200 hours (not taking the support structure into account). The engine mount will weigh around 5.42 kg (titanium has a density of 2,710 kg/m^3). The raw material cost of titanium is around €300 [42], combining this with 200 hours of labor, the engine mount will

cost around €7,630 (excluding the energy costs and supporting structure cost).

The conclusion is that the labor hours of a printer is the most cost driving factor (not including the energy costs). To make the aircraft more viable and cost efficient, the build rate should be improved with a minimum of increasing the cost of buying such a printer. A more exact cost estimation was not possible because there was no data available about the raw material costs of the polymers, build rate of the polymer printers and the exact power consumption.

7.9 Market Analysis

Creating a fully additively manufactured LSA is a manufacturing challenge just as much as it is a design challenge. An important prerequisite is to find a cheap AM machine that can create large, precise and strong parts. The price of this aircraft could be more expensive compared to traditional LSA since it is futuristic and innovative concept. Typical price ranges for existing LSA and ULA are listed in Table 7.5.

Table 7.5: LSA and ULA prices [43, 44, 45, 46]

Airplane	Manufacturer	Category	Price [US $]
Cessna Skycatcher	Cessna	LSA	112,000
Champ	American Champion Aircraft	LSA	102,900
Fox	Appollo Aircraft	LSA	66,450
BushCaddy LSA	BushCaddy	LSA	111,900
SUPER Sport Club	CubCrafters	LSA	127,500
Patriot 150	Aircraft Manufacturing and Development	LSA	90,000
SR Sport	Cirrus	LSA	120,000
Aerolite 103	Aerolite	ULA	15,900
Ultraclub kit	Belite	ULA	6,495
Proculb Lite kit	Belite	ULA	9,995
1500R SPORT	Mini-max	ULA	6,480

As it can be seen in Table 7.5, there is large difference in price between an ULA and a LSA. It should be noted that most ULA come in kits and must be assembled by the buyer: The assembly cost is not in the price. In addition the philosophy of buying a kit and assembling it complies with that of the printed airplane. Since the aircraft being designed will resemble more a LSA the cost can be closer to that of a LSA. As mentioned before, since the airplane will be manufactured entirely using AM it is probable that its price will be more than the typical LSA. In addition, the nature of the manufacturing process will allow the buyer to add personal touches. Taking these enhanced features a reasonable price range for such an aircraft is in the US $\$ 200,000 - 250,000$ range. Unfortunately, such a price range does not seem achievable with respect to today's prices for additively manufactured objects, but may change in the future. Today's realistic cost would be above US $\$ 1,000,000$. The objective of this project is rather a feasibility study that AM techniques can be used to create a fully functioning airplane rather than making a market viable airplane.

In order to use AM as a viable production technique for airplane parts, a lot of innovations in the technology should be made. Innovations in order of producing larger parts (less joints), higher production rate (decrease production time per part) [47] and in order of higher accuracy (when producing larger parts). Like already explained, the realistic costs of a fully functioning airplane will exceed US $\$ 1,000,000$. However, by using a blend of traditionally manufacturing and AM the price can be reduced significantly.

7.10 Sensitivity Analysis

A sensitivity analysis investigates the sensitivity of a design (solution) for a change in major system parameters. Changing the layout or position of an aircraft component or changing a design parameter can have major effects on the rest of the design. In this section only the sensitivity analysis of the use of Additive Manufacturing will be elaborated, the change of the main components can be found in the Midterm Report [3].

Using Additive Manufacturing to build large parts is a risk that should be taken into account. Current technologies at *LayerWise* [18] do not allow building of large parts. The company is planning to scale things up, as described in Section 4.3, but often things do not go as planned. When it would be impossible to print large parts, more joints would be required which automatically lead to a weight increase. Furthermore some parts like the landing gear might not be strong enough when joined together instead of manufactured in one piece, and some reinforcements might be needed. Adding reinforcements will also lead to a weight increase.

Not only big parts can be an issue, small parts that require higher level of detail can cause conflicts as well. Some manufacturing techniques will not provide enough detail so local thicknesses might have to be increased in order to facilitate printing tolerances. Scaling up obviously causes a weight increase.

These weight increases are difficult to measure since it is not yet known if any reinforcements will be needed. Some of the parameters defined in the Midterm Report [3] are still open to changes and can have an influence on the mass or power budget. Parameters that still can influence the mass budged are listed in Table 7.6. Parameters with impact on the power budget are listed in Table 7.7.

Parameters with Impact on Mass Budget

Operational Empty Weight (OEW) This growth factor assesses how the MTOW increases if a generic aircraft item adds another percent to the OEW. For this purpose a miscellaneous item with 1 % of the OEW is added in the Class-II weight estimation. The snowball effect causes an increase of the Maximum Take-off Weight of 1.28 %.

Specific fuel consumption, c_p The specific fuel consumption c_p is one decisive input parameter in Breguet's endurance equation. Consequently, the total mass fuel fraction M_{fuel} for the mission decreases as a result of which the fuel weight W_{fuel} grows. Finally, a 1 % increase in specific fuel consumption causes a 0.11 % growth in MTOW.

Lift-to-Drag ratio, L/D This is one of the major parameters indicating an aircraft's aerodynamic performance level. An increase in L/D yields an increase in M_{fuel} which in turn means that a lower fuel weight W_{fuel} can be achieved. Feeding the new fuel fraction into the Class-II weight estimation one obtains a weight decrease of 0.10 % in MTOW.

Maximum lift coefficient, C_{Lmax} An increase in maximum lift coefficient C_{Lmax} increases the attainable wingloading W/S. The two parameters are directly proportional to each other. As a result, the required lifting surface area is reduced. Keeping the aspect ratio constant, the wingspan decreases. Feeding these changes into the Class-II weight estimation one obtains a weight reduction of 0.12 % in MTOW.

Table 7.6: Ranking of growth factors regarding the MTOW estimation

Parameter	Growth factor MTOW [%]
OEW	+1.28
Specific fuel consumption, c_p [−]	+0.11
Lift-to-Drag ratio, L/D [−]	−0.11
Maximum lift coefficient, $C_{L_{max}}$ [−]	−0.12

Parameters with Impact on Power Budget

Maximum lift coefficient, $C_{L_{max}}$ An increased lift coefficient translates to an increased wing-loading requirement. At this new wing-loading, the power-loading W/P is decreased by 0.53 %. Together with the change in MTOW the new power requirement is increased by 0.33 %.

Oswald efficiency factor, e The span efficiency factor plays a decisive part in the determination of the maneuvering requirement. Increasing e by 1 % first increases the power-loading W/P by 0.75 % which then reduces the overall power budget by 0.88 %.

Table 7.7: Ranking of growth factors regarding the power estimation

Parameter	Growth factor power [%]
Maximum lift coefficient, $C_{L_{max}}$ [−]	+0.33
Oswald efficiency factor, e [−]	−0.88

7.11 Sustainability Analysis

The sustainability analysis of this aircraft consists of two parts: the first one is an overall analysis of the AM industry and the second compares two parts of the aircraft with their traditionally manufactured counter-parts. However, before starting the sustainability analysis, certain assumptions need to be stated.

Assumptions

Creating an integral sustainability analysis of aircraft parts produced using AM compared to ones produced using traditional methods can be a meticulous process. Hence some processes and/or components of the production chain can be omitted for simplicity. Such components include:

- The electrical consumption for lighting and heating of the manufacturing facility producing a part, whether it is traditionally or AM printed.
- The electrical consumption of computers used for creating TO models, performing FEM analysis, TO and any numerical analysis and documentation related to the creation of the part.
- The sustainability of the electricity production process, since 1 kW produced by a solar panel will have lower CO_2 emission than 1 kW produced by a coal plant.
- The transportation of the ore (bauxite for aluminum, and various minerals for titanium) from the mine to the refinement plant will not be taken into account. Indeed processing of the ore into a pure element is necessary regardless of the production method used on the material.

Sustainability of AM over Traditional Manufacturing

The cost of material transportation in the aircraft industry will be developed in this report to compare the carbon footprint of AM transport and traditional manufacturing transport. The fly-to-buy ratio for traditionally manufactured aircraft parts is about 3% to 5% [48]. On the other hand using exclusively AM could lead to a fly-to-buy ratio of 50% [48]. It is this ratio that has the biggest impact on sustainability. Indeed since the purified ore needs to be shaped into a product or part in a specialized facility, the less material this facility needs to order, the lower the carbon footprint of the transport process. The carbon footprint of transportation is generally measured in grams of CO_2 rejected by one ton of material being transported over one kilometer. Large aircraft manufacturers do not produce and assemble all their parts in one unique workshop thus in addition to transporting the raw material to a manufacturing company it is also necessary to move the material from the manufacturing workshop to the assembly workshop. This is the case, for instance, for Airbus [49]. However, since an AM facility can be located in multiple locations, it can be assumed that it would be located within the assembly facility, hence removing an entire transportation component of traditional manufacturing.

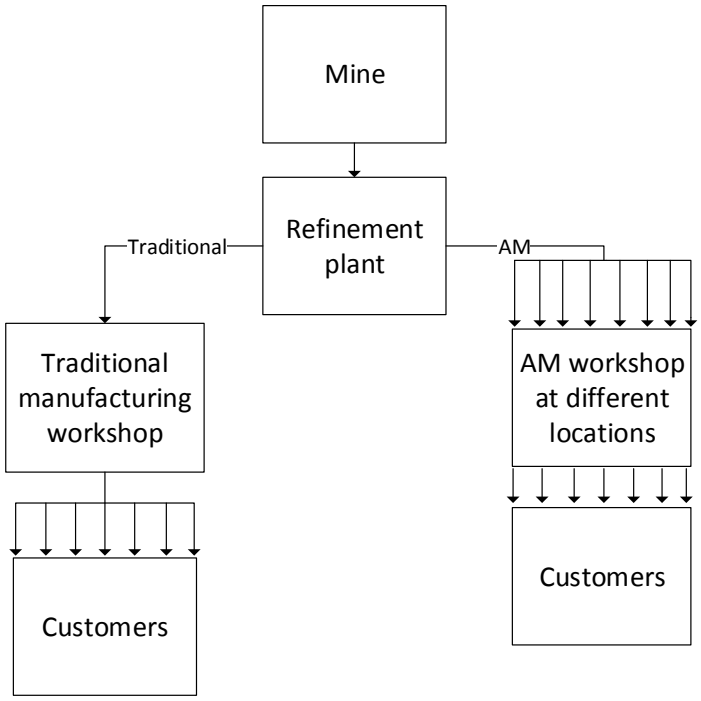

Figure 7.8: Transport route of manufacturing material in the aerospace industry

Taking into account the fly-to-buy ratio, traditional manufacturing will require 10 to 15 times more material than AM, hence the carbon footprint of traditional manufacturing, with respect to transport, is 10 to 15 times higher. In addition to carbon emissions that damage the Earth's atmosphere, bio-hazards need to be taken into account. Such hazards include the toxicity of the materials used as well as the amount of energy required to use the machines and any other product (such as lubricant) that the process requires.

Traditional manufacturing machines, such as CNC machines, require a high use of lubrication and cooling fluids. Such cutting fluid can be damaging for the human worker as well as the environment [50]. Fortunately, such liquids are not required for AM. On the other hand a study lead by Brent Stephens et al. [51] showed that desktop printers using ABS produce Utra Fine Particules (UFP) that can be very harmful to the lung and cardio-vascular system. These emission are however of little

impact since they are of the same level, for one machine, than the amount of UFP emitted when using an electric cooking pan.

Another factor to take into consideration is the energy consumption of AM machines and compare it to that of traditional manufacturing machines. The electricity consumption needs to be related to the amount of parts produced by the machine because initializing and/or warming up the material to be processed can represent most of the energy use if only one part needs to be printed. A study by Faludi [52] showed that for minimal use, FDM and BJ, consume less electricity per part per year than a CNC. Moreover, when the machines are used at their full potential, CNC is the least electricity consuming process.

Finally, the plastic used for about half AM machines is ABS which is an oil based plastic that is detrimental for the environment. PLA plastic (it is biodegradable) can also be used but it is less strong than ABS. Hence the user of the AM machine must choose between strength or sustainability. Today, both PLA and ABS are commonly used [53].

Airplane's Parts Comparison

The wings have been described in Section 4.5. They are composed of root section made out of aluminum and a tip section (that is effectively a spar) is made out of a polymer, namely *Tusk Somos Solidgrey 3000 ®*. The internal structure is covered by a foil. Both the metal and the plastic part are printed in one piece, making such a wing almost impossible to manufacture using traditional methods (though the spar could be made using Vaccum Infusion). In order to obtain a consistent sustainability analysis, this wing should be compared to a typical LSA wing layout consisting of two I-beam spars held parallel to each other with rib. For LSA, a cloth or foil usually recovers the wing as well. As far as the production process is concerned, the ribs are press-formed and punched; the I-breams are welded. Table 7.8 shows the electricity consumption, the recyclability of the material used and the waste material of the AM wing and the traditionally manufactured wing. Table 7.8 also compares these values if ten airplanes are made as well as hundred.

Table 7.8: Sustainability of the wing manufacturing [54]

	AM		Traditional	
Batch size	10	100	10	100
Energy	$120 - 170$ MJ/kg for VP and DED	No change in energy per kg	9.6 kW for I-beam welding	No change in energy per kg
Waste	Support structure, material near the part being made and surface finish	No increase in waste per part	Slug removed due to punching, surface finish	No increase in waste per part
Recyclability	Most metals and some plastics	No influence on recyclability per part	Most metals used	No influence on recyclability per part

Contrarily to the wings, the fuselage section, described in Section 4.6, is much similar to a fuselage structure that would be made with traditional manufacturing. Indeed the struts made using VP can easily be made out of aluminum using a metal extrusion process. Once more the sustainability of each fuselage will be compared in Table 7.9.

Table 7.9: Sustainability of the fuselage frame manufacturing [55, 54, 56]

	AM		Traditional	
Batch size	10	100	10	100
Energy	$75 - 150$ MJ/kg for VP	No change in energy per kg	N/A for metal extrusion	No change in energy per kg
Waste	Support structure, material near the part being made and surface finish	No increase in waste per part	Material in the "dead metal zone", surface finish	Reduced wast per part
Recyclability	Sumo tusk is recyclable	No influence on recyclability per part	Most metals used	No influence on recyclability per part

Discussion

Overall, the real impact on sustainability of this aircraft is difficult to evaluate. Indeed, using AM will limit the carbon footprint this aircraft produces during transportation but on the other hand, the AM machines requires much more energy. The real environmental impact of such an aircraft would require an intensive investigation on all components of the aircraft's life and all of the assumptions stated should be taken into account. Such an evaluation could not happen until the end of life of the aircraft. The aircraft's life time required is of twenty flights, hence the aircraft's use contributes little to its overall carbon footprint. This airplane is designed to demonstrate the feasibility of an additively manufactured aircraft and the sustainability can further be improved by choosing AM facilities that use electricity from clean power plants. Finally, this aircraft is unique and produced in a batch size of one. Compared to a large batch as it is customary in LSA, a single prototype can never compete in sustainability.

Chapter 8

Future Work

This Final chapter of the report deals with the next step that would need to be taken to have a flying airplane. First, the airworthiness requirements are a crucial set of prerequisites that the aircraft needs to fulfill if one wishes to flight the airplane. A non exhaustive list of such requirements is listed in the first section of this chapter. In the subsequent section, a set of future design developments and structure improvements are listed. These improvements aim at increasing the efficiency of additive manufacturing and better complying with the airworthiness requirements.

8.1 Airworthiness Compliance Plan

To be sure that the designed aircraft can be registered and actually be flown, the team did set up a meeting with mr. A. Klut and mr. E. Bakker, two inspectors at the Inspectie Leefomgeving en Transport (ILT). The main conclusion that can be drawn from the meeting with ILT is that there are two important steps in getting an airworthiness certificate, being getting a proof of registration, and getting an airworthiness certificate.

Proof of Registration

The first step in the total registration process is getting the proof of registration. This should be the most easy part in the whole process. Any person just can go to the aircraft authorities, pay a registration fee of €70 and obtain a tail number. As strange as it sounds, these authorities will not check if the object to register is actually able to fly. After the proof of registration is obtained it is time for step two: obtaining an airworthiness certificate.

Airworthiness Certificate

Obtaining an airworthiness certificate is the hardest part in the registration process. To complete this step, certain regulations should be met. These regulations are the so called Certification Specifications (CS). Since there are a lot of CS set by European Aviation Safety Agency (EASA) that are the same for every aircraft, the team has scanned through all CS part 23, and highlighted the main risks considering this project [57]. For a special airworthiness certificate, around 600 CS should be met, for a regular airworthiness certificate this value goes up to 1700. The difference between the special- and regular certificate is the fact that with a special airworthiness certificate the aircraft only can operate on Dutch territory. Since the aircraft should operate from Lelystad and it can be easily remain with Dutch territory, only the 600 requirements for the special certificate have to be met.

For these CS the used fabrication methods or selected materials do not play any role, as long as the CS are met.

Besides the standard Certification Specifications, also extra extra requirements, called Certification Review Item (CRI), should be met. These CRI's should focus on Additive Manufacturing in particular, explaining extra possible risks that may occur using AM techniques as manufacturing process. Important CS and extra CRI's are listed below in more detail.

CS by EASA

Important CS are listed below:

CS 23.171:	*The aeroplane must be longitudinally, directionally and laterally stable.*
CS 23.251:	*There must be no vibration or buffeting severe enough to result in structural damage.*
CS 23.305:	*The structure must be able to support limit loads without detrimental, permanent deformation.*
CS 23.307:	*Compliance with the strength and deformation requirements of CS 23.305 must be shown for each critical load condition.*
CS 23.605:	*The methods of fabrication used must produce consistently sound structures.*
CS 23.613:	*Material strength properties must be based on enough tests of material meeting specifications to establish design values on a statistical basis.*
CS 23.629:	*It must be shown, ... , that the aeroplane is free from flutter.*
CS 23.641:	*The strength of stressed skin wings must be proven by load tests or by combined structural analysis and load tests.*
CS 23.693:	*Control system joints (in push-pull systems) that are subject to angular motion, except those in ball and roller bearing systems, must have a special factor of safety of not less than 3.33*

CRI's set by the team

The CRI's that are set by the team, and thus contain extra risk using Additive Manufacturing Techniques, are liested below:

CRI 1:	*The fuel tank should be made of material that will not be affected by the fuel.*
CRI 2:	*The reproducibility of the parts made by using Additive Manufacturing must be proven.*

Several of these requirements have been included in the overall requirements for the aircraft (such as CS 23.171), however others require more in depth investigation and might require changes to the design. However, when it is believed all requirements are fulfilled, an external expert has to be contacted who then will check all CS and CRI's. To convince the expert that that all single components are safe, for instance that joints will not break and the aircraft as a whole is safe to operate, a great deal of tests will be needed. These tests will require the manufacturing of many components, the inspectors even estimated it will take approximately three complete aircraft that should be manufactured before enough tests can be provided to convince the external expert and consequently obtain the airworthiness certificate.

The manufacturing and testing of extra parts will require a large investment, both in time and financial resources. Another problem can be that there are only three experts in the Netherlands allowed to provide an airworthiness certificate, so the availability of these experts can be an issue as well. For that reason obtaining an airworthiness certificate is an important part of the future project activities.

8.2 Future Design Developments

At this final stage of the project, the design has reached a fair amount of detail. Reflecting on the degree of progress that has been made it can be confirmed that requirement AMA-Con.-Sched.-1 is satisfied. However, to actually realize the design, more research and design activities need to be performed next to the airworthiness compliance plan described in Section 8.1. These recommended future activities are described in this section, where they are differentiated into general, additively manufacturing related tasks, structural design activities, subsystem design procedures as well as verification and validation procedures. All future action items are also summarized in a project development logic, shown in Figure 8.1. Moreover, a preliminary timeline of these activities is outlined in a Gantt chart which is illustrated in Figure 8.2.

Additive Manufacturing

Considering the application of AM technologies for structural parts, the fatigue behavior of such additively manufactured parts has proven to be a major uncertainty. For this matter, additional safety factors of 2 are applied to increase reliability and safety. Researching fatigue characteristics of the desired processes and materials can significantly reduce the ambiguity in design and thereby, reduce applied safety factors and in turn realize weight savings. In a similar manner, the curing characteristics of polymers processed with Vat Polymerization need to be further analyzed, as mentioned in Section 4.5. Additionally, for some components the current build volumes are slightly exceeded, more specifically, for the fuselage structure and the main landing gear. The targets for increased build volume are based on demands from industry, the progress on this matter needs to be tracked to see if it is indeed possible to manufacture these parts.

For the mentioned action items, it may prove useful to contact manufacturers and establish collaborations where possible. Furthermore, detailed printing plans need to be developed for each component. These shall include, build direction, support structures and similar. Once the printing plans are finalized the preliminary production and assembly plan can be completed.

Lastly, since the designed aircraft is an experimental demonstrator, the plan for the flight tests needs to be designed. These shall focus on features and data that can improve the application of Additive Manufacturing in aerospace structures.

Structural Design

For the structural design the level of detail varies for the aircraft components. The major action items per component are stated in the following.

Wings. The current wing design does not provide the weight savings that could have been expected from AM technology. The major reason is again the high safety factor applied. This stresses the importance of the already mentioned research in fatigue properties of additively manufactured parts. Next to this, a foil material needs to be chosen which wraps the lattice structure which still needs to be sized. Additionally, the Topology Optimization of the root section needs to be validated. Especially, the integration of wing root and fuselage structure requires a review and a more detailed design. On the other side, the wing tip sections have to be analyzed in terms of aeroelasticity. Last, the control surfaces need to be designed structurally.

Fuselage. The fuselage is fully sized, but can be further optimized. Weight savings are expected from a cross-section refinement of the truss structure as well as the shear panels. Both are currently constant thickness structures and can be further refined. Furthermore, the nodes, where multiple

trusses join, can be improved by application of Topology Optimization software. A particular area of interest shall be the landing gear integration.

Vertical Tail. The vertical tail is, at this stage, the most developed structure in the aircraft. Still, some more weight can be saved by iterating the internal beam structure. For instance, the current solid struts can be made hollow. Additionally, the validation of the Topology Optimization needs to be finished of.

Landing Gear. As previously mentioned, the integration of landing gear and fuselage can be detailed further. Additionally the internal structure of the aerodynamic fairing is still to be developed. Here, a trabecular structure shall be investigated. Optionally, the team may invest time in an additively manufactured wheel design.

Propeller. While the propeller is aerodynamically designed, it still needs to be structurally sized.

Engine Mount. The engine mount can also be detailed further. As this part is most evidently exposed to fatigue loads, the efficiency of the damping rubber mounts shall be tested experimentally. This test is to be designed, executed and analysed. In addittion, the shaft support has to be designed.

Joints. The current design features components made from a variety of materials. Joining of these different materials may not always prove easy. Therefore, test specimens are to be developed and tested to gain insight on the connection properties. In case of adhesive bonding, the strength and scatter of the bond are to be determined as well. Then, the knowledge from these tests is to be integrated in detailed joint designs.

Subsystems Design

The first focus of the further subsystem refinement is on stability and control, while a second area of interest lies on the internal aircraft layout.

For stability and control it would be most helpful if the team can design and perform a windtunnel test to validate acquired CFD data, stability calculations and predicted aerodynamic performance. If targets are not met, for instance the stall criteria, a slot design can be developed to increase the aircraft's maximum lifting capabilities. Considering the control surface design, relatively large surfaces are used. While the reason for this originates from the structural wing design, this unconventional layout needs to be verified. Connected to this is the design of a (de)augmentation system for the actuation of the control surfaces.

For ground stability on the other hand, the steering system which is operated by differential braking is to be validated. Regarding the internal aircraft layout, the furnishing and the fuel system, including fuel pump, hose system as well as the air intake for the engine need to be finalized. Moreover, the safety system requires a detailed structural integration into the fuselage design.

Verification & Validation

Several verification and validation activities related to the structural design have already been described. In addition to these, more verification and validation tasks are to be carried out. On the one hand these tasks relate to the CFD analysis which was performed. For this purpose, a windtunnel test seems most suitable.

On the other hand, a case study concerning Topology Optimization was carried out. Future work may contain a FEM analysis which compares the stress levels obtained by the Direct Image Correlation. Alternatively, the case study can be redesigned with the experience gained during the

first experiment. In this case, care needs to be taken that the obtained displacements are sufficiently large to obtain precise strain measurements from the DIC. A second point of interest in a consecutive case study could be the evaluation of the anisotropic behavior of the printed specimen.

Other verification and validation activities may touch upon stability and control as well as other subsystems. These tasks are not defined yet in detail.

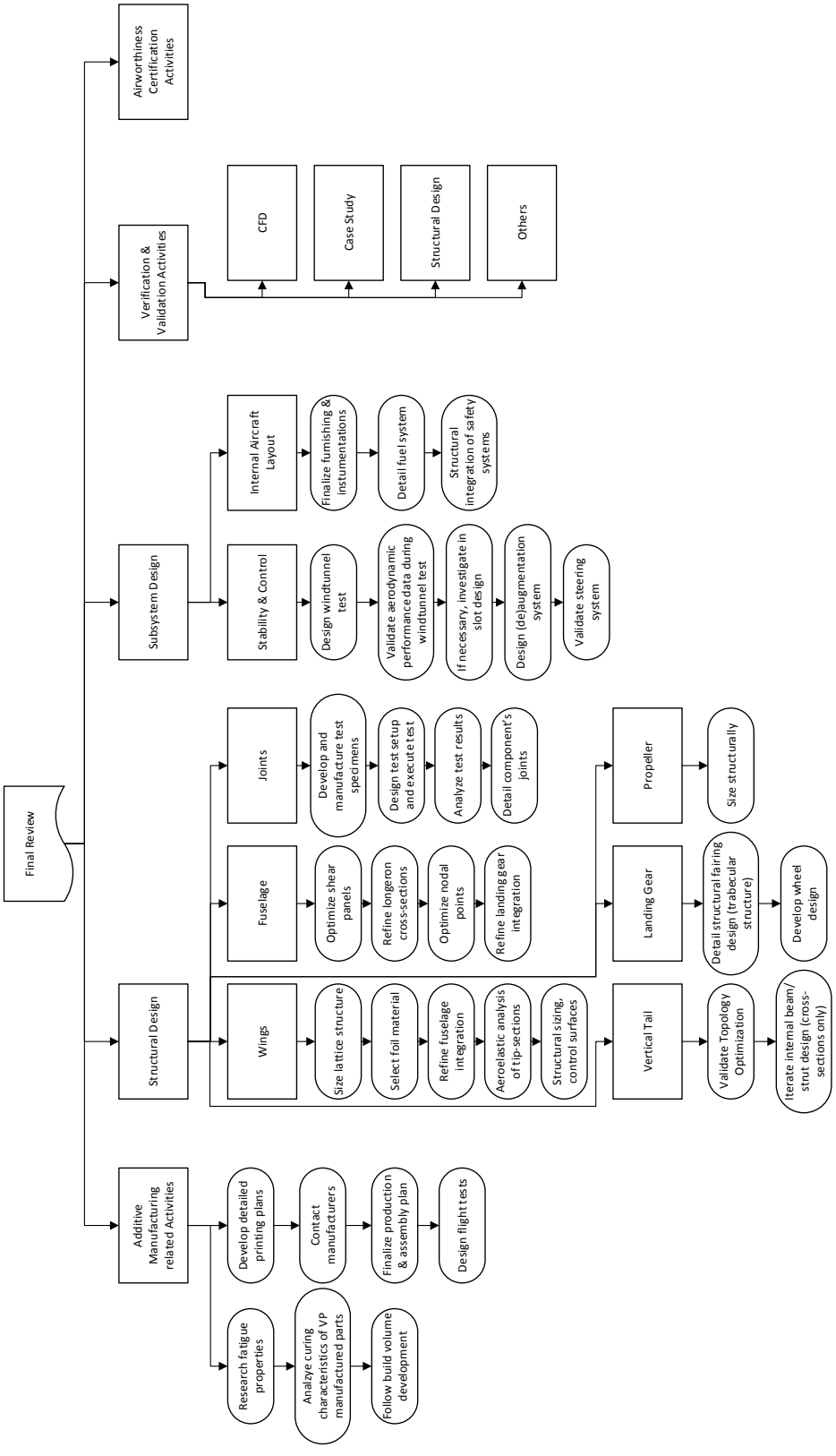

Figure 8.1: Project development logic

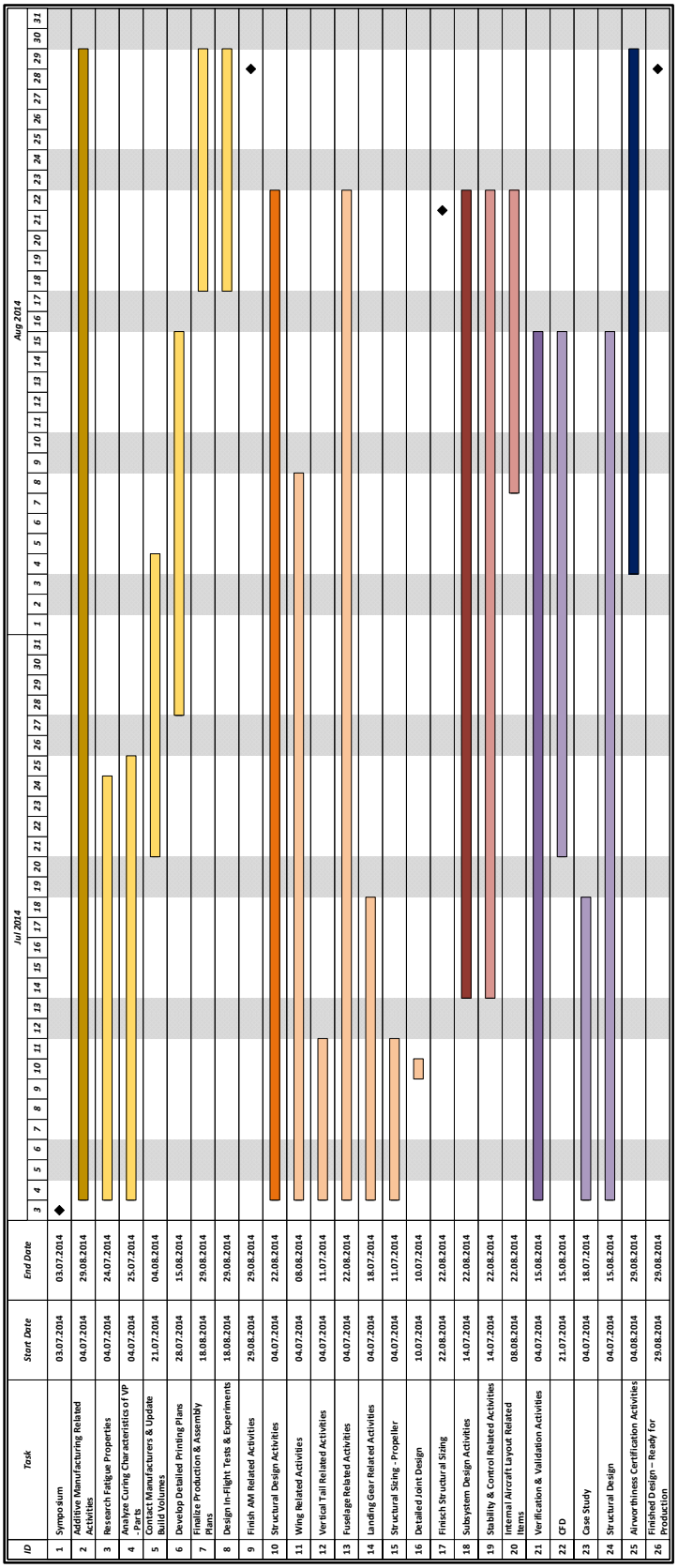

Figure 8.2: Future work Gantt chart

Chapter 9

Conclusion & Recommendations

The Design Synthesis Exercise's purpose of group 12 was to assess the feasibility of designing a personal aircraft using only Additive Manufacturing (AM) techniques for the airframe construction. As for most engineering problems, given enough time and money, everything is possible, but more interesting is to determine whether the technologies' benefits are worthwhile to invest further research into them. Therefore, the challenges associated with using AM for load bearing structures have been investigated in more detail, starting at the conceptual design phase up to the final assembly plan.

Although AM offers immense freedom of design, enabling highly efficient structural and aerodynamic solutions, it also brings along its own limitations. At the moment, the build volume is largely process dependent and for the majority of technologies it is rather small ($\leq 1\,m^3$), resulting in a larger number of joints required. The largest state-of-the-art manufacturing machines feature a build envelope of $2.1 \times 0.8 \times 0.7\,m$ for Vat Polymerization, a polymer processing technique and a build volume of $2.0 \times 1.5 \times 0.75\,m$ for Direct Energy Deposition a process working with metals. Currently there are however uncertainties present regarding fatigue and and anisotropic behavior of additively manufactured parts, driving the applied safety factors above average.

Regarding the design process, AM requires a rethinking of the approach strategy to a design problem. Compared to classical manufacturing processes, AM provides almost total design freedom; so much, that it proves difficult to find a starting point in the design phase. Thus, the concept selection process in this particular project has often been intuitively driven. Furthermore, the various opportunities can stretch the conceptual design phase and thereby, prevent progress into the detailed design. Furthermore, once a novel concept has been developed, conventional analyses and sizing methods may not be applicable to the desired design. At the same time, it is inappropriate to initiate a full FEM analysis at such an early stage in the project. To cope with this new design environment, adjusted or even revolutionized systems engineering methodologies are required to assess the feasibility and to perform the initial sizing of a concept.

An alternative way to approach the detailed design process is the use of Topology Optimization (TO) software. This tool iteratively optimizes the structure of a component with its underlying load cases based on a FEM analysis. However, the conversion process from TO output to a design interpretation in CAD software currently appears to be complex and time-consuming. This pipeline therefore requires more research to accelerate the development speed of additively manufactured parts.

Two major parts have been designed using TO software: the vertical tail and the wing roots. The possibilities of combining this design principle with Additive Manufacturing technologies became clearly visible. However, a comparison with the weight estimates of a Class II estimation revealed that the designed structures are 52 % and 23 % heavier than expected at this stage, respectively for the

vertical tail and the wing structure. Though, the reason for this excessive weight lies in the additional safety factors that have been applied to cover the uncertainty in material behavior rather than in the working efficiency of the Topology Optimization software. Thus, more research in the fatigue and anisotropic behavior of additively manufactured parts is recommended to overcome this current disadvantage.

Besides the technical aspects, a market and cost analysis revealed that time and cost requirements associated with AM are still high, especially when considering series production. A cost estimation showed that the landing gear production would cost $\sim$ €$10,000$, while the engine mount is estimated to cost $\sim$ €$8,000$, considering one time production. For larger parts, such as the wing structure a cost estimation has not been performed yet. However, costs are expected to scale with part volume. Therefore, an aircraft featuring a fully additively manufactured airframe cannot compete with its conventional counterparts yet.

In conclusion, Additive Manufacturing has shown its potential and the possibility to print a complete airframe structure, but for the moment it is advisable to only use AM as a tool to add value to specific aircraft components. The high costs associated with it, make it suitable for parts with a high impact on the overall weight of the aircraft. In the aerospace industry a minor weight saving can already yield a large fuel reduction, justifying the higher cost for the part in the long term. That does however not mean that everything should be printed, such as the skin for the aircraft. The keyword for the future of AM in the aerospace industry is therefore “added value”.

References

[1] Saaty, T., *Group Decision Making: Drawing Out and Reconciling Differences*, RWS Publications, Pittsburgh, PA, 2008. 4

[2] Barten, K. P. A. M., De Bie, M., Cheylus, T. P. A., van de Grift, I., Jux, C., van der Linden, S., Opgenoord, M. M. J., Peelman, S. H. M., Stoter, K. F. S., and van Zanten, F. J., "Baseline Report - Printing the Personal Aircraft of Tomorrow," Tech. rep., Delft University of Technology, May 2014. 4, 71, 73

[3] Barten, K. P. A. M., De Bie, M., Cheylus, T. P. A., van de Grift, I., Jux, C., van der Linden, S., Opgenoord, M. M. J., Peelman, S. H. M., Stoter, K. F. S., and van Zanten, F. J., "Midterm Report - Printing the Personal Aircraft of Tomorrow," Tech. rep., Delft University of Technology, May 2014. 6, 7, 51, 60, 71, 73, 75

[4] Lowry, J., "Propeller Aircraft Performance and The Bootstrap Approach: Background," http://www.allstar.fiu.edu/aero/BA-Background.htm, Accessed: April 30, 2014. 8

[5] Advanced Flight Systems Inc., "Mode S Transponder," http://www.advanced-flight-systems.com/Products/Transponder/Transponder.html, Accessed: April 30, 2014. 8

[6] Sadraey, M., *Aircraft Design: A Systems Engineering Approach*, Wiley, Chichester, West Sussex, U.K, 2013, http://faculty.dwc.edu/sadraey/Chapter%206.%20Tail%20Design.pdf, Accessed: June 17, 2014. 12, 13, 17, 19

[7] Raymer, D., *Dan Raymer's Simplified Aircraft Design for Homebuilders*, Design Dimension Press, Los Angeles, CA, 2003. 12, 13, 14, 17

[8] Roskam, J., *Airplane Design - Part III: Layout Design of Cockpit, Fuselage, Wing and Empennage: Cutaways and Inboard Profiles*, DARcorporation, Lawrence, Kan, 1986. 13, 20, 28, 65

[9] Husa, B., "Airfoil Selection," http://sats.aeroengineer.net/articles.html, Accessed: June 1, 2014. 14, 15, 16

[10] La Rocca, G., "Aerospace Design and Systems Engineering Elements II," http://www.blackboard.tudelft.nl, 2012, Accessed : September, 2012. 15

[11] Selig, M. S., Guglielmo, J. J., Broeren, A. P., and Giguère, P., *Summary of Low-Speed Airfoil Data*, SoarTech Publications, Virginia Beach, Virginia, USA, 1995. 15

[12] Ackroyd, J. A. D., "The Spitfire Wing Planform: A Suggestion," *Journal of Aeronautical History*, Vol. 2013, No. 2, February 2013, pp. 121–135. 15

[13] Drela, M., "XFOIL Subsonic Airfoil Development System," http://web.mit.edu/drela/Public/web/xfoil/, Accessed: May 19, 2014. 15, 110

[14] Deperrois, A., "XFLR5 - General Description," http://www.xflr5.com/xflr5.htm, Accessed: May 19, 2014. 18

[15] Deperrois, A., "XFLR5 Analysis of Foils and Wings Operating at Low Reynolds numbers," Tech. rep., Guidelines for QFLR5 v0.03, October 2009, https://engineering.purdue.edu/~aerodyn/AAE333/FALL10/HOMEWORKS/HW13/XFLR5_v6.01_Beta_Win32(2)/Release/Guidelines.pdf Accessed: June 17, 2014. 19

[16] Hepperle, M., "JavaProp Applet," http://www.mh-aerotools.de/airfoils/javaprop.htm, Accessed: June 6, 2014. 20

[17] Rotax Aircraft Engines, "Installation Manual for Rotax Engine Type 912 series," http://www.flyrotax.com/portaldata/5/dokus/d04967.pdf, Accessed: June 3, 2014. 21, 45

[18] LayerWise, "Technology - Technical Specifications," http://www.layerwise.com/technology/technical-specifications/, Accessed: June 16, 2014. 26, 46, 56, 75

[19] Roland Berger Strategy Consultants, "Additive Manufacturing - A game changer for the manufacturing industry?" http://www.rolandberger.com/media/pdf/Roland_Berger_Additive_Manufacturing_20131129.pdf, Accessed: June 18, 2014. 26, 46

[20] Granta Design Limited, "CES EduPack 2013," Version 12.2.13. 26, 102

[21] Materialise, "Stereolithography Material Properties," http://manufacturing.materialise.com/sites/default/files/public/AMS/Updated%20datasheets/ams_datasheets_stereolitography.pdf, Accessed: May 1, 2014. 27, 30, 39, 102

[22] Materialise, "FDM Material Properties," http://manufacturing.materialise.com/sites/default/files/public/AMS/Updated%20datasheets/ams_datasheets_fdm.pdf, Accessed: May 1, 2014. 27, 51, 102

[23] FAA, "Federal Aviation Regulations - Part 23," Tech. rep., U.S. Department of Transportation, January 2005, Accessed from http://www.flightsimaviation.com/data/FARS/part_23-441.html on June 17, 2014. 28

[24] Detego, "Belite Aircraft Wing Design," http://www.homebuiltairplanes.com/forums/light-stuff-area/11041-challenge-you-all-46.html, Accessed: June 17, 2014. 33

[25] HPWizard, "Tire friction and rolling resistance coefficients," http://hpwizard.com/tire-friction-coefficient.html, Accessed: June 17, 2014. 35

[26] Mattheck, C., *Secret Design Rules of Nature*, Forschungszentrum Karlsruhe GmbH, D-76021 Karlsruhe, 2007. 41, 101

[27] Sadraey, M., *Landing Gear Design*, Daniel Webster College, http://faculty.dwc.edu/sadraey/Chapter%209.%20Landing%20Gear%20Design.pdf, Accessed: May 21, 2014. 43, 52

[28] Edwards, P. and Ramulu, M., "Fatigue performance evaluation of selective laser melted Ti–6Al–4V," *Elsevier*, January 2014. 46

[29] BRP Powertrain GmbH & CO KG, "Why 912 iS Sport - Facts," http://www.flightevolution.com/en/Why-912-iS-Sport, Accessed: May 22, 2014. 51

[30] Ultralight News, "BRS Vertical Launch system," http://www.ultralightnews.ca/brs/brs_vls.htm, Accessed: June 12, 2014. 52

[31] Experimental Aircraft Info, "Aircraft Firewall Preparation," http://www.experimentalaircraft.info/articles/aircraft-firewall-preparation.php, Accessed: June 16, 2014. 52

[32] Stratasys, "Additive Manufacturing; Aerospace – Defence," http://www.manitoba-aerospace.mb.ca/pdfs2/james_janeteas.pdf, Accessed: June 17, 2014. 52

[33] Stratasys, "Ultem™ 9085 Production-Grade Thermoplastic for Fortus 3D Production Systems," http://www.stratasys.com/~/media/Main/Secure/Material%20Specs%20MS/Fortus-Material-Specs/Fortus-MS-ULTEM9085-01-13-web.ashx, Accessed: June 17, 2014. 52

[34] Dutta, B. and Froes, F. H., "Additive Manufacturing of Titanium Alloys," *Advanced Materials & Processes*, February 2014, pp. 18–23. 56

[35] DM3D Technology LLC, "Products & Services - 3D Printing," http://www.dm3dtech.com/index.php?option=com_content&view=article&id=194&Itemid=817, Accessed: June 19, 2014. 56

[36] Mulder, J. A., van Staveren, W. H. J. J., van der Vaart, J. C., de Weerdt, E., in 't Veld, A. C., and Mooij, E., *Flight Dynamics Reader* , February 25, 2013. 65, 66

[37] Lutze, F.H., "Maneuvering Flight," http://www.dept.aoe.vt.edu/~lutze/AOE3134/maneuvering.pdf, Accessed: June 14, 2014. 66

[38] La Rocca, G., Verhagen, W., Curran, R., and Gill, E., "AE3211-I Systems Engineering and Aerospace Design," http://www.blackboard.tudelft.nl, 2014, Accessed : February, 2014. 70, 71

[39] University of Arizona, "Direct vs. Indirect Costs Introduction," http://www.sps.arizona.edu/financialcompliance/directindirect/05_02_Direct%20vs.%20Indirect%20Costs%20Introduction_for%20Web%20Site.pdf, Accessed: June 24, 2014. 73

[40] Harold Averkamp, "Indirect Cost," http://www.accountingcoach.com/terms/I/indirect-cost, Accessed: June 19, 2014. 73

[41] Baumers, M., Tuck, C., Wildman, R., Ashcroft, I., Rosamond,E., and Hague, R., "Combined build-time, energy consumption and cost estimation for direct metal laser sintering," http://utwired.engr.utexas.edu/lff/symposium/proceedingsArchive/pubs/Manuscripts/2012/2012-71-Baumers.pdf, Accessed: June 19, 2014. 73

[42] McKenna, B, "Why 3D Systems Corp. and Arcam AB Could BE Big Winners Because of This New U.K. Development," http://www.fool.com/investing/general/2014/02/13/why-3d-systems-corporation-and-arcam-ab-could-be-b.aspx, Accessed: June 19, 2014. 73

[43] Aviation Bull, "Light Sport Aircraft Comparison," http://www.aviationbull.com/light-sport-aircraft-comparison, Accessed: April 29, 2014. 74, 102

[44] Aerolite 103, "AeroLite 103, Ready to fly," http://www.uflyit.com/aerolite_103_prices.htm, Accessed: April 29, 2014. 74, 102

[45] Belite, "Pricing and Store," http://www.beliteaircraft.com/how-to-buy/, Accessed: April 29, 2014. 74, 102

[46] Team Mini-Max , "Mini-Max Aircraft Comparison Chart," http://www.teammini-max.com/aircraft/comparison-chart/, Accessed: April 29, 2014. 74, 102

[47] Royal Academy of Engineering, "Additive manufacturing: opportunities and constraints," http://www.raeng.org.uk/news/publications/list/reports/Additive_Manufacturing.pdf, Accessed: June 18, 2014. 74

[48] David Dornfeld, "Degrees of Perfection," http://green-manufacturing.blogspot.nl/2010/07/degrees-of-perfection.html, Accessed: June 17, 2014. 77

[49] Zuliani J.M. , Jalabert G., "L'industrie aéronautique européenne : organisation industrielle et fonctionnement en réseaux," http://www.cairn.info/zen.php?ID_ARTICLE=EG_342_0117, Accessed: June 19, 2014. 77

[50] Department of Health and Human Services, "Niosh Health Hazard Eevalution Report," Tech. rep., Diamond Chain Company, September 2007, http://www.cdc.gov/niosh/hhe/reports/pdfs/2005-0227-3049.pdf, Accessed: June 19, 2014. 77

[51] B. Stephens, P. Azimi, Z. T., "Ultrafine particle emissions from desktop 3D printers," *Elsevier*, 2013, http://www.sciencedirect.com/science/article/pii/S1352231013005086, Accessed: June 17, 2014. 77

[52] Jeremy Faludi, Cindy Bayley, S. M., "Comparing Environmental Impacts of Additive Manufacturing vs. Traditional Machining via Life-Cycle Assessment," Tech. rep., University of California, Berkeley, Departement of Mechnical Engineering, http://www.faludidesign.com/work/publications/Additive%20Mfg%20vs.%20Machining.pdf, Accessed: June 19, 2014. 78

[53] Absplastic, "PLA vs. ABS Plastic – The pros and cons," http://www.absplastic.eu/pla-vs-abs-plastic-pros-cons/, Accessed: June 19, 2014. 78

[54] M. Baumers, C. Tuck, R. I. R., "Energy Inputs To Additive Manufacturing: Does Capacity Utilization Matter?" Tech. rep., Additive Manufacturing Research Group, Wolfson School of Mechanical and Manufacturing Engineering, Loughborough University, Loughborough, LE11 3TU, UK, August 2011, http://utwired.engr.utexas.edu/lff/symposium/proceedingsArchive/pubs/Manuscripts/2011/2011-03-Baumers.pdf, Accessed: June 17, 2014. 78, 79, 102

[55] J. Gronostajski, H. Marciniak, A., "New methods of aluminium and aluminium-alloy chips recycling," *Elsevier*, 2000. 79, 102

[56] I. Bagudancha, M.L. Garcia-Romeua, I. J., "The effect of process parameters on the energy consumption in Single Point Incremental Forming," *Elsevier*, 2013. 79, 102

[57] European Aviation Safety Agency, "Certification Specifications for Normal, Utility, Aerobatic, and Commuter Category Aeroplanes - CS-23," http://easa.europa.eu/system/files/dfu/CS-23%20Amendment%202%20(corrigendum).pdf, Accessed: June 6, 2014. 80

[58] París, J., Martínez, S., Navarrina, F., Colominas, I., and Casteleiro, M., "Topology Optimization of Aeronautical Structures with Stress Constraints: General Methodology and Applications ," *Proceedings of the Institution of Mechanical Engineers, Part G: Journal of Aerospace Engineering*, April 2012. 107

[59] Bendsøe, *Topology Optimization Theory, Methods, and Applications*, Springer Berlin Heidelberg, Berlin, Heidelberg, 2004. 107

[60] Sigmund, O. and Petersson, J., "Numerical instabilities in topology optimisation: A survey on procedures dealing with checkerboards, mesh-dependencies and local minima," *Structural Optimisation*, , No. 16, February 1998, pp. 68–75. 108

[61] Hora, P., Berisha, B., and Manopulo, N., "Comparison of Bending Behavior for Different Element Types," Principles of Nonlinear Finite-Element-Methods, 2013, Accessed : November, 2013. 108

[62] OpenFOAM, "The Opensource CFD Toolbox," http://www.openfoam.com/, Accessed: June 18, 2014. 110

[63] Drela, M., "XFOIL: An Analysis and Design System for Low Reynolds Number Airfoils," *Low Reynolds Number Aerodynamics, Springer-Verlag Lecture Notes in Engineering 54*, 1989. 110

[64] Drela, M., "XFOIL Documentation," http://web.mit.edu/drela/Public/web/xfoil/xfoil_doc.txt, Accessed: June 18, 2014. 110

[65] Lafountain, C., Cohen, K., and Abdallah, S., "Use of XFOIL in Design of Camber-Controlled Morphing UAVs," *Computer Applications in Engineering Education*, Vol. 20, No. 4, 2012, pp. 673–680. 110

[66] Deperrois, A., "About XFLR5 Calculation and Experimental Measurements," Tech. rep., Guidelines for QFLR5 v0.03, October 2009, Accessed from http://www.xflr5.com/docs/Results_vs_Prediction.pdf on June 19, 2014. 110, 111

[67] Anderson, J., *Fundamentals of Aerodynamics*, McGraw-Hill, New York, 2011. 110

[68] Fahner, T., "Theory & Application - CFD Workshop DUT Racing - ActiFlow," . 111, 112

[69] Jenny, P. and Kleiser, L., "Turbulent Flows - Lecture Notes - HS 2010," 2013, Last Revised : February 9, 2011. 111

[70] Schlichting, H., *Boundary-layer theory*, Springer, Berlin New York, 2000. 112

[71] ANSYS Fluent, "Fluent 6.3 User Guide - Near-Wall Mesh Guidelines," http://aerojet.engr.ucdavis.edu/fluenthelp/html/ug/node518.htm, Accessed: June 22, 2014. 112

Nomenclature

Greek Symbols

Symbol	Description	Units
α	Angle of Attack	$^\circ$
β	Sideslip Angle	$^\circ$
δ_e	Elevator Deflection Angle	$^\circ$
ε	Elongation	–
$\varepsilon_{failure}$	Failure Strain	%
$\varepsilon_{t_{0.75R}}$	Twist at 0.75 radius	$^\circ$
η	Efficiency	%
η_{loiter}	Propeller Efficiency During Loiter	–
η_{max}	Propeller Efficiency During Maximum Power	–
μ	Friction Coefficient	–
ν	Kinematic Viscosity	m^2/s
ϕ	Heat Deflection Temperature	$^\circ C$
ρ	Density	kg/m^3
σ	Normal Stress	Pa
σ_{ult}	Tensile Ultimate Stress	Pa
σ_y	Tensile Yield Stress	Pa

Roman Symbols

Symbol	Description	Units
A	Aspect Ratio	–
b	Wing Span	m
n_b	Number of Blades	–
b_{VT}	Wing Span Vertical Tail	m
c	Chord Length	m

C_D	Drag Coefficient	–
C_d	Two Dimensional Drag Coefficient	–
C_h	Hinge Moment Coefficient	–
C_L	Lift Coefficient	–
C_l	Two Dimensional Lift Coefficient	–
C_{L_α}	Lift Rate Coefficient	–
C_{l_α}	Two Dimensional Lift Rate Coefficient	–
$C_{L_{max}}$	Maximum Lift Coefficient in Clean Configuration	–
$C_{l_{max}}$	Maximum Two Dimensional Lift Coefficient	–
C_m	Moment Coefficient	–
$C_{m0.25c}$	Moment Coefficient around the Quarter Chord Point	–
C_{m_α}	Moment Rate Coefficient	–
C_{n_β}	Static Directional Stability Coefficient, $= \partial C_n / \partial \beta$	–
c_p	Propeller Specific Fuel Consumption	$N/s/W$
c_{VT}	Tail Volume Coefficient of the Vertical Tail	–
D	Drag	N
d	Diameter	m
d_s	Spinner Diameter	m
E	Young's modulus	Pa
e	Oswald Factor, respectively Span Efficiency Factor	–
F	Force	N
g	Gravitational Acceleration	m/s^2
h	Height	m
i_w	Incidence Angle	$^\circ$
L	Lift	N
L/D	Lift to Drag Ratio	–
L_{VT}	Moment Arm of the Vertical Tail	m
M	Mach Number	–
$MTOW$	Maximum Take-off Weight	N
n	Load Factor	–
n_1	Positive Limit Maneuvering Load Factor	–

n_2	Negative Limit Maneuvering Load Factor	–
N_{crit}	Amplification Factor	–
n_j	Load Factor on Wheels at Landing Impact	–
OEW	Operational Empty Weight	N
P	Power	W
RC	Climb rate	m/s
Re	Reynolds Number	–
S	Wing Surface Area	m^2
S_{VT}	Surface of Vertical Tail	m^2
T_{cruise}	Thrust During Cruise	N
T_{max}	Maximum Thrust	N
V	Velocity	m/s
V_A	Design Maneuvering Speed	m/s
V_C	Design Cruising Speed	m/s
V_D	Design Diving Speed	m/s
V_{EAS}	Equivalent Airspeed	m/s
V_F	Design Flap Speed	m/s
V_{loiter}	Design Loiter Speed	m/s
V_{max}	Maximum Airspeed	m/s
V_S	Stalling Speed at the Design Maximum Weight with the Flaps Retracted	m/s
V_{S0}	Stalling Speed at the Maximum Weight with the Wing Flaps Fully Extended	m/s
W	Weight	N
W/P	Power Loading	N/W
W_{PL}	Payload Weight	N
W/S	Wing Loading	N/m^2
x_{ac}	X-Location of the Aerodynamic Center	m
x_{np}	X-Location of the Neutral Point	m
x_{wing}	X-Location of the Wing	m

List of Abbreviations

ABS Acrylonitrile Butadiene Styrene. 77

ADAHRS Air Data Attitude Heading Reference System. 54, 55

ADC Air Data Computer. 54

AHP Analytical Hierarchy Process. 4, 16

AM Additive Manufacturing. I, IV, V, 1, 2, 4–6, 20, 22–26, 28, 30–33, 37, 41–43, 45–48, 56, 57, 65, 66, 69, 70, 73, 74, 76, 77, 79, 81, 82, 87, 88

ATOM Abaqus Topology Optimisation Module. I, 95

BJ Binder Jetting. 77

CAD Computer Aided Design. 28, 29, 31, 36, 87, 96, 99

CAS Calibrated Airspeed. 60

CATIA Computer Aided Three dimensional Interactive Application. 29, 96

CFD Computational Fluid Dynamics. I, 18, 19, 59–64, 83, 98–101

CG Center of Gravity. 10–12, 22, 37, 43, 50, 52, 62, 64, 65

CNC Computer Numerical Control. 77

CRI Certification Review Item. 81

CS Certification Specifications. 80, 81

DATCOM United States Air Force Stability and Control Data Compendium. 10, 11, 19

DED Direct Energy Deposition. 22, 26, 33, 36, 39, 56, 57, 87

DES Detached Eddy Simulation. 99

DIC Direct Image Correlation. 67, 68, 83, 84

DNS Direct Numerical Simulation. 99

DSE Design Synthesis Exercise. iv, I, 1, 71, 87

EASA European Aviation Safety Agency. 80

ECU Engine Control Unit. 53, 55

EFIS Electronic Flight Instrument System. 54

EICAS Engine Indicating and Crew Alerting System. 54, 55

EMS Engine Management System. 53

FAA Federal Aviation Administration. 60, 62, 63, 66, 92

FAR Federal Aviation Regulations. 28

FDM Fused Deposition Modeling. 27, 51, 52, 77

FEM Finite Element Method. 2, 24, 28, 31, 32, 35, 48, 67, 68, 76, 83, 87, 95–97

FFD Functional Flow Diagram. 4, 94

GAW General Aviation Whitcomb. 15–18, 36

GPS Global Positioning System. 54

HIC Human Interface Connectors. 53

HIP Hot Isostatic Pressing. 56

ILS Instrument Landing System. 54

ILT Inspectie Leefomgeving en Transport. I, 80

LCD Liquid Crystal Display. 54

LES Large Eddy Simulation. 99

LLC Limited Liability Company. 56

LLT Lifting Line Theory. 98

LSA Light Sport Aircraft. IV, V, 1, 13, 14, 16, 60–62, 66, 72–74, 78, 79

MDZ Minimum Drag Zone. 16, 17

MFD Multi-Function Display. 54, 55

MTOW Maximum Take-off Weight. 14, 44, 60, 75

NACA National Advisory Committee for Aeronautics. 14–18, 28, 36

NASA National Aeronautics and Space Administration. 15

OEW Operational Empty Weight. 5, 7, 75

PBF Power Bed Fusion. 22, 26, 44

PFD Primary Flight Display. 54, 55

PLA Polylactic Acid. 67, 77

PPSU Polyphenylsulfone. 28, 51

RAMS Reliability, Availability, Maintainability and Safety. 59

RANS Reynolds-averaged Navier Stokes. 99

RPM Revolutions Per Minutes. 20, 21, 54, 61

SLM Selective Laser Melting. 26, 44, 46, 56, 57

SST Shear Stress Transport. 99, 100

TO Topology Optimization. IV, 2, 24, 25, 28–32, 35, 36, 41, 67–70, 76, 82, 83, 87, 88, 95, 96, 102

UFP Utra Fine Particules. 77

ULA Ultra Light aircraft. 73

UV Ultra Violet. 27, 57

VHF Very High Frequency. 54

VI Vaccum Infusion. 78

VLM Vortex Lattice Method. 98, 99

VOR VHF Omni Directional Radio Range. 54

VP Vat Polymerization. 27, 28, 30, 31, 33, 39, 51, 56, 57, 72, 78, 82, 87

List of Figures

List of Tables

Appendix A

List of Requirements & Targets

Requirements & targets to perform the mission technically

Performance requirements

# ID	Type	Requirement	Owner
AMA-Tech.-Perf.-End.-1	R	The aircraft shall be able to loiter for two hours under the specified design conditions.	M.O.
AMA-Tech.-Perf.-End.-2	T	The design airspeed for loitering shall be an airspeed of 85 kts CAS. This means that at this airspeed the aircraft should fly most efficiently during loitering.	M.O.
AMA-Tech.-Perf.-End.-3	T	The design altitude for loitering shall be 4,000 ft AGL.	M.O.
AMA-Tech.-Perf.-Climb-1	T	The aircraft shall have a maximum attainable climb rate of 800 ft/min in sea level conditions.	M.O.
AMA-Tech.-Perf.-Man.-1	R	The aircraft should be able to pull a $2.5g$ pitch-up maneuver at the design loiter speed.	M.O.
AMA-Tech.-Perf.-FD-1	R	The aircraft shall be able to be trimmed at all times.	M.O.
AMA-Tech.-Perf.-FD-2	R	The aircraft shall be longitudinally statically stable.	M.O.
AMA-Tech.-Perf.-FD-3	R	The aircraft shall be longitudinally dynamically stable.	M.O.
AMA-Tech.-Perf.-FD-4	R	The aircraft shall be laterally statically stable.	M.O.
AMA-Tech.-Perf.-FD-5	R	The aircraft shall have a convergent Dutch Roll eigenmotion.	M.O.

Manufacturing requirements & targets

# ID	Type	Requirement	Owner
AMA-Tech.-Manu.-1	R	At least all load carrying structural elements of the aircraft shall be fabricated using AM techniques.	S.P.
AMA-Tech.-Manu.-2	R	Only current AM techniques shall be used in the design.	S.P.
AMA-Tech.-Manu.-3	R	Cables, pulleys and fasteners altogether shall never contribute to more than 10 % of the airframe mass.	C.J.

Structural requirements & targets

# ID	Type	Requirement	Owner
AMA-Tech.-Struct.-Loads-1	R	The aircraft shall be able to withstand a load factor on the wheels (n_j), computed as defined per ASTM F2245-07a, Section 5.2.4.1.	M.O.
AMA-Tech.-Struct.-Loads-2	R	The positive limit load factor (n_1) of the aircraft shall not be less than +4.0 at V_A.	M.O.
AMA-Tech.-Struct.-Loads-3	R	The negative limit load factor (n_2) of the aircraft shall not be greater than −2.0 at V_A.	M.O.
AMA-Tech.-Struct.-Loads-4	R	The aircraft's structure shall be able to withstand positive and negative gusts of 7.5 m/s nominal intensity at V_F with the flaps fully extended.	M.O.
AMA-Tech.-Struct.-Loads-5	R	The aircraft's structure shall be able to withstand, with flaps retracted, (1) positive and negative gusts of 15 m/s at V_C; (2) positive and negative gusts of 7.5 m/s at V_D.	M.O.
AMA-Tech.-Struct.-Maint.-1	T	Each component of the structure shall be accessible within two hours by two skilled technicians.	S.P.

Requirements & targets derived from constraints

Derived from scheduling

# ID	Type	Requirement	Owner
AMA-Con.-Sched.-1	R	The conceptual design, preliminary design and 60% of the detailed design phase shall be performed by the 10 members of DSE Group 12 within 10 weeks.	M.O.

FAA regulations

# ID	Type	Requirement	Owner
AMA-Con.-FAA-1	T	The aircraft shall be certifiable in the LSA category from the FAA.	M.O.
AMA-Con.-FAA-2	R	The aircraft shall be operated under a special airworthiness certificate in the FAA LSA experimental aircraft category.	M.O.
AMA-Con.-FAA-1-1	R	The maximum take-off weight of the aircraft shall not exceed 1,320 lbs (598.7 kg).	M.O.
AMA-Con.-FAA-1-2	R	The maximum stalling speed of the aircraft without the use of lift-enhancing devices (V_S) shall not exceed 45 kts CAS at maximum take-off weight and most critical center of gravity.	M.O.
AMA-Con.-FAA-1-3	R	The airspeed in level flight with maximum power shall not exceed 120 kts CAS under standard atmospheric conditions at sea level.	S.P.

AMA-Con.-FAA-1-4	R	The maximum seating capacity of the aircraft shall not exceed two persons, including the pilot.	M.O.
AMA-Con.-FAA-1-5	R	The aircraft shall use a single engine.	M.O.
AMA-Con.-FAA-1-6	T	The aircraft shall use a reciprocating engine.	M.O.
AMA-Con.-FAA-1-7	R	The aircraft shall be using a fixed-pitch propeller or ground-adjustable propeller.	S.P.
AMA-Con.-FAA-1-8	R	The aircraft shall have a fixed landing gear.	S.P.
AMA-Con.-FAA-1-9	R	The aircraft shall have a non-pressurized cabin.	S.P.

Sustainability restrictions

# ID	Type	Requirement	Owner
AMA-Con.-Sust.-1	T	The aircraft shall at least be as sustainable as comparable aircraft in the LSA category.	S.P.
AMA-Con.-Sust.-2	T	The operational lifetime of the aircraft shall be at least twenty flights.	S.P.

Operational restrictions

# ID	Type	Requirement	Owner
AMA-Con.-Oper.-1	R	The aircraft shall be a single-seat aircraft.	M.O.
AMA-Con.-Oper.-2	R	The aircraft shall be capable of operating off runway 05/23 at Lelystad Airport.	S.P.
AMA-Con.-Oper.-1-1	R	The maximum payload weight for the aircraft shall be 100 kg.	M.O.
AMA-Con.-Oper.-1-2	T	The cockpit width shall be minimum 24” or 0.6 m .	S.P.
AMA-Con.-Oper.-1-3	T	The cockpit height shall be minimum 42” or 1.1 m.	S.P.
AMA-Con.-Oper.-1-4	T	The cockpit depth shall be minimum 48” or 1.2 m.	S.P.
AMA-Con.-Oper.-2-1	R	The maximum take-off ground-roll distance shall be no more than 1250 m.	S.P.
AMA-Con.-Oper.-2-2	R	The maximum landing ground-roll distance shall be no more than 1250 m.	S.P.

Appendix B

Functional Flow Diagram

A Functional Flow Diagram (FFD) describes in a logical and chronological order what functions need to be performed by a system or a product. This mission functional flow diagram shows the functions that will be performed to achieve a successful mission. The mission of the airplane is basic; it shall loiter for two hours. Establishing such an FFD guarantees that no functions required to have a successful flight will be omitted.

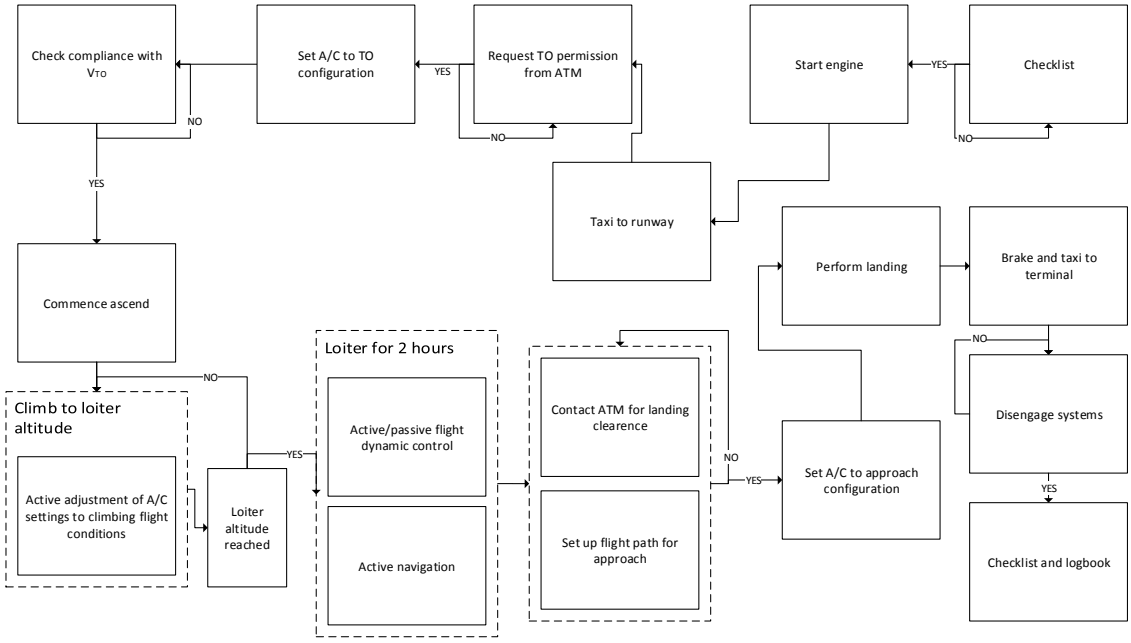

Figure B.1: Mission functional flow diagram

Appendix C

Details on Topology Optimization

The whole design process of this aircraft depends heavily on the use of numerical structural analysis tools. Topology Optimization is used as a guide for the design of the vertical tail and the wing root sections, while a structural FEM analysis is also used separately for the verification of the design. All these tools are described in this appendix, while also some results for these computations are presented.

Several software packages provide the required FEM and TO algorithms. Some of them are freeware, but they are not as good as commercial ones and are at times slow and buggy. Within the commercial software, Dassault Systèmes' Abaqus and Altair stand out with their Abaqus Topology Optimisation Module (ATOM) and OptiStruct, respectively, which are packages specifically designed for TO. For the Altair Optistruct package a dedicated student license is available. However, that license only allows for mesh sizes of at most 10,000 nodes. This restriction of model size seems to render that software package not useful for optimizing large parts such as the vertical tail. Delft University of Technology does however provide a license for the Abaqus package. The ATOM license is however not included in this license. After contact with Dassault Systèmes and Ir. Jan Hol from TU Delft, it was decided to request an evaluation license for ATOM for the limited period of 30 days. This license is therefore used to perform all TO optimization.

C.1 Topology Optimization Theory & Application

In topology optimization different formulations can be used to obtain the most adequate design. For instance, one can optimize for stiffness, eigenfrequency, stress, et cetera. However, the most widely used formulation tries to minimize strain energy (i.e. maximize stiffness), while putting a constraint on the volume or weight of the part. The reason for this is that this is one of the least computational intensive optimization tasks with still very useful output. More recently, different optimization approaches are used which focus on stress and/or displacement constraints. Such a method has several advantages over the stiffness maximization approach, such as preventing chequerboard modes, guaranteeing the feasibility of the solution and more realistic and reliable formulations. However, such a method is more computationally intensive since the underlying problem formulation is more complicated [58]. Therefore, every TO computation for this project optimizes for stiffness under a volume constraint. More information on Topology Optimization can be found in Reference [59].

In the Abaqus ATOM package, for this form of optimization the "Condition-based optimization" is chosen over the "General optimization (sensitivity-based)", mostly because it is much faster for the chosen optimization formulation. This software package uses the "density-based approach" towards TO. As such, during the computation it tries to find the optimal density distribution for each element. For instance, one element can have a density of 0.0, another might have 0.4 and yet another is very

highly loaded and therefore requires a density of 1.0. The output is therefore a material distribution with different densities for every element. This output can subsequently be converted to an isosurface file by connecting all elements with the same value. Most commonly used for this ”isosurface value” is a value between 0.2 and 0.3. For most designs an isosurface value of 0.2 is used to prevent omitting important details from the result. This isosurface can subsequently be smoothed in Abaqus to yield more useable parts for post-processing.

These isosurfaces are the focal point of problems between the TO and subsequent post-processing. These surfaces (in the form of an .STL file) can be easily submitted to a 3D printer, as was done for the case study model. However, using them in CAD design software is more of a problem. They can be loaded into CATIA, but due to their complex nature they cannot be converted to solids. That means every result has to be fully redrawn in CATIA, but since it is a surface it is also hard to measure all dimensions correctly. This all results in a less optimal TO and CAD integration, requiring a great deal of manual rework before yielding a useable end result.

Lastly, another point of attention for the Topology Optimization is the possible dependence of the solution on the mesh resolution [60]. Due to time constraints it was not possible to check this for an optimization used in the project. Thus, this should be investigated in a later stage. Regarding the element size of the models, these were mostly chosen as small as the computational resources would allow for. This mostly meant that the mesh size was sufficiently coarse to run within ten hours. Furthermore, two types of meshes have been used: Meshes with quad cells and one with triangular cells. For FEM quad cells are preferred for their higher accuracy under bending deformation, but it can be difficult to generate them on a complex geometry [61]. Therefore, where the geometry allows it quad cells are used (only the case study model, Figure C.1(a)), otherwise triangular cells are employed (vertical tail and wing-root sections, Figure C.1(b)).

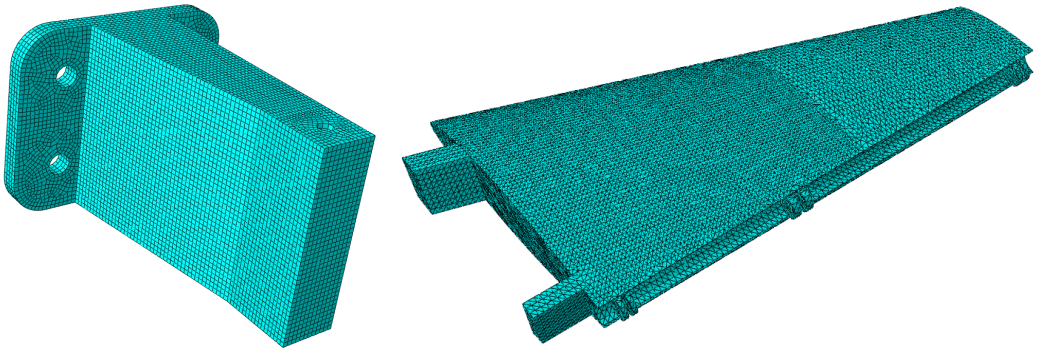

(a) Quad cell mesh (As used in case study model)

(b) Tri cell mesh (As used for vertical tail model)

Figure C.1: Different mesh types used for FEM and TO

C.2 Additional Results

For the vertical tail a final FEM analysis is performed to verify the design. A detail of these results focused on the root section of the vertical tail and is shown in Figure C.2. The deflections in the skin at the root are quite high, but further investigation is required to see if that is due to the mesh size of the FEM analysis or if it is indeed a problem in the design. This uncertainty is the result of the coarse mesh on the skin, which is only two elements thick (with triangular elements). According to Hora [61], a beam with only two elements in thickness direction can sometimes yield a 300% larger deflection than is measured experimentally. Therefore, it has to be investigated whether this is also the case

for the current mesh, which was not done immediately because of the high demand on computational resources it would imply.

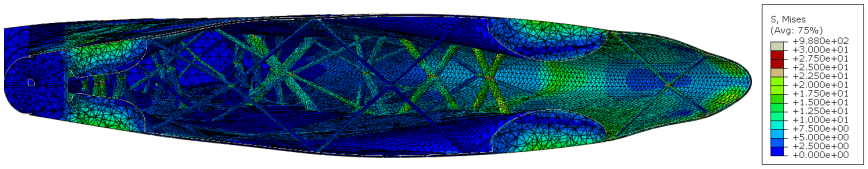

(a) Bottom view (deflection scale factor = 4.138)

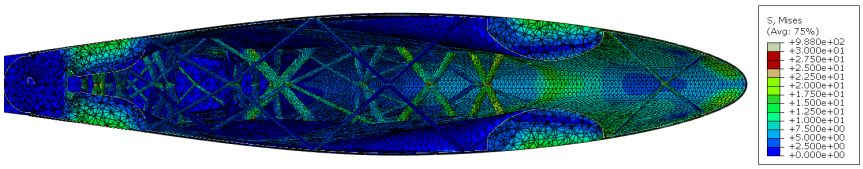

(b) Bottom view, undeformed

Figure C.2: FEM analysis of the current vertical tail design for load case 3 (with safety factor 3.0). Von Mises stresses are indicated in $[MPa]$.

Appendix D

Details on Computational Fluid Dynamics

For the aerodynamic analysis of the design multiple numerical fluid dynamics analysis tools are used. Firstly, more straightforward analysis tools like `XFOIL` are used to select proper airfoils for the individual wings and the vertical stabilizer. To then verify and adapt the overall aerodynamic design the 3D numerical analysis program `XFLR5` is used. However, since it was identified that blanketing is a large risk for the tandem aircraft, a more accurate estimation on the aerodynamics is required. Therefore, also the CFD software `OpenFOAM` [62] is used. This appendix describes these numerical tools as well as their use in the project.

D.1 Simple Analysis Tools

For the airfoil selection and load estimations on the vertical tail, `XFOIL` has been used extensively. It is an inviscid linear-vorticity panel method developed by Drela [13]. The viscous layer influence on the potential flow is accounted for by superimposing source distributions on the airfoil and wake. Both laminar and turbulent boundary layers are accounted for, where the e^n-type amplification formulation determines the transition point [63]. This mostly all happens in the software itself and the team did not deal with most of it. However, the user does have to specify one important parameter for the analysis: N_{crit} from the e^n-type amplification formulation. This directly determines the transition point between laminar and turbulent flow and thereby influences lift and drag enormously. Drela [64] does give some guidelines on which value for N_{crit} to select. The standard value for N_{crit} which is applicable to most windtunnels is 9. However, for sailplanes it ranges from 12-14 and for motorgliders between 11-13. Therefore, for N_{crit} a value of 12 is used throughout the whole aerodynamic analysis.

The airfoils could also have been selected on the basis of CFD results, but the computational demands and demands on resources would be much higher. Moreover, those CFD results would not be more accurate than `XFOIL`, as `XFOIL` is known for providing accurate results at low Reynolds numbers [65].

For a first estimate of the 3D aerodynamic performance of the aircraft, `XFLR5` has been used. The 2D analysis is heavily based on `XFOIL`, while the 3D analysis can either use a Lifting Line Theory (LLT), Vortex Lattice Method (VLM) or 3D panel method combined with VLM. In Reference [66], these three methods are compared to one another and to experimental results. The conclusion was that VLM was the best option for most analyses, with the 3D panel/VLM being slightly more accurate. However, for the VLM method the influence of thickness on the aerodynamic forces is neglected [67]. Considering the difference in C_{L_α} between the front and aft wing is important for the stability of the aircraft (as explained in Section 3.1), the estimation of this parameter is important. The thickness and its distribution over the airfoil do have an influence on the C_{L_α} of the wing and should therefore

not be neglected. Consequently, the 3D panel/VLM method is used for all XFLR5 analyses throughout the whole design process, since this method does take the thickness into account.

Furthermore, it has been decided to not take the fuselage into account in the XFLR5 analysis, since according to its own developers, this adds more nuisance than accuracy to the solution [66]. Therefore, the model shown in Figure D.1 is used for all XFLR5 analyses. Another problem in XFLR5 is that it is known to have some problems with large changes in Reynolds number over the span, as is the case with delta and elliptical wings. Furthermore, XFLR5 cannot solve at high angles of attack when stall occurs, which is the reason why the result for the tandem wings in Figure 3.8 only continues up until $\alpha = 10.5°$. Due to these limitations of XFLR5 and the high risk associated with high angles of attack for a tandem aircraft a more advanced aerodynamic analysis using CFD is required.

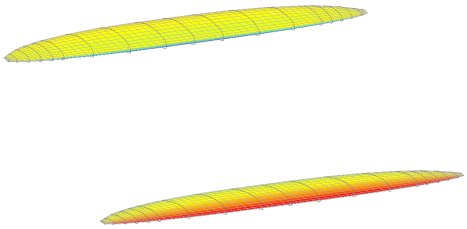

Figure D.1: Model used in XFLR5 analysis

D.2 OpenFOAM CFD Analysis

For more advanced aerodynamic analysis the OpenFOAM software package is used extensively. Reasons for this are, amongst others, that it is open-source and a cluster running of this software is made available to the team by the Formula Student Team Delft. Especially since the aircraft has a tandem wing configuration, the interference between the two wings is important, thereby requiring a more accurate aerodynamic simulation. Within OpenFOAM a Reynolds-averaged Navier Stokes (RANS) simulation is executed using the simpleFOAM solver. A RANS simulation is used as that is widely used in industry for its lowest computational resources and is less research based as the other simulations such as Large Eddy Simulation (LES), Detached Eddy Simulation (DES) and Direct Numerical Simulation (DNS). The simpleFOAM solver is be used as that is most applicable to general external aerodynamics and the flow can still be assumed incompressible with the low Mach numbers the aircraft will fly at. Because a transient CFD computation would require too much computational time, only steady state CFD computations are performed. As mentioned before, a cluster with 40 quadcore computers is used to execute all CFD computations.

For the turbulence model, the selection was limited to the k-ω-SST turbulence model and the Spalart-Allmaras model. The k-ω-SST model is widely used in the automotive industry and the Spalart-Allmaras model is more in use in the aircraft industry [68, 69]. Early in the detailed design phase the CAD model from the final concept was meshed and run with these two different turbulence models. The residuals for the iterative solver are presented in Figure D.2, from which can be derived that the overall residuals for the Spalart-Allmaras turbulence model are lower. The CFD computations were stopped at 3000 iterations, since the residuals are already relatively constant from 2000 onwards. However, a constant residual means there is still fluctation in the end result (for instance in the total lift). For the k-ω-SST model the standard deviation of that fluctuation between iterations 2500 and 3000 was 42.4, while for the Spallart-Allmaras turbulence model that standard deviation was only 1.3. Although this does not necessarily mean one turbulence model is better than the other, it was still decided to choose the Spallart-Allmaras model because it would most likely yield more useable results.

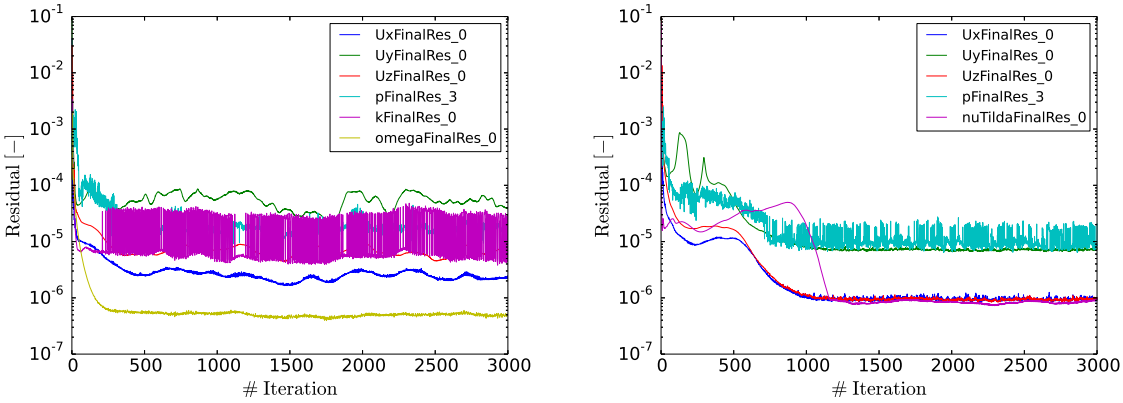

(a) k-ω-SST (b) Spalart-Allmaras

Figure D.2: Comparison in residuals between k-ω-SST and Spalart-Allmaras turbulence model

The mesh for the performed CFD computations is an unstructured mesh. On this relatively simple geometry (see Figure D.3(a)), a structured mesh could also be used but then the time spent on meshing would increase tremendously. Since no sideslip angles are modeled with CFD, the flow field is symmetric and therefore only the right side of the aircraft is modeled in CFD. Furthermore, the mesh is tetrahedral mesh but with prism cells near the boundary to solve the boundary layer correctly. The mesh around the aircraft can be seen in Figure D.3(b), while a detail of it with a prism layer is shown in Figure D.3(c). The mesh is relatively fine as the mesh size of the lifting surfaces ranges from 4 mm to 10 mm and on the fuselage from 10 mm to 15 mm. It has also been attempted to solve on a coarser mesh, but the confidence in those results was not high because it could not capture the boundary layer or the wake of the front wing with a high enough resolution. To capture that boundary layer accurately, a five cell thick prism layer has been added. For the height of the first prism layer the $y+$ [1] value is very important. For $y+$ values in the order of 1 (meaning a very fine mesh), the turbulence model can solve the boundary layer directly. For $y+$ values in between 30 and around 200, wall functions have to be employed which reduce the accuracy somewhat but allow for a much coarser mesh [68, 71]. Therefore, wall functions are used while the height of the prism layer was chosen such that the $y+$ value was in that range (around 100-180). This resulted in a height for the first prism cell of 3 mm, with the final mesh size in the order of ten million cells.

To validate the CFD a more extensive mesh independence study has to be performed. Furthermore, wind tunnel tests should be conducted on the model, which are also required to investigate the stability in more detail as explained in Section 7.2. However, as a first check also results from literature could be used to validate the CFD against. Since aerodynamics is not the main focus of this project, it was decided to postpone these activities to allow for more time spent on the structural details.

[1] The $y+$ value relates the local mesh size with local flow properties (such as viscosity, density and velocity), several assumptions of the wallfunctions is only valid in a certain range of $y+$ [70].

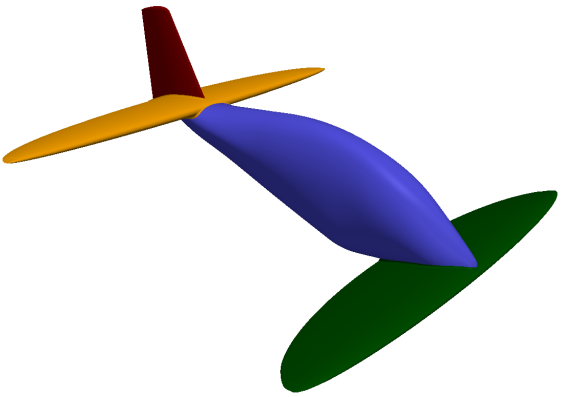

(a) CFD with separate patches

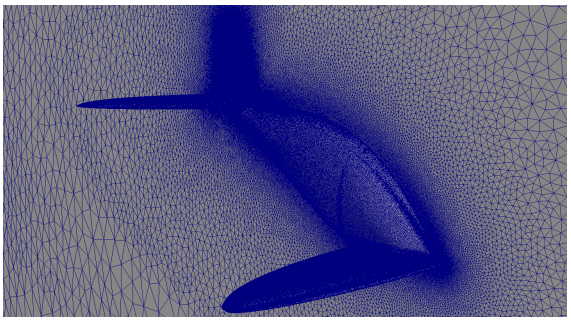

(b) Mesh in proximity of the aircraft: very fine around the aircraft, coarser towards the farfield

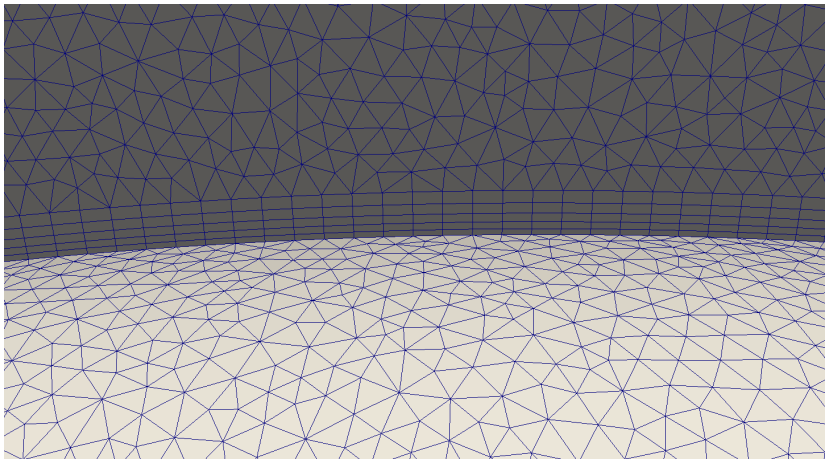

(c) Prism layer around the aircraft

Figure D.3: CFD geometry and mesh

Appendix E

Technical Drawings

In this appendix, technical drawings of the vertical tail and fuselage structure are shown. In the first, the vertical tail technical drawing, different section cuts in the tail show the internal structure of it, which is designed using Topology Optimization. Secondly, the technical drawing of the fuselage truss structure shows the locations of the trusses in the beams.

Section view C-C

Section view G-G

Section cut A-A

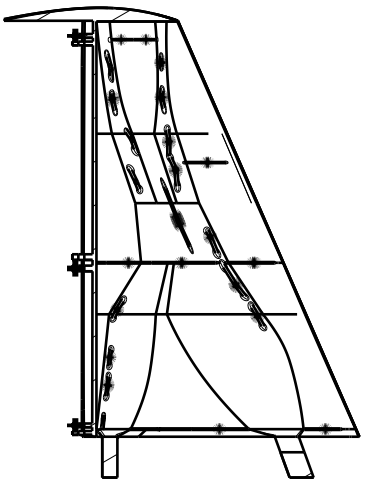

Section view D-D

Section view H-H

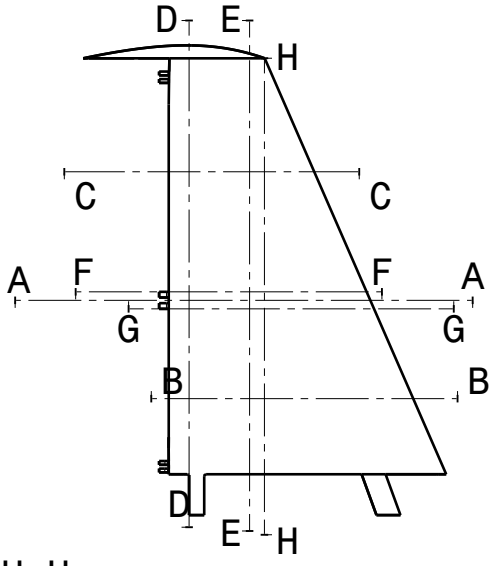

Front view
Scale: 1:20

Section view E-E

Section view F-F

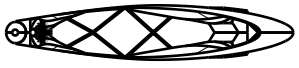

Section view B-B

E. Technical Drawings

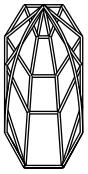

Front view

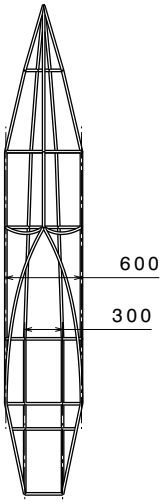

Top view

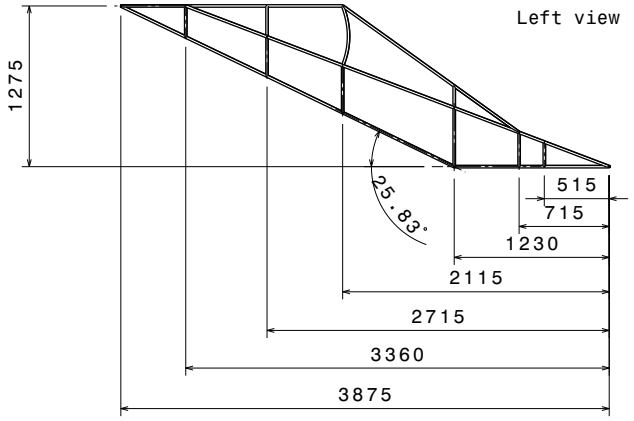

Appendix F

Organisational Breakdown & Project Planning

In the following the work distribution for the contents of the detailed design phase is given in Table F.1, while an overview of the performed activities is illustrated in the Gantt Chart, shown in Figure F.1.

Table F.1: Work distribution for the detailed design phase

Team Member	Tasks
K. Barten	Structural Design (Fuselage); Design Evaluation (Performance Analysis, Compliance Matrix)
M. De Bie	Structural Design (Landing Gear, Engine Mount); CATIA (Engine Mount); Subsystem Design (Steering & Braking, Electronics & Data Acquisition); Design Evaluation (Risk-, Cost- & Market Analysis)
T. Cheylus	Design for- & Analysis of Stability and Control (Major); Design Evaluation (Sustainability)
I. van de Grift	Structural Design (Joints); CATIA (Main Responsible); Subsystem Design (Internal Layout, Furnishing)
C. Jux	Structural Design (Wings, Initial setup Fuselage) ; CATIA (Wings), Future Work
S. van der Linden	Structural Design (Landing Gear, Engine Mount, Joints); Design Evaluation (RAMS)
M. Opgenoord	Topology Optimization (incl. Case Study); Structural Design (Vertical Tail); Stability and Control (Initial setup); Aerodynamics (incl. CFD); CATIA (Vertical Tail); Manufacturing, Assembly & Operations
S. Peelman	Structural Design (Landing Gear); Subsystem Design (Safety Systems); Design Evaluation (Sensitivity Analysis)
S. Stoter	Topology Optimization (incl. Case Study); Structural Design (Joints); Design Evaluation (RAMS)
F. van Zanten	Stability and Control ($2.5g$ Pull-up Maneuver); Propeller Design

F. Organisational Breakdown & Project Planning

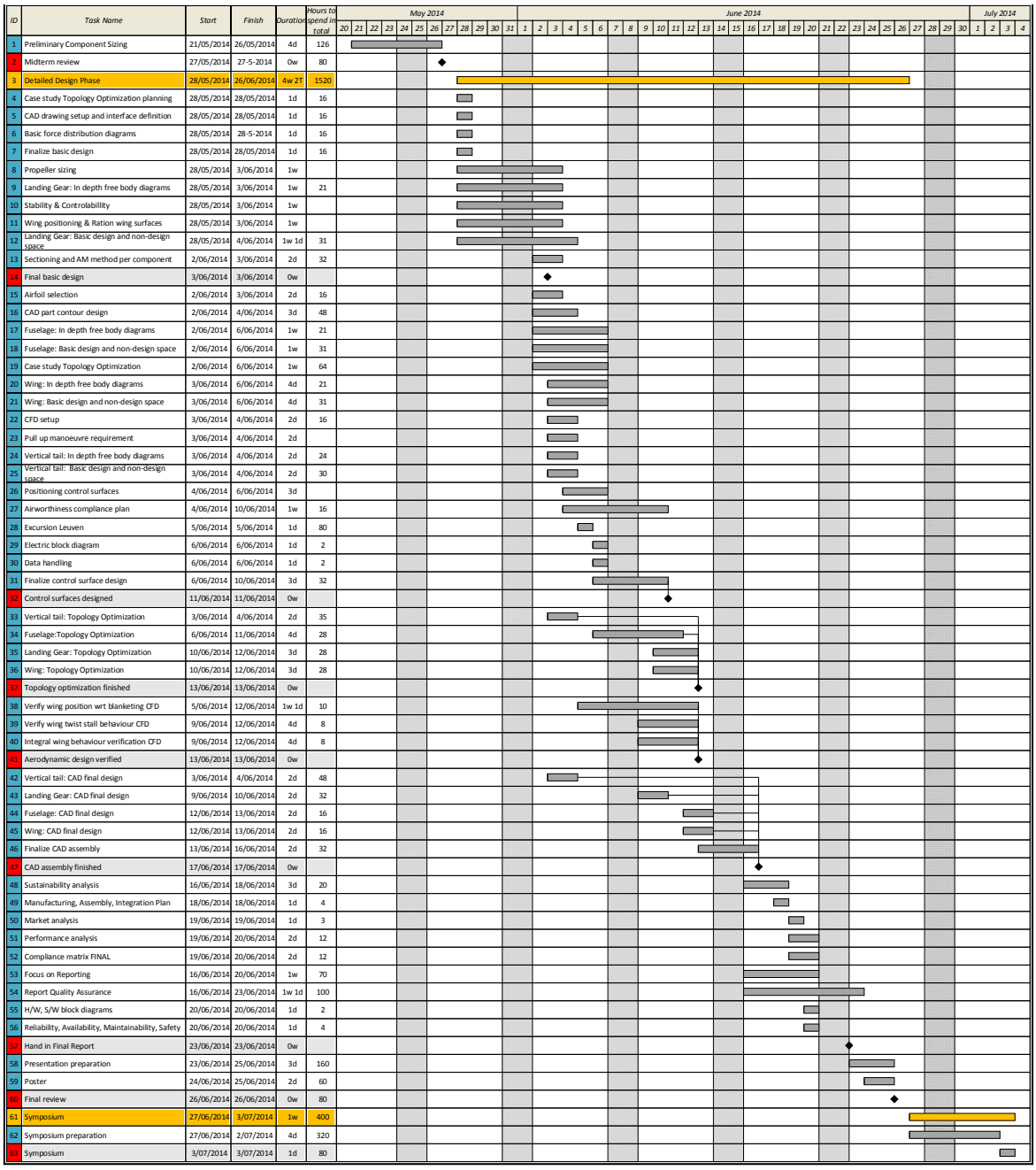

ID	Task Name	Start	Finish	Duration	Hours to spend in total
1	Preliminary Component Sizing	21/05/2014	26/05/2014	4d	126
2	Midterm review	27/05/2014	27-5-2014	0w	80
3	Detailed Design Phase	28/05/2014	26/06/2014	4w 2T	1520
4	Case study Topology Optimization planning	28/05/2014	28/05/2014	1d	16
5	CAD drawing setup and interface definition	28/05/2014	28/05/2014	1d	16
6	Basic force distribution diagrams	28/05/2014	28-5-2014	1d	16
7	Finalize basic design	28/05/2014	28/05/2014	1d	16
8	Propeller sizing	28/05/2014	3/06/2014	1w	
9	Landing Gear: In depth free body diagrams	28/05/2014	3/06/2014	1w	21
10	Stability & Controlability	28/05/2014	3/06/2014	1w	
11	Wing positioning & Ration wing surfaces	28/05/2014	3/06/2014	1w	
12	Landing Gear: Basic design and non-design space	28/05/2014	4/06/2014	1w 1d	31
13	Sectioning and AM method per component	2/06/2014	3/06/2014	2d	32
14	Final basic design	3/06/2014	3/06/2014	0w	
15	Airfoil selection	2/06/2014	3/06/2014	2d	16
16	CAD part contour design	2/06/2014	4/06/2014	3d	48
17	Fuselage: In depth free body diagrams	2/06/2014	6/06/2014	1w	21
18	Fuselage: Basic design and non-design space	2/06/2014	6/06/2014	1w	31
19	Case study Topology Optimization	2/06/2014	6/06/2014	1w	64
20	Wing: In depth free body diagrams	3/06/2014	6/06/2014	4d	21
21	Wing: Basic design and non-design space	3/06/2014	6/06/2014	4d	31
22	CFD setup	3/06/2014	4/06/2014	2d	16
23	Pull up manoeuvre requirement	3/06/2014	4/06/2014	2d	
24	Vertical tail: In depth free body diagrams	3/06/2014	4/06/2014	2d	24
25	Vertical tail: Basic design and non-design space	3/06/2014	4/06/2014	2d	30
26	Positioning control surfaces	4/06/2014	6/06/2014	3d	
27	Airworthiness compliance plan	4/06/2014	10/06/2014	1w	16
28	Excursion Leuven	5/06/2014	5/06/2014	1d	80
29	Electric block diagram	6/06/2014	6/06/2014	1d	2
30	Data handling	6/06/2014	6/06/2014	1d	2
31	Finalize control surface design	6/06/2014	10/06/2014	3d	32
32	Control surfaces designed	11/06/2014	11/06/2014	0w	
33	Vertical tail: Topology Optimization	3/06/2014	4/06/2014	2d	35
34	Fuselage:Topology Optimization	6/06/2014	11/06/2014	4d	28
35	Landing Gear: Topology Optimization	10/06/2014	12/06/2014	3d	28
36	Wing: Topology Optimization	10/06/2014	12/06/2014	3d	28
37	Topology optimization finished	13/06/2014	13/06/2014	0w	
38	Verify wing position wrt blanketing CFD	5/06/2014	12/06/2014	1w 1d	10
39	Verify wing twist stall behaviour CFD	9/06/2014	12/06/2014	4d	8
40	Integral wing behaviour verification CFD	9/06/2014	12/06/2014	4d	8
41	Aerodynamic design verified	13/06/2014	13/06/2014	0w	
42	Vertical tail: CAD final design	3/06/2014	4/06/2014	2d	48
43	Landing Gear: CAD final design	9/06/2014	10/06/2014	2d	32
44	Fuselage: CAD final design	12/06/2014	13/06/2014	2d	16
45	Wing: CAD final design	12/06/2014	13/06/2014	2d	16
46	Finalize CAD assembly	13/06/2014	16/06/2014	2d	32
47	CAD assembly finished	17/06/2014	17/06/2014	0w	
48	Sustainability analysis	16/06/2014	18/06/2014	3d	20
49	Manufacturing, Assembly, Integration Plan	18/06/2014	18/06/2014	1d	4
50	Market analysis	19/06/2014	19/06/2014	1d	3
51	Performance analysis	19/06/2014	20/06/2014	2d	12
52	Compliance matrix FINAL	19/06/2014	20/06/2014	2d	12
53	Focus on Reporting	16/06/2014	20/06/2014	1w	70
54	Report Quality Assurance	16/06/2014	23/06/2014	1w 1d	100
55	H/W, S/W block diagrams	20/06/2014	20/06/2014	1d	2
56	Reliability, Availability, Maintainability, Safety	20/06/2014	20/06/2014	1d	4
57	Hand in Final Report	23/06/2014	23/06/2014	0w	
58	Presentation preparation	23/06/2014	25/06/2014	3d	160
59	Poster	24/06/2014	25/06/2014	2d	60
60	Final review	26/06/2014	26/06/2014	0w	80
61	Symposium	27/06/2014	3/07/2014	1w	400
62	Symposium preparation	27/06/2014	2/07/2014	4d	320
63	Symposium	3/07/2014	3/07/2014	1d	80

Figure F.1: DSE Gantt Chart

Faculty of
Aerospace Engineering
Kluyverweg 1
2629 HS Delft
The Netherlands

www.tudelft.nl